RCA REVIEW

a technical journal

RADIO AND ELECTRONICS
RESEARCH · ENGINEERING

VOLUME XV   **MARCH 1954**   **NO. 1**

RCA REVIEW

a technical journal

RADIO AND ELECTRONICS
RESEARCH • ENGINEERING

CONTENTS

RCA REVIEW

BOARD OF EDITORS

REPUBLICATION AND TRANSLATION

A SYSTEM FOR RECORDING AND REPRODUCING TELEVISION SIGNALS*

By

Harry F. Olson, W. D. Houghton, A. R. Morgan,
Joseph Zenel, Maurice Artzt, J. G. Woodward.
and J. T. Fischer

Research Department, RCA Laboratories
Princeton, N. J.

Summary—A system for recording and reproducing television signals by means of magnetic tape has been developed. This system will accommodate both monochrome and color pictures. For monochrome pictures, two channels are used, one for the video signal and one for the sound signal. These signals are recorded as two tracks on ¼-inch magnetic tape. For color pictures, five channels are used: video channels for the color signals red, green and blue and the synchronizing channel and an audio channel. These signals are recorded as five tracks on ½-inch magnetic tape. An electronic servomechanism provides the speed constancy required for the reproduction of television signals from magnetic tape. The present tape speed is 30 feet per second. The recorded and reproduced frequency band is over 3 megacycles. There is a description of a demonstration which included side-by-side showing of a direct picture, and the same picture recorded and immediately played back.

INTRODUCTION

A SYSTEM for recording and reproducing television signals by means of magnetic tape has been developed. This system will handle both monochrome and color pictures. The elements of the system and several demonstrations are described in the sections which follow.

TAPE

The tape used in this development consists of a cellulose acetate base coated with a red iron oxide. The acetate base is .0017 inch in thickness. The iron oxide coating varies among different makes from .0004 to .0007 inch in thickness. The width of the tape for color television is ½ inch, and that for monochrome television is ¼ inch. In the case of monochrome, ½ inch tape may be used with two parallel programs on one tape. The coercive force of the tape used in the demonstration is 250 oersteds. The residual magnetization is 770 gausses.

---

* Decimal Classification: R583.15.

TAPE TRANSPORT MECHANISM

The tape transport mechanism has been designed to limit any sudden speed changes to a very minute quantity and thereby prevent jitter in the pictures. The order of constancy required can be illustrated by stating that a sudden speed change of one part in a million
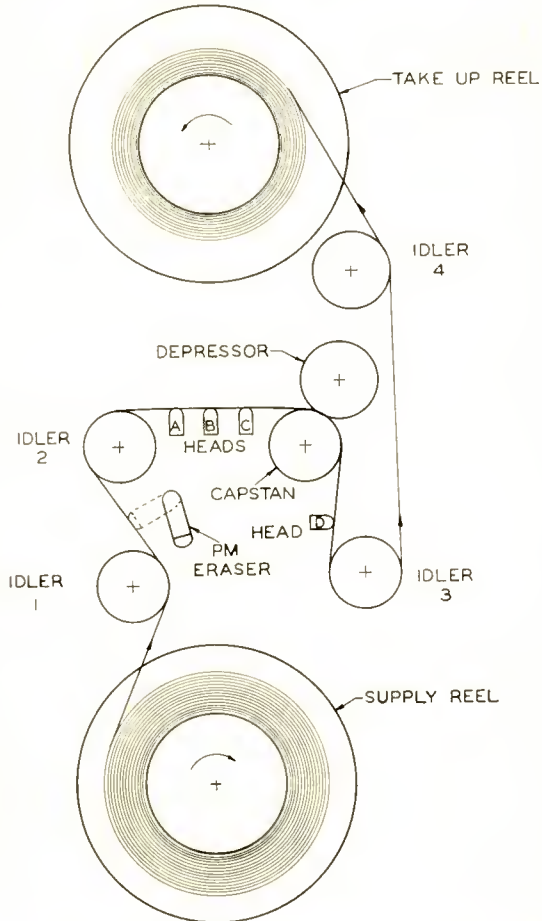
Fig. 1—A schematic diagram of the tape transport mechanism.

will put a jog of about $\frac{1}{5}$ inch in the picture on a 12-inch kinescope. In addition, any slow drifts in speed have to be limited to considerably less than one picture element per scanning line.

A schematic diagram of the tape transport system is shown in Figure 1. A photograph is shown in Figure 2.

The basic speed of the tape feed is determined by a capstan driven at approximately 30 revolutions per second and having a circumference of one foot. Sudden changes in capstan speed are filtered out by a flywheel. Bearings on this capstan-flywheel assembly must be
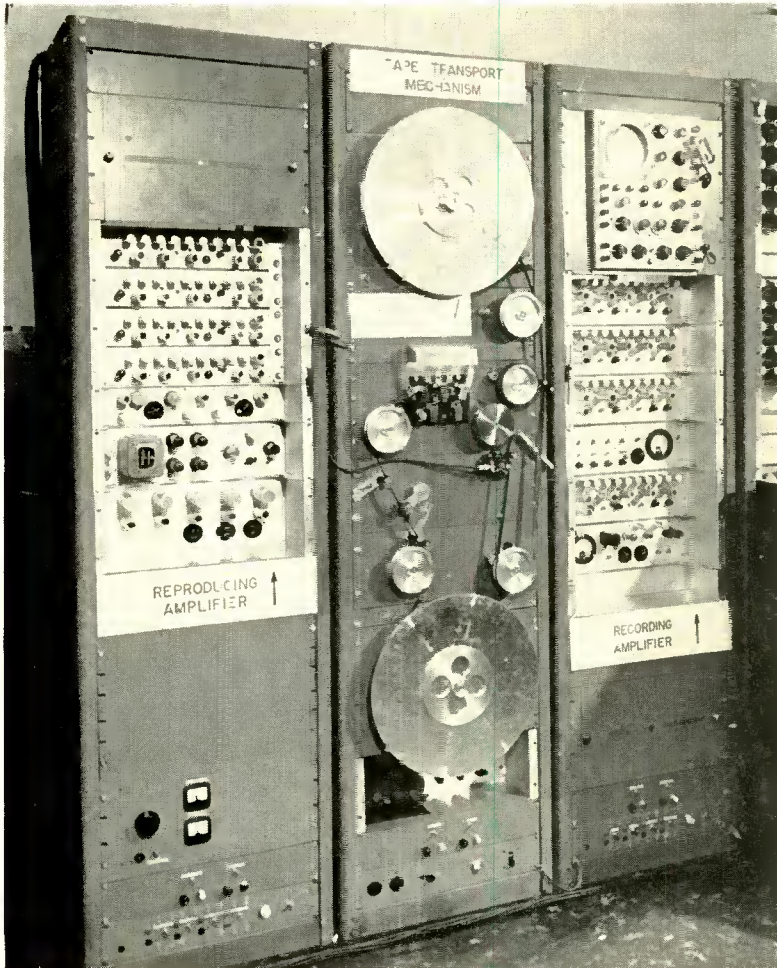
Fig. 2—The system for recording and reproducing television signals by means of magnetic tape.

very smooth and perfectly aligned, and both static and dynamic balance of all parts must be precise.

Even with accurate tape speed established by the capstan, tension in the tape supply and take up must be held very exact or momentary changes in tape position will be introduced by stretch in the tape.

Tension is maintained constant on the supply by driving a generator from the supply reel shaft, and using feedback to control the generator load to a constant tension load. The control must hold over a speed range of from 400 revolutions per minute (with a full reel) to over 860 revolutions per minute (when reel is empty).

The take up reel is motor driven and has its feedback circuit arranged so that a constant tension on pull-out is obtained. Both supply and take up tensions are held constant whether the reels are empty or full.

Figure 1 shows a diagram of the complete transport mechanism. Four fixed idler pulleys are used to guide the tape from supply reel over the heads and capstan, and onto the take up reel. A rubber surfaced idler is sprung against the capstan to act as a depressor in holding the tape on the capstan for speed determination.

The tape reels are an important part of the tape transport mechanism. The reel must not have excessive inertia if a practical starting time is to be achieved. The reel must be accurately balanced if full advantage is to be had from the constant tension reel drives.

The playing time of a reel full of tape is dependent on the diameter of the reel, the thickness of the tape, and the speed of the tape. The present reels shown in Figures 1 and 2 are 17 inches in diameter and have a hub 8 inches in diameter. The present tape is .0021 inch in thickness. A full reel contains approximately 7000 feet of tape. This length of ½ inch tape weighs 4.3 pounds and will play approximately 4 minutes at 30 feet per second. An objective of current research is to handle 15 minutes of program time using reels 19 inches in diameter. A fifteen minute reel could be considered a unit reel for television programing. Longer shows would be handled by using two reproducers alternately, as is done in motion picture theater presentations.

RECORDING AND REPRODUCING HEADS

The enormity of the problem of recording video signals on magnetic tape is obvious to anyone acquainted with the art of recording sound on magnetic tape. Application of the techniques employed for recording sound on tape seems almost futile when the demands of video recording are enumerated. To be more specific, a simple calculation will show that a frequency of 4 megacycles per second recorded on a tape traveling at 30 feet per second results in a wave length, on the tape, of less than 1/10,000 of an inch. Quite obviously the effective gap length of the recording and reproducing heads must be considerably less than the wave length to be recorded. One must accept the

problem of producing heads having exceedingly small effective gap lengths.

Further thought will point out the fact that the head gaps must be straight if the tape is to be recorded on one head and reproduced on another head, without loss of over-all performance.

The electrical and magnetic performance of the heads is all the more formidable for the reason that some 16 to 18 octaves of frequency range must be covered. The magnetic path of the heads must be made of a material that will maintain a high permeability over the entire frequency range. The coil which surrounds the magnetic path of the head must produce a reasonable electrical impedance over the frequency range. It is particularly important that the electrical impedance be free of resonances in the higher frequency range.

The physical configuration of the heads must satisfy a number of conditions. Firstly, the assembled head must be stable with time
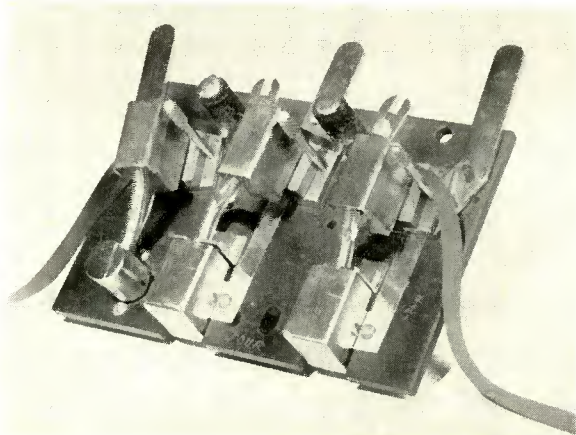
Fig. 3—The sound and video magnetic recording and reproducing heads.

against such adversities as temperature and humidity cycles. Secondly, the head must have good wear resistance to the abrasive effect of the passage of tape. Thirdly, the head must be physically small to allow for the grouping of multiple channels, such as in the color recording and reproducing procedures. Finally, there are numerous other mechanical requirements such as mounting of the heads, shielding of the electrical connections, head position adjustments, etc.

Redoubtable as the above requirements may be, it has been possible to develop a set of heads that appears to be a reasonable solution to all the problems. Figure 3 is a photograph showing the present arrangement of the head assembly for recording the color video signals

on tape. The left-hand head is for recording the sound. The central head is the video recording head, which is made up of four elemental heads to provide four channels. The right-hand head is the video reproducing head, which also contains four elemental heads. The sound reproducing head is placed at a point following the tape drive capstan, for the sake of expediency only. In a final design, both video and sound heads would probably be incorporated in a single unit. It may be noted that the sound recording head is positioned so that the sound track is centered between two of the video tracks.

Tests have established that the frequency response of the heads is uniform with a reasonable signal-to-noise ratio up to approximately 3.5 megacycles per second. The impedance of the elemental head is substantially free of resonances to the highest frequency. The wear properties of the heads, although not completely examined, have been satisfactory.

Audio System

In conventional magnetic tape recording systems used for audio frequency work, the tape usually moves past the recording and reproducing heads at a speed in the neighborhood of 1.25 feet per second. With such systems, careful design and adjustments are necessary if one is to succeed in recording and reproducing the higher audio frequencies, say above 10,000 cycles, because of the extremely short wave lengths of these higher frequencies. In the video tape recording system where the tape speed is 30 feet per second, the situation with respect to recording audio frequencies is reversed. It is now more difficult to record and reproduce the lower audio frequencies at useful levels above noise because of the extremely long wave lengths of the lower frequencies. For example, a 100-cycle tone recorded by the video tape system has a wave length of nearly 4 inches, while the same tone recorded on a conventional audio tape recorder has a wave length of only 1/10 inch or less.

A consideration of the problem of recording and reproducing the lower audio frequencies, together with the requirement of a complete absence of cross talk between the audio track and the adjacent video tracks recorded on the tape, led to the use of a modulated-carrier method of recording the audio signals in the present system. Thus, the audio frequencies are not recorded directly on the tape. Instead, a high-frequency carrier signal is recorded, and this carrier is amplitude modulated by the audio-frequency signals. Upon playback from the tape, the modulated carrier is amplified and demodulated to give the reproduced audio signals.

A block diagram of the audio recording and playback system is shown in Figure 4. The frequency of the carrier is 150 kilocycles. The recording and reproducing amplifiers both employ tuned circuits having a pass band centered at the carrier frequency. The audio recording and reproducing heads are essentially the same as those used in the video channels. A switching arrangement not shown in the block diagram can be used to connect the audio amplifier input directly to the audio input of the modulator. This permits listening to the audio program without first passing the signal through the tape system.

Video System for Color

The block diagram of Figure 5 shows the basic components required
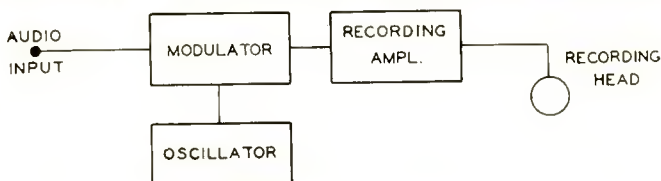
AUDIO RECORDING SYSTEM
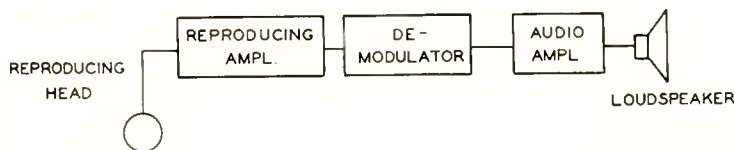
AUDIO REPRODUCING SYSTEM

Fig. 4—A schematic diagram of the electronic elements used in recording and reproducing the audio signals on magnetic tape.

for recording a composite color video signal such as obtained from the video output from a television receiver or microwave radio relay.

As shown, the composite color video is coupled to a color demodulator which produces, on separate outputs, the three color video signals (red, green, and blue), and the separate synchronizing components. The four signals thus obtained are coupled to their respective recording heads through four recording amplifier units.

The sound or audio signal which may be obtained from the audio output of a television receiver is coupled to the audio recording head

through a fifth recording amplifier unit as described in the preceding section.

The recording amplifier units provide both phase and frequency compensation in order to obtain the desired flux pattern on the tape.

The signals, as shown in Figure 5, are recorded on five separate tracks on the magnetic tape. There is one track for each of the primary color video components (red, green, and blue), one for the associated synchronizing information and one for the audio or sound signal.
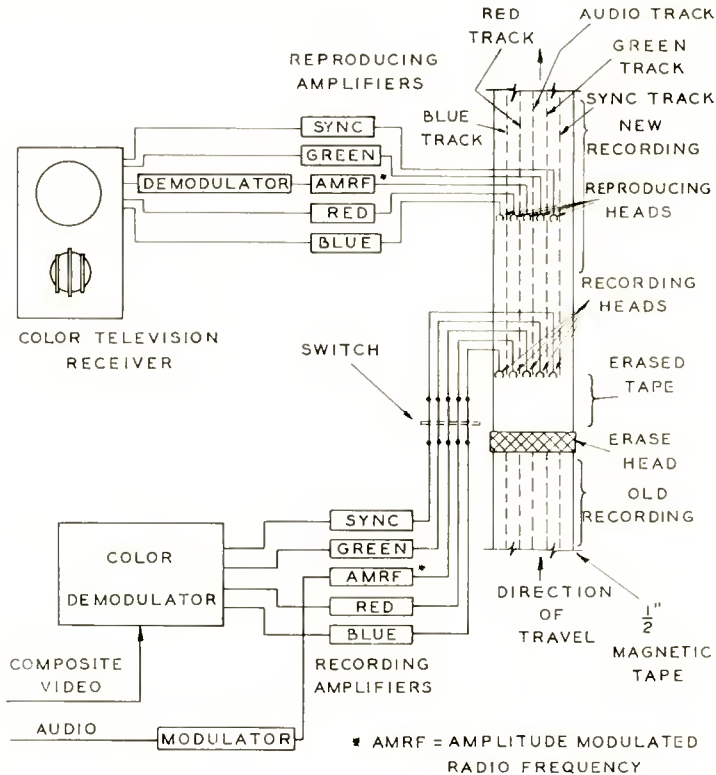
Fig. 5—A schematic diagram of the electronic elements used in recording and reproducing the color video signals and audio signals on magnetic tape.

Referring again to Figure 5, as the tape travels in an upward direction, the erase head first removes all previous information from the tape and conditions the tape for recording. The tape then travels past the recording heads where new information is impressed. The information is stored on the tape in the form of a flux pattern which corresponds to the signal.

The energized tape then travels past the five reproducing heads

which are used for reproducing or monitoring purposes. The reproducing heads generate electrical signals which correspond to the flux patterns stored on the tape.

Since the reproducing heads do not change the flux pattern on the tape, any desired number of reproductions may be had by merely running the tape through the machine with the erase and recording heads de-energized.

The erase head is a specially designed permanent magnet which subjects the individual elements of the tape to reversing magnetic fields and leaves the tape in a fixed magnetic condition. This head is physically removed from the tape path when the erasing operation is not desired.

In order to de-energize the recording heads, there is provided an on–off switch which permits the removal of all signals from these units.

Each of the recording amplifiers contains a special biasing unit. This unit applies an appropriate signal to the tape so that the full magnetic amplitude range may be used for the video signal. That is, the "black" level of the video wave is made to occupy a particular value on the magnetic characteristic of the tape. The "white" signal components then vary the magnetic pattern relative to this value.

The output signals from the magnetic tape are essentially in the form of the output signals from a television color camera. To use these signals to modulate a television transmitter, it is necessary to form a composite signal of FCC Standard Signal Specifications just as is done with camera signals at a studio. One difference exists in the use of magnetic tape output, for here the synchronizing signals are reconstituted and related to the information recorded on the tape.

Video System for Monochrome

When black and white television signals are to be recorded on magnetic tape, only two tracks on a ¼-inch tape are required. As shown in Figure 6, one track is used to carry the complete video signal and the other is used for the associated audio signal.

The video signal is coupled to the video recording head by means of a recording amplifier. This amplifier inserts the required phase and frequency compensation to permit the desired flux pattern to be formed on the tape.

The audio signal is coupled to the audio recording head by means of an audio recording amplifier. The audio system consists of a carrier generator, modulator, and amplifier as described earlier.

As in the case of color, any previously recorded information is removed from the tape by a specially designed permanent magnet

erase and conditioning head. The tape then travels past the recording heads and on to the reproducing heads. The recording heads record the video and sound signals on the tape in the form of a flux pattern which corresponds to the signal as described for the color system.

The reproducing heads generate a signal which corresponds to the flux pattern on the tape. The video signal, generated by the video recording head, is coupled to a video reproducing amplifier where amplitude and phase correction is applied. The output from the reproducing amplifier is the complete video signal which may be applied to
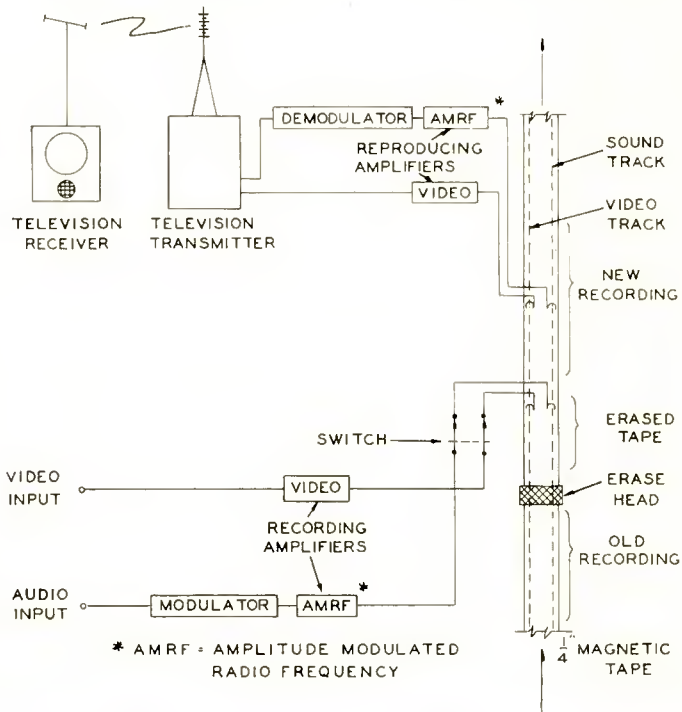
Fig. 6—A schematic diagram of the electronic elements used in recording and reproducing the monochrome video signals and audio signals on magnetic tape.

a television transmitter as shown.

The signal from the audio reproducing head is coupled to a demodulator and amplifier as described in a preceding section.

The complete video and sound signals may then be transmitted in a standard television channel and may be received by conventional black and white television receivers.

Comparison of Photographic Film and
Magnetic Tape Systems

In conventional kinescope recording methods, the television picture is displayed on a kinescope. A special motion picture camera photographs the kinescope image and records the program sound. The film negative is chemically processed and the desired number of prints made. In order to reproduce the television signal, another apparatus is required. This apparatus includes a special television camera that picks up the image produced by a motion picture projector. A diagram of the kinescope recording method is shown in Figure 7.

Figure 8 shows a diagram of the magnetic tape recording method. The television picture and sound signals are fed directly to the record-
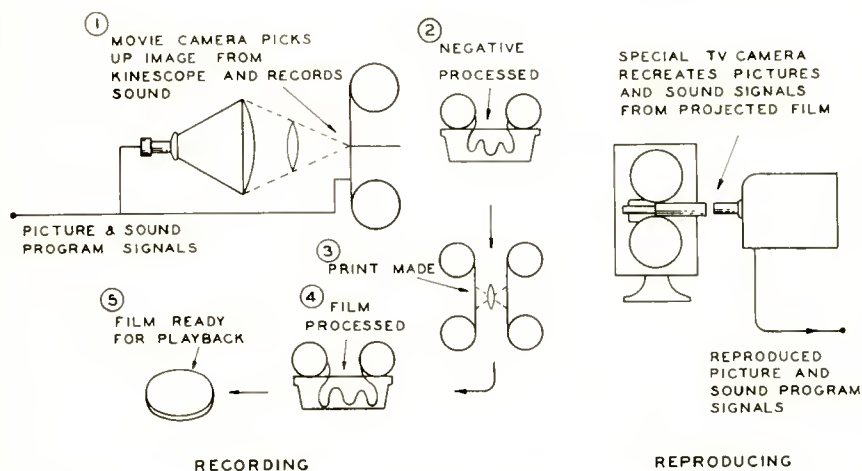
Fig. 7—A schematic diagram of the system for recording and reproducing a television program by means of photographic film.

ing system where the electrical signals are stored on tape in magnetic form. The magnetic tape requires no processing. The program may be reproduced from the tape by using the same unit which recorded it. As in motion picture practice, when a lengthy program is to be recorded and reproduced, two tape transport units with suitable switching may be used.

Description of the System Used for Demonstration

The schematic diagram of Figure 9, shows all of the essential elements used in the demonstrations of the recording and reproduction of color television signals by means of magnetic tape. All of the pro-

gram material originated in a television studio in New York. The picture was picked up by means of a color television camera. The output of the camera was fed to standard studio-type video equipment to produce a composite video color signal. The output of the microphone was fed to standard studio-type audio equipment. The audio signal was carried by a telephone line from New York to Princeton. The composite video signal was carried by microwave radio relay from New York to Princeton. The audio signal was fed to the modulator of the recording equipment. The composite color video signal was demodulated into the red, blue, and green video signals and the synchronizing signal by means of a color demodulator. These signals were sent to the input of the recording system. The outputs of the synchronizing, red, blue, and green video recording amplifiers and the sound modulator were
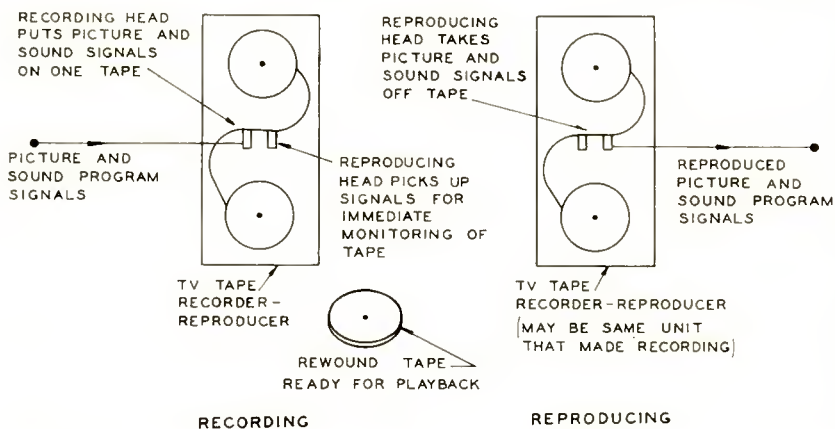
Fig. 8—A schematic diagram of the system for recording and reproducing a television program by means of magnetic tape.

fed to the recording heads. In reproducing, the outputs of the reproducing heads were fed to the synchronizing, red, blue, and green video amplifiers and the sound demodulator. The outputs of the amplifiers correspond to the direct red, blue, and green video signals and the audio signal. The direct signals and the reproduced signals were fed to a switch gear. The output of the switch gear was fed to two color television receivers. Each of the color receivers was equipped with a tri-color kinescope for the reproduction of the picture and a loud-speaker for the reproduction of the sound. By means of the switch gear it was possible to switch both receivers to the direct signals or both receivers to the reproduced signals or one to the direct signal and one to the reproduced signal.

THE DEMONSTRATIONS

Four similar demonstrations were given, one in the morning and one in the afternoon of December 1 and 2. All of the program material originated in a television studio in New York. The actress was Margaret Hayes. The direction was by Herbert Swope, Jr.
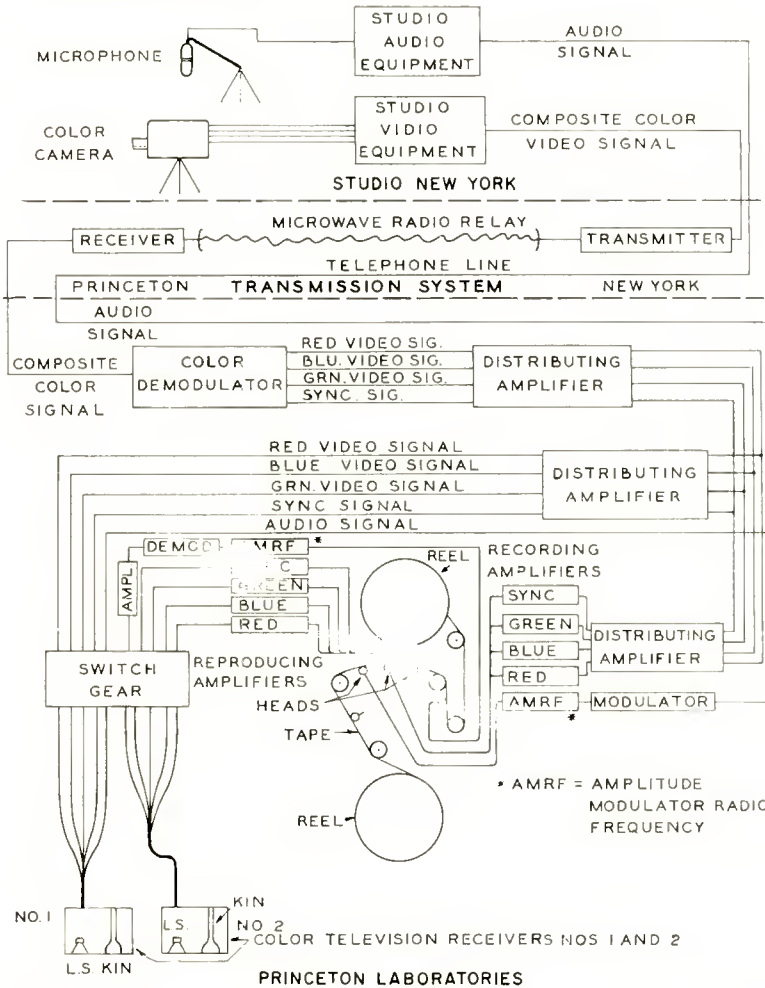
Fig. 9—A schematic diagram of the elements of the system used in demonstrating the recording and the reproducing of television signals by means of magnetic tape.

The following program was presented:

1. The reproduction of a magnetic tape recording of a monochrome

television signal containing an introductory message by Margaret Hayes. The tape was recorded several days before the demonstration.

2. The reproduction of a magnetic tape recording of a color television signal containing a Christmas sketch by Margaret Hayes. The tape was recorded several days before the demonstration.

3. The reproduction of a magnetic tape recording of a monochrome television signal containing a Victorian sketch by Margaret Hayes. The tape was recorded several days before the demonstration.

4. In this part of the demonstration, a live program from the studio, consisting of a Victorian sketch by Margaret Hayes, was fed by microwave radio relay to both receivers. Halfway through the sketch, one receiver was switched to the signal reproduced by the magnetic tape so that a comparison could be made of the direct and reproduced pictures. The delay introduced between the direct and reproduced pictures was the time required for the tape to travel from the recording to the reproducing head. Since this is only 4 milliseconds, the delay is imperceptible. This test demonstrated the fidelity of the reproducing system.

5. The tape recorded in Part 4 was rewound and played back.

Results

In a complex operation such as video recording, it is difficult to derive a figure of merit which will permit an objective evaluation of the system. The opinions of a sufficiently large number of observers, however, give a good indication of the success of the system. The demonstrations described above were shown to several hundred members of the press, industry, and other diverse interests. The magnetically reproduced monochrome and color pictures were considered to be very nearly as good as the pictures received by direct transmission.

In addition to the quality of pictures, the magnetic system has two other notable advantages over the more conventional film recording. These are reduced costs and the fact that instantaneous playback is possible. It has been estimated that the cost of recording a monochrome program on tape will be about 10 per cent of what it would cost to record the same program on film. The corresponding figure for a color program would be about 5 per cent. This difference in cost is due in part to the fact that the tape may be erased and reused a great number of times.

In kinescope recording it is necessary to process the film before

the recorded pictures can be viewed. This usually requires several hours. The instantaneous playback feature of the tape system permits simultaneous recording and monitoring of the recorded picture. The advantages of such a feature are self evident.

A SYMMETRICAL-TRANSISTOR PHASE DETECTOR FOR HORIZONTAL SYNCHRONIZATION*

By

BERNARD HARRIS AND ALBERT MACOVSKI

Industry Service Laboratory, RCA Laboratories
New York, N. Y.

Summary—This paper describes the application of a developmental symmetrical transistor as a balanced phase detector for controlling the horizontal oscillator of a television receiver. A high degree of balance and uniformity of performance under unfavorable conditions of transistor symmetry and temperature has been obtained. The transistor phase detector was used to control a stabilized multivibrator type of horizontal oscillator having a sensitivity of approximately 150 cycles per second per volt. Approximately ten volts of single-ended sawtooth and thirty volts of single-ended sync were required to produce a pull-in of 120 to 180 cycles per second.

Wide variations in the absolute values of transistor parameters and in the degree of symmetry resulted in less than 0.5-volt unbalance in the absence of sync. Laboratory measurements indicated that the performance was relatively unaffectd by temperatures up to 55° C. These results were obtained with transistors having values of r_c, I_{co}, and α_{cb} which varied as much as 3:1 when the collector–emitter roles were interchanged.

Symmetrical transistors are constructed in the same way as conventional junction transistors with the exception that the collector and emitter junctions are made identical. The circuit was tested with two varieties of symmetrical transistors. One had both junctions 15 mils in diameter, the other had both junctions 45 mils in diameter. The two varieties of transistors performed equally well.

COMPARISON OF THE TRANSISTOR AND DIODE PHASE DETECTOR

THE transistor phase detector may be compared with a conventional double-diode phase detector. As shown in Figure 1, both circuits provide an error voltage which is positive or negative, depending upon whether the sync pulse arrives before or after the center of the sawtooth retrace interval. In the double-diode phase detector, this desirable balanced characteristic is obtained by peak rectification of the composite sync-sawtooth voltages applied to each of the diodes, and by subtracting these two peak voltages to produce the required error voltage. In the transistor circuit, a similar characteristic is obtained by making use of the symmetrical property of the transistor, i.e., the ability of the transistor to conduct in either

---

* Decimal Classification: R583.13.

18

direction, as shown by the family of curves in Figure 2. By gating the transistor on with the sync pulse, the sawtooth coupling capacitor is charged toward the instantaneous voltage of the sawtooth during the sync pulse interval; this produces an error voltage across the
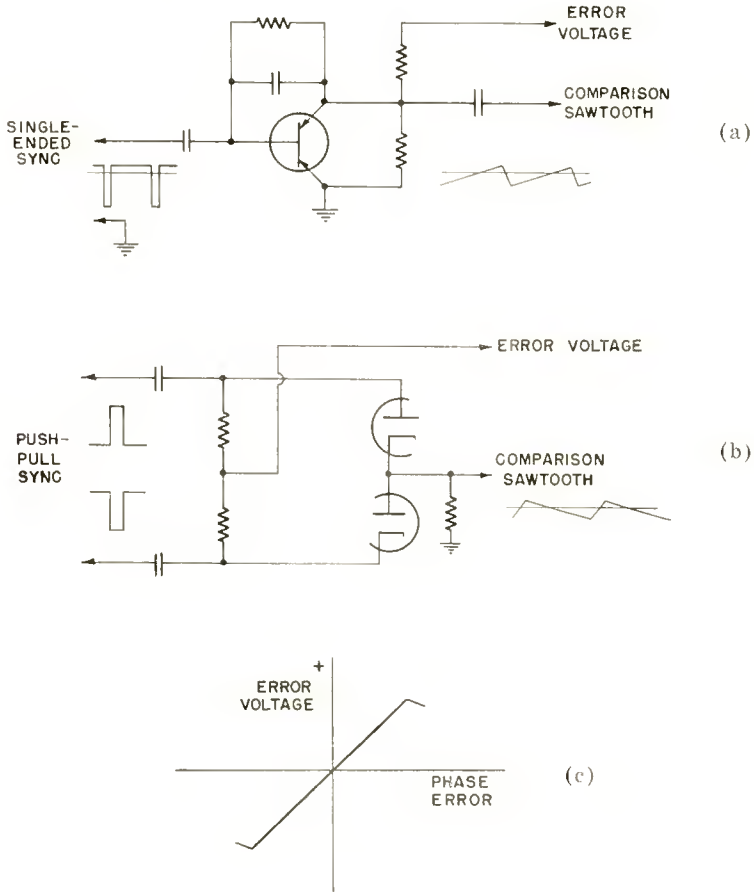
Fig. 1—Comparison of (a) symmetrical transistor phase detector, and (b) conventional double diode phase detector. The corresponding control characteristic is shown in (c).

sawtooth coupling capacitor which depends on the relative phase of the sync and sawtooth.

For both the transistor and the diode phase detector, the error voltage is relatively insensitive to the amplitude of the sync signal as long as the peak-to-peak value of the sync exceeds the peak-to-peak
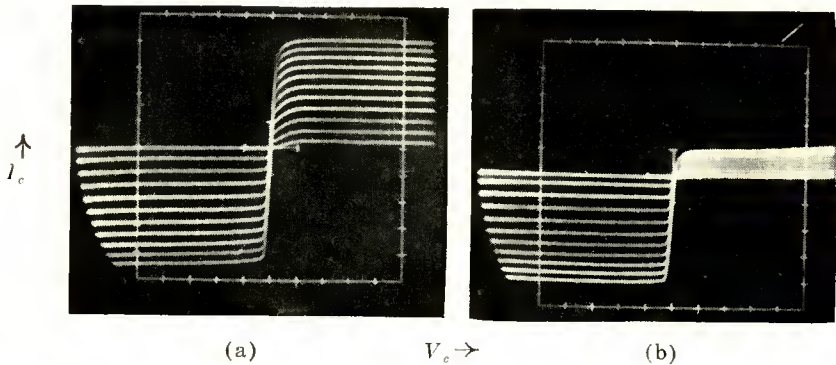
Fig. 2—Collector-current curves for (a) symmetrical and (b) asymmetrical
transistors, for constant base current.

sawtooth. In addition, both detectors are balanced so that random
noise does not contribute to the direct-current output of the detectors.
In the absence of sync, as when switching between channels, the control
voltage of both detectors remains relatively unchanged so that the
oscillator continues to run synchronously.

TRANSISTOR PHASE DETECTOR

A basic transistor phase detector circuit is shown in Figure 3.
Because of transistor symmetry, two arrows are used to designate the
fact that either element can serve as the emitter or the collector,
depending upon the applied potentials. Either element is therefore
referred to as a "collector–emitter." The operation of the circuit
depends on the transistor conducting only when the sync pulses are
present. Thus, if the instantaneous sawtooth voltage on the collector–
emitter is positive at the instant the sync pulse "gates" the base, the
transistor conducts and produces a negative error voltage across C_2;
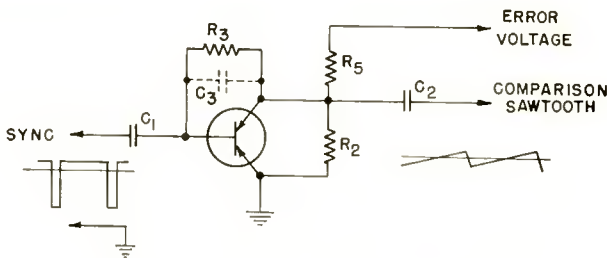
Fig. 3—Basic transistor phase detector circuit.

if the phase is such that the collector-emitter is negative, C_2 is charged to produce a positive error voltage. In this way, the transistor acts as a bidirectional switch charging C_2 to essentially the instantaneous sawtooth potential at the time of sync arrival.

Since it is essential for the transistor to be cut off between sync pulses, capacitive coupling of the sync is used to permit the equivalent diode formed by the base and the collector–emitter to clamp the sync peaks to ground. For the transistor to be cut off between sync pulses, the base voltage during this interval must remain more positive than the peak positive collector–emitter voltage; i.e., the peak-to-peak sync voltage at the base must exceed the peak-to-peak sawtooth.

Normal operation also requires that the collector current during the sync interval be sufficiently large to charge the sawtooth coupling capacitor to the instantaneous voltage of the sawtooth during the sync interval. The amount of collector current which flows during the sync interval is dependent primarily on the amount of base current, and thus primarily on the back impedance of the base. As some transistors have too high a back base impedance, shunting a resistor R_3 from the base to the collector is necessary to provide sufficient base and collector current.

Balance Considerations

When a constant-current generator is used to supply the sync, removing the sync is equivalent to floating the base. If the transistor capacitances to ground are neglected, any net charge developed across the sawtooth coupling capacitor is then due to transistor asymmetry. The resultant polarity of this unbalance voltage reverses when the transistor collector–emitter roles are reversed.

The voltage at the base in the absence of sync, when the base impedance to ground is high, is shown in Figure 4. This waveform may be understood by noting that the base-to-emitter voltage must be approximately zero over the sawtooth cycle. Thus, during the negative part of the sawtooth, when the grounded electrode is the emitter, the base voltage is approximately zero; during the positive part of the sawtooth, when the ungrounded electrode is the emitter, the base-to-ground voltage is approximately the same as the positive part of the sawtooth.

In the absence of sync the transistor will be turned on by the base current resulting from the capacitance between base and ground. Transistor nonlinearity results in the corresponding collector current developing an error voltage. As the base driving impedance is in-

creased by reducing the driving capacitor, the resulting unbalance decreases. However, a small base driving capacitor results in compression of the sync signal at the base, so that a larger sync amplitude is required to cut off the transistor between sync pulses.

The addition of capacitor C_3, shown dotted in Figure 3, permits the use of a large sync coupling capacitor while maintaining balance. This is accomplished by providing equal base currents over each half of the sawtooth cycle. Since the base-to-emitter voltage is approximately zero, C_3 causes a base current, during the time that the sawtooth is negative, that is similar to the base current through C_1 during
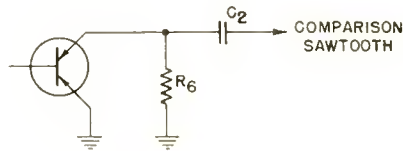
Transistor circuit

Collector–emitter voltage

Base-to-ground voltage

Fig. 4—Waveforms in the absence of sync when the base circuit impedance is high.

the time that the sawtooth is positive. Therefore when C_1 is approximately equal to C_3, it is possible to supply the sync through a larger capacitor and still maintain balance. As the sync at the base is now approximately one half of the applied sync, the required minimum peak-to-peak sync voltage is twice the peak-to-peak sawtooth. The values of C_1 and C_3 are limited by the capacitance which their series combination shunts across the sync source impedance. Too large a value integrates the leading edge of the sync pulse and results in excessive picture shift with respect to the raster.

Temperature Effects

One of the effects of increasing temperature is the reduction of the output impedance of the transistor under cutoff conditions. To prevent distortion of the sawtooth, and consequent phase shift of the picture with respect to the raster, a low sawtooth driving impedance
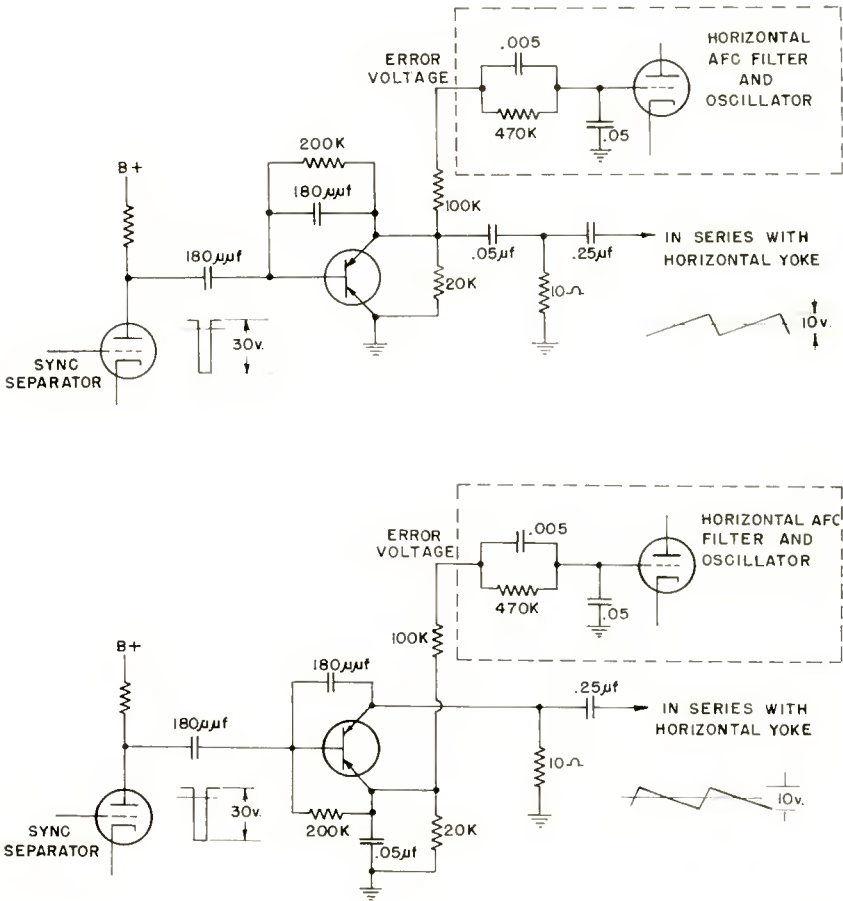
Fig. 5—Phase-detector circuits which operate with either polarity of comparison sawtooth.

and a relatively large sawtooth coupling capacitor C_2 are necessary. Resistor R_2 is connected between the collector-emitter and ground in order to provide the proper time constant for the automatic-frequency-control loop.

CPS

VOLTS
+1.0

BALANCE

180

120

60

PULL-IN

(a) NORMAL CONNECTION

VOLTS
+1.0

BALANCE

CPS

180

120

60

PULL-IN

(b) TRANSISTOR REVERSED
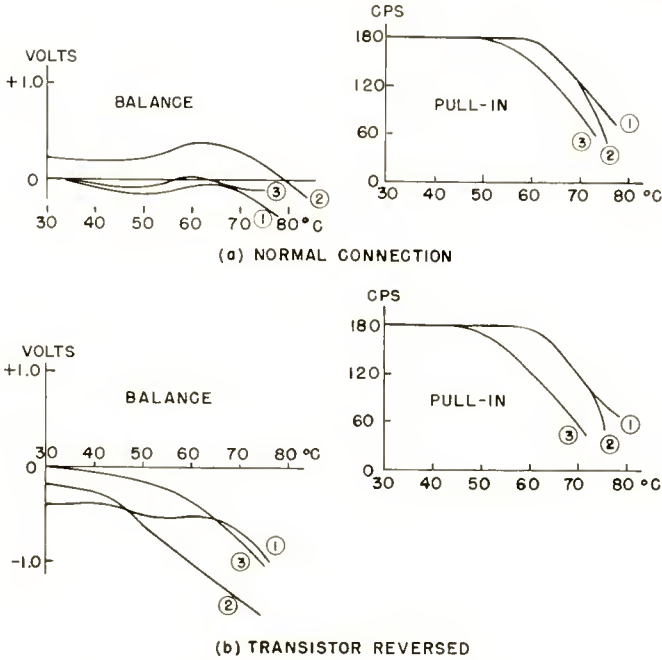
Another effect of increasing temperature is the reduction of the back base impedance. This produces excessive sync crushing at the base, as a result of which the sync amplitude becomes insufficient to cut off the transistor between sync pulses. To avoid this, either the amount of sync can be increased or the sync driving impedance can be lowered.

Transistor Parameters

Unit	α_{oe}	α_{cb}	r_b ohms	r_o Meg-ohms	$I_{co} @ -10v$ ma	Comments
1	.950	19	280	.440	.02	Typical
	.947	17	230	.218	.03	
2	.986	68	530	.660	.02	Abnormal α_{cb}
	.966	28	550	.685	.02	asymmetry
3	.960	23	470	1.17	.02	Abnormal r_o
	.955	21	340	.40	.04	asymmetry

Fig. 6—Effect of variation of transistor parameters on balance and pull-in. The two sets of values given for each transistor correspond to the reversal of the emitter and collector roles.

Circuit Details

Figure 5 shows the transistor phase detector applied to representative receiver circuits. While the basic operation of each circuit shown is the same, the appropriate circuit must be used in conjunction with the proper sawtooth polarity in order to obtain the correct sense of oscillator control. Both circuits require negative sync which is available with conventional circuitry.

Ten volts of sawtooth were supplied to the transistor from a low-impedance source by placing 10 ohms between the horizontal yoke blocking capacitor and ground. This method provides a linear low-impedance sawtooth source, the phase of which accurately represents the beam deflection. Thirty volts of negative sync were supplied directly from the sync separator output.
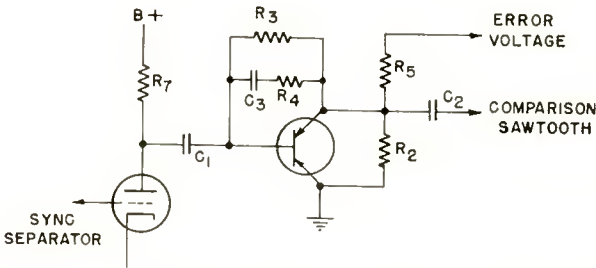
Fig. 7—Balance is obtained by adding a resistor R_4 approximately equal to the sync source impedance.

Figure 6 shows the circuit performance with a typical developmental symmetrical transistor, and with two asymmetrical transistors. For most of the symmetrical units tested, the unbalance was under half a volt. All of the units, however, provided a pull-in of 120 to 180 cycles per second that was relatively unaffected by temperature up to 55°C. Above this temperature the performance was limited by compression of the sync signal at the base. The possible effects of operation at elevated temperatures for extended periods were not investigated.

The amount of sync compression in the circuit of Figure 6 can be decreased by further reducing the sync driving impedance, as shown in Figure 7. This is accomplished by increasing the capacitance of C_1. Balance is restored by similarly increasing C_3 and by adding a

resistor R_4 in series with C_3 so that the balance is maintained as a result of the equality of the sync driving resistance and the resistance R_4. Since the driving resistance is the parallel combination of the sync output tube r_p and the sync output load resistance R_7, it is necessary to make R_7 small in comparison with r_p, in order that the balance not be affected by variations in r_p. This places a greater burden on the sync separator than is present in the circuit of Figure 5.

INVESTIGATION OF ULTRA-HIGH-FREQUENCY
TELEVISION AMPLIFIER TUBES*

By

Wen Yuan Pan

RCA Victor Home Instrument Division,
Camden, N. J.

Summary—This paper considers the use of a radio-frequency amplifier stage in an ultra-high-frequency television receiver. The degree of improvement in receiver performance which can be obtained from such an amplifier using currently available ultra-high-frequency amplifier tubes is discussed.

The planar type tubes tested offer good noise figure and gain at both very-high and ultra-high frequencies, and exhibit a high degree of amplifier stability. In the developmental cylindrical-type tube (pencil triode) which was used for the comparative tests, it was necessary to sacrifice some of the performance in order to achieve moderate cost. It gave stable performance, but its gain and noise factor were not as good as those of the planar-type tubes. The miniature tubes tested are limited by feedback within the amplifier stage for high gain operation.

The stability of ultra-high-frequency amplifier operation can be evaluated, with a fair degree of accuracy, by observing the variation of input impedance while detuning the plate circuit. Such variation also affects the input match and input circuit detuning.

Based on the present status of amplifier tubes, no really substantial advantage is assured by using ultra-high-frequency amplifiers in television receivers, particularly when considering the element of cost. None of the existing tubes is completely adequate when judged in terms of cost and performance.

Introduction

FIELD observers are in substantial agreement that the present television coverage on ultra-high-frequency (UHF) channels is inferior as compared to that on very-high-frequency (VHF) channels. One of the major limiting factors in television coverage is the signal-to-noise ratio. On that basis the *approximate* difference between the present VHF and UHF television pictures can be calculated. The figures can only be approximate because of two uncertain factors affecting television coverage.

1. Cosmic and man-made noises—These noises generally decrease rapidly as frequency increases. However, cosmic noise depends upon the installation and the site of the receiving antenna, and man-made noise is highly irregular in ampli-

---

* Decimal Classification: R339.2.

tude and duration. The effect of such noises on receiver performance cannot be evaluated exactly.

2. The power absorption coeffcients of different objects standing in the way of the wave travel are complicated functions of frequency. VHF waves would lose relatively less power to obstacles such as trees and buildings. In free space, and within the line of sight, this factor does not make a great difference.

Under conditions relatively free of cosmic and man-made noises and free of obstacles in the way of wave travel, the relative signal-to-
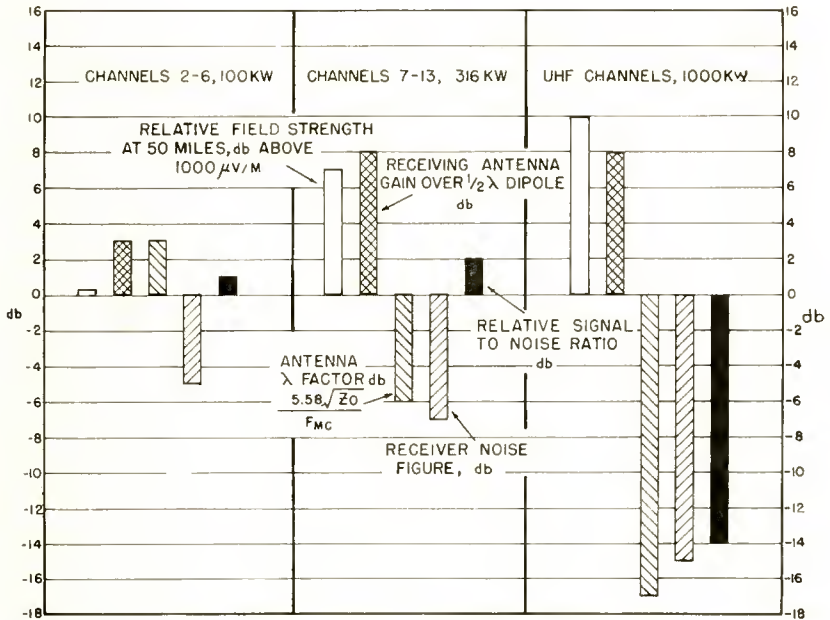
Fig. 1—Relative signal-to-noise ratios of VHF and UHF television receivers at 50 miles from stations.

noise ratios of present-day VHF and UHF receivers with typical antennas at a distance of 50 miles from the respective stations are analyzed graphically in Figure 1.

Relative Field Strength—The field strength in decibels above 1 millivolt per meter at a given distance at UHF is comparable to that at VHF for the same effective radiated power (e.r.p.) and the same transmitting-antenna height. According to regulations of the Federal Communications Commission, the maximum permissible e.r.p. is 100

kilowatts on channels 2-6 (54-88 megacycles), 316 kilowatts on channels 7-13 (174-216 megacycles), and 1000 kilowatts on channels 14-83 (470-890 megacycles). Therefore, the maximum permissible free space field strength for UHF is greater than that for VHF.

Receiving-Antenna Gain—Among the popular television antennas now in use commercially, the gain of the UHF antennas over a half-wave dipole is generally greater than that of the VHF antennas.

Receiving-Antenna λ Factor—The receiving-antenna λ factor converts the signal field strength to signal voltage across the receiver input impedance. With a given receiver noise factor, the signal-to-noise ratio of a television picture depends chiefly upon the signal which is developed across the receiver input impedance. The λ factor for a half-wave dipole is inversely proportional to the signal frequency; therefore, it is highly in favor of VHF.

Receiver Noise Factor—The average noise factor of present commercial UHF receivers is about 10 decibels higher than that of VHF receivers.

Taking these four factors into consideration, it is found that the present UHF television receiver performance, insofar as signal-to-noise ratio is concerned, is approximately 15 decibels inferior to VHF receiver performance.

When considering cosmic and man-made noises and the wave absorption coefficients of the obstacles, the 15-decibel figure has to be revised. The signal-to-noise ratios indicated by the solid black blocks in Figure 1 are relative. At a distance of 50 miles from a 1000-kilowatt station with a transmitting-antenna height of 1000 feet above average terrain, the absolute or actual signal-to-noise ratio of a UHF receiver would be high enough to give a good picture. Pictures at approximately 50 miles from stations on channels 46 and 33 are shown in Figures 5 and 6.

THE UHF PROBLEM

The problem which is of greatest concern is how to liquidate the 15-decibel deficit. Careful examination of important factors affecting television coverages reveals that the antenna λ factor, the cosmic and man-made noises, and the wave absorption coefficient characteristics are inherent, but the maximum e.r.p., the receiving antenna gain, and the receiver noise factor, more or less follow engineering progress.

The e.r.p. is limited by the power capabilities of presently used

transmitting tubes and is also bound by the FCC regulations, while the receiving antenna gain at UHF is limited by the antenna directivity, frequency selectivity, and also by the physical size of the antenna. These two sets of factors are beyond the scope of this paper.

At present, practically all commercial UHF tuners employ a crystal diode mixer without radio-frequency (r-f) amplification. The tuner noise factor ranges from 12 to 20 decibels. This wide range of noise factors is largely due to the variations between crystal diodes and variations in mixer loss and mixer impedances with varying oscillator excitation and other operating conditions. More uniform and somewhat lower receiver noise factor may be secured by using one or more stages of r-f amplification preceding the mixer.
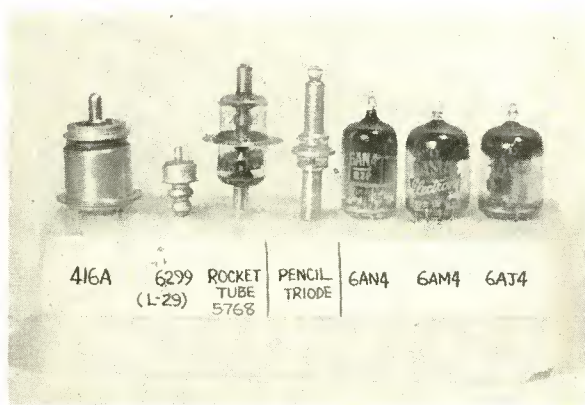
Fig. 2—Samples of UHF amplifier tubes.

UHF Amplifier Tubes

For the purpose of this investigation, a number of tube types both commercially available and in developmental status were tested. These are arbitrarily classified into three general groups. Sample tubes of each group are shown in Figure 2.

1. Miniature-type tubes including 6AJ4, 6AM4 and 6AN4, and a developmental tube.

2. Cylindrical-type developmental tube (pencil triode).

3. Planar-type tubes including 416A, 5768, 6BA4, and the 6299, frequently referred to as the L29.

These tubes were tested and compared in commercial-type circuits
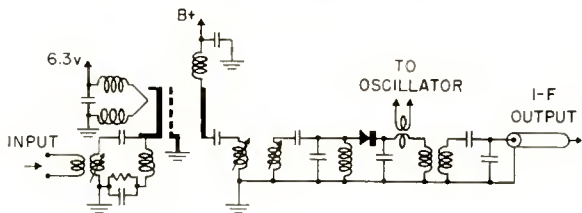
Fig. 3—A typical UHF television tuner using commercial circuits.

at frequencies below 890 megacycles. A typical circuit used for this investigation is shown in Figure 3. The unloaded Q of the circuit is considerably lower than the Q of a resonant cavity; therefore, some of the advantages of the planar and cylindrical types of tubes are lost. The results obtained by means of the circuit of Figure 3 may not be representative of the optimum performance of each tube type although each is operated under the same conditions.

RELATIVE NOISE FACTORS

Of the tubes under consideration, the noise factor of the planar type is the lowest, that of the cylindrical type of the pencil triode variety next, and that of the miniature type the highest. Figure 4 shows the tuner noise factors when using a one-stage grounded-grid amplifier and 14-decibel mixer noise factor.

Fig. 4—Noise factor of receiver with one-stage grounded-grid r-f amplifier.

The shaded areas illustrate the noise factor ranges of some television receivers now on the market. A television receiver using a developmental pencil triode amplifier stage offers a lower noise factor on all channels than present commercial receivers. On UHF channels the noise factor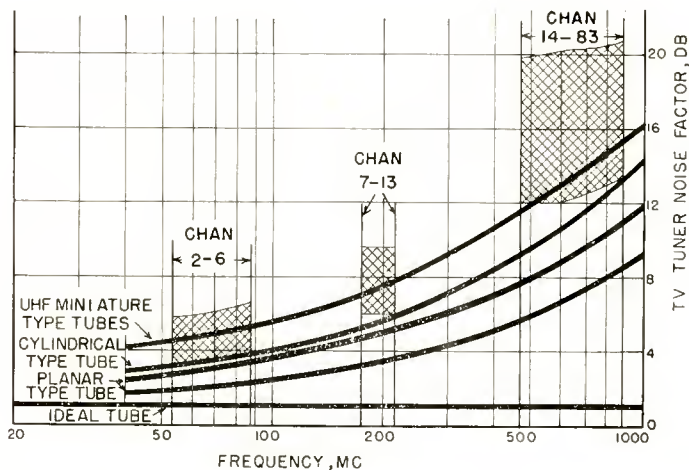s of the 5768 rocket tube and the L29 tube are about 2 decibels lower than the pencil triode tested, and the 416A is about 4 decibels lower. The commercial miniature-type tubes are comparatively inferior, about 2-3 decibels higher in noise factor than the pencil triode tested, although some developmental miniature tubes have shown improved performance. The present developmental pencil triode is a compromise between performance and cost; it does not represent the best that can be achieved by a cylindrical-type tube.

Five UHF tuners were constructed; each consisting of an r-f amplifier stage, a 1N82 crystal diode mixer, a 6AF4 oscillator, and a triode-connected 6CB6 grounded-grid i-f amplifier. In the r-f amplifier stages, a 416A, 5768 rocket tube, L29, pencil triode, and a good miniature tube are used. The mixer noise factor of all five tuners is 14 decibels.

FIELD OBSERVATIONS

The first field comparison was made at Browns Mills, N. J. on channel 46, station WFPG in Atlantic City, N. J., radiating about 20 kilowatts at a height of 430 feet above average terrain. Browns Mills is 41 air miles northwest of the station, and the receiving antenna is 90 feet below the line of sight. Figure 5 shows the picture qualities of these tuners, together with a good, an average, and a poor commercial receiver. The difference in noise factor between the 416A planar-tube tuner and the miniature-tube tuner is about 6 decibels on channel 46, which makes an apparent difference in signal-to-noise ratio at Browns Mills. The picture obtained from the miniature-tube tuner is comparable to, or may be slightly better than that from the good commercial receiver; it is definitely superior to the pictures from the average and poor commercial receivers. The picture produced by the tuners using the L29 and the 5768 rocket tube respectively are slightly better than that of the pencil triode tuner but somewhat poorer than that of the 416A tuner.

The second field observation was made at Haddon Heights, N. J., on channel 33, station WEEU, at Reading, Pennsylvania, radiating about 130 kilowatts at a height of 1050 feet. The receiving antenna is 53 air miles from the station and 290 feet below the line of sight. The comparative results on channel 33, as shown in Figure 6, are in substantial agreement with those observed on channel 46, shown by

UHF TUNERS USING ONE R-F AMPLIFIER STAGE
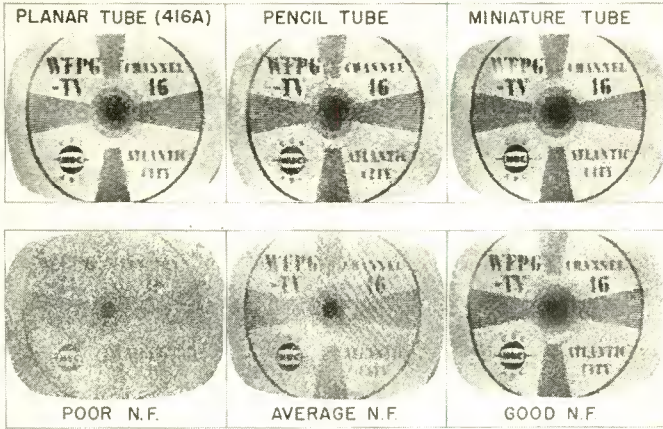
PRESENT COMMERCIAL TUNERS – NO R-F AMPLIFIER

Fig. 5—Picture qualities of station WFPG, channel 46, Atlantic City, N. J.; received at Browns Mills, N. J., 41 miles from transmitter.

Figure 5. Theoretically, as the frequency goes down, the noise factor of a UHF tuner with an r-f amplifier stage decreases while that of a commercial tuner using a crystal-diode mixer without r-f amplification would remain practically unchanged if it were properly designed. The

UHF TUNERS USING ONE R-F AMPLIFIER STAGE
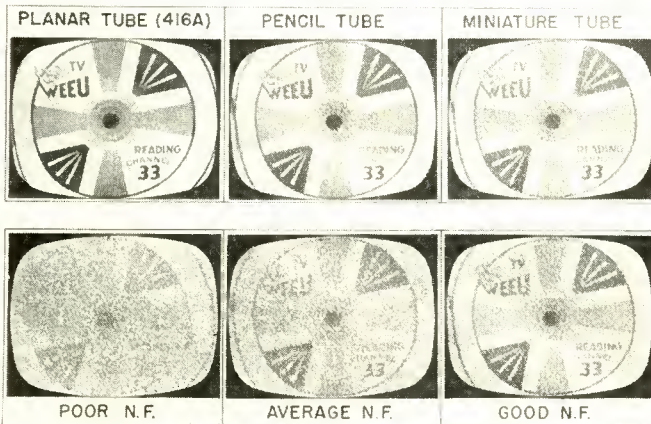
PRESENT COMMERCIAL TUNERS – NO R-F AMPLIFIER

Fig. 6—Picture qualities of station WEEU, channel 33, Reading, Pa.; received at Haddon Heights, N. J., 53 miles from transmitter.

decrease in noise factor from channel 46 to 33, however, is no more than 1.0 decibel, the difference was not very noticeable. To verify this fact the tuners were aligned on channel 83 (884-890 megacycles). In Figure 7 the pictures from the good commercial receiver and the miniature-tube tuner are almost of the same quality. The good commercial receiver picture may be even slightly superior if both pictures are examined closely. Furthermore, the difference between the best picture produced by a planar-tube tuner and the picture produced by an average commercial receiver is narrowed down to some extent. This set of pictures was taken at the laboratory by modulating a UHF signal-generator with a video signal. The time of exposure was about
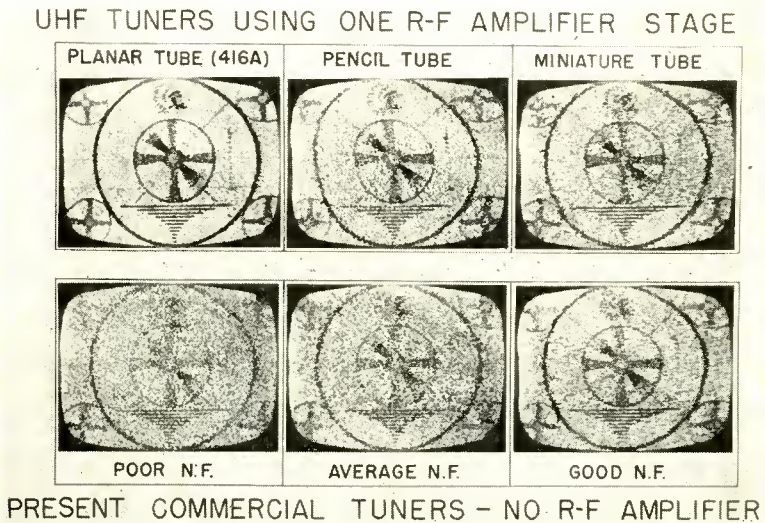
Fig. 7—Picture qualities on channel 83.

1/30 second and therefore the noise was not integrated much during the photographic process.

The improvement in the best picture over the picture of the average commercial receiver closes the gap of the 15-decibel deficit of UHF television as compared to VHF. As might be expected, however, tube performance is closely related to cost. The high-cost planar tubes provide low noise, high gain, and very good stability. The medium-cost cylindrical-type pencil tube gives somewhat poorer noise and gain performance but is equally stable. The relatively inexpensive miniature tubes now commercially available are marginal in performance on all three counts.

Amplifier Gain and Stability

The noise factor of a television tuner using an r-f amplifier stage is also affected by the noise factor of the mixer which follows the r-f amplifier, and by the d-c input power to the amplifier tube. The effect of the mixer noise on the over-all tuner noise factor decreases as the amplifier gain increases, and the amplifier gain usually increases with the d-c input power to the amplifier tube. Furthermore, a higher d-c input power also lowers the amplifier noise factor slightly, due to greater cathode current density and probably other effects. The effect of d-c input power on the amplifier noise factor of a miniature tube,
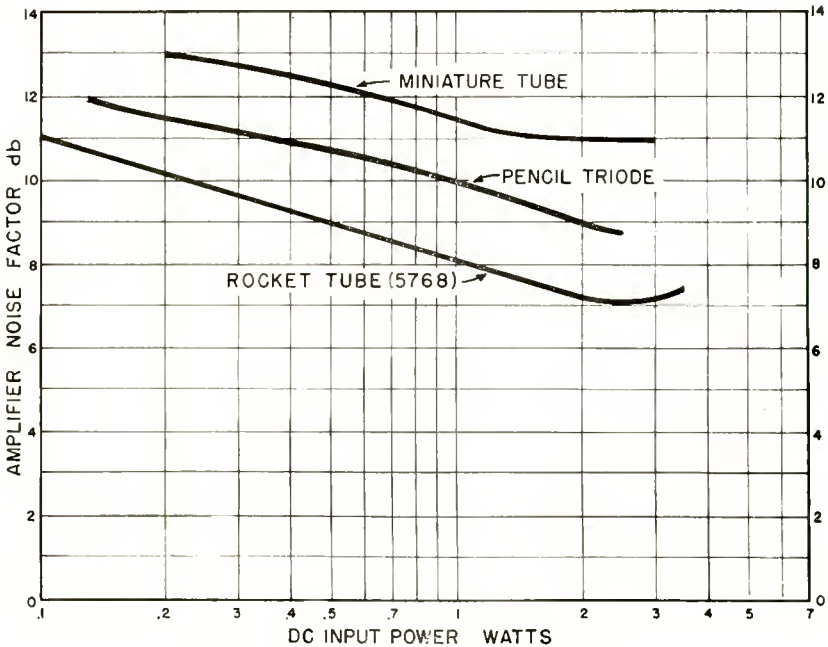
Fig. 8—Relative UHF amplifier noise factor.

a pencil triode, and a rocket tube is indicated in Figure 8. Unfortunately, there is a practical limit to the maximum amount of d-c input power which can be applied to an amplifier tube. The planar and cylindrical-type tubes are usually limited by the plate dissipation capabilities, while the miniature tubes are usually limited by the stability of amplifier operation. One of the goals in design, therefore, is to secure the maximum amplifier gain without causing excessive dissipation and excessive feedback.

The function of d-c input power on amplifier gain at channel 46 is shown in Figure 9. The slopes of curves representing some commercial miniature-type tubes are seen to increase beyond certain d-c input power, as shown by the dotted portions of such curves. Regeneration probably takes place somewhere along such dotted portions. Similar results are obtained at 890 megacycles at which the useful amplifier gain is slightly reduced, particularly in the miniature-type tubes.

There is no exact way of measuring the degree of amplifier stability. The gain as a function of the d-c input power curve is only an approxi-
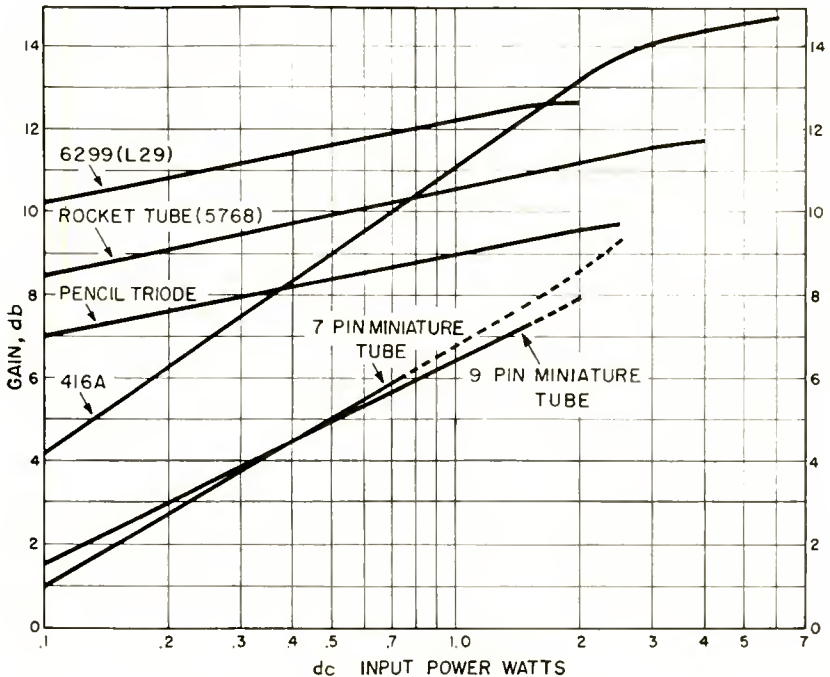
Fig. 9—Relative UHF amplifier gain.

mate measure. An alternative method is to observe the passband characteristics while increasing the amplifier gain. In the case of the miniature tubes, a high-gain amplifier is often oscillatory when the plate circuit is far detuned. When oscillation takes place, the plate current usually changes, either drawing more current or drawing less current than the plate current under stable operating conditions. The amplifier is aligned to 857-869 megacycles, the center frequency of which falls in channel 79, using a miniature-type tube. By detuning

the plate circuit, one miniature-type tube becomes oscillatory over the frequency bands as indicated by the shaded areas of Figure 10, while another miniature-type tube also becomes oscillatory, but over fewer and narrower frequency bands, as indicated by the solid areas. In one case the plate current increases and in the other case decreases when oscillation occurs. It is difficult to conclude from such information how stable either tube is, but one tube is less stable than the other. Oscillation caused by plate-circuit detuning does not usually happen to the planar or the cylindrical tubes. Instability is, of course, caused by some form of feedback, either inside the amplifier tube or through the external amplifier circuits. In a typical single-stage grounded-grid
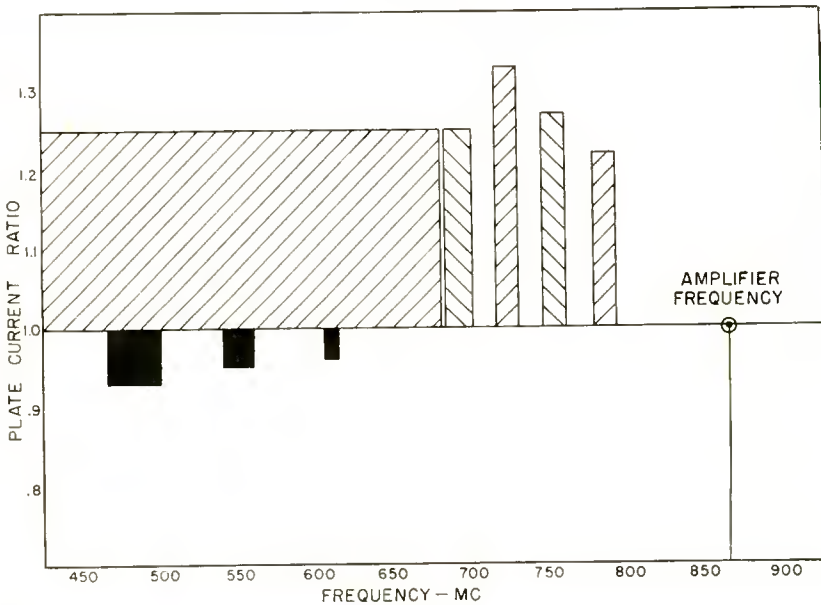
Fig. 10—Oscillatory frequency bands when amplifier plate circuit is far off-tuned.

UHF amplifier the feedback inside the tube usually limits the useful amplifier gain and amplifier performance. Such inside-the-tube feedback, illustrated in Figure 11, can be divided into at least three paths of considerable importance.

    1. The obvious source of feedback is by way of the interelectrode capacitances. The feedback factor is a minimum at a frequency such that C_3 and L_G are in series resonance. This frequency occurs at about 700 megacycles for the 416A tube.
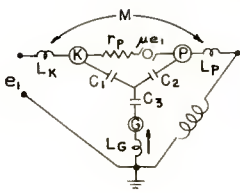
M = MUTUAL INDUCTANCE – COUPLING
BETWEEN PLATE LEAD L_P &
CATHODE LEAD L_K

L_G = GRID LEAD INDUCTANCE

FEED-BACK PATHS:

1. FLOW OF PLATE CURRENT INDUCES A VOLTAGE $\omega M i_p \angle \theta_1$ IN THE CATHODE CIRCUIT DUE TO "M"

2. FLOW OF PLATE CURRENT THROUGH L_G INTRODUCES A VOLTAGE $\omega L_G i_p \angle \theta_2$ IN THE CATHODE CIRCUIT

3. FEED-BACK THROUGH THE CAPACITANCE T- NETWORK, MINIMUM ONLY WHEN C_3 & L_G ARE IN SERIES RESONANCE

Fig. 11—Feedback in a UHF amplifier.

It occurs at a considerably lower frequency for the miniature-type tube.

2. In miniature types the cathode and the plate leads inside the tube are loosely coupled to each other; the flow of current in the plate lead induces a voltage in the cathode circuit.

3. The grid lead inductance is another potential source of feedback. The flow of plate current again introduces a voltage in the cathode circuit through the grid lead.

These two voltages added to the cathode circuit as a result of the flow of plate current have the same frequency dependence and same general phase relationship. Low grid-lead inductance and good shielding between plate and cathode leads are, therefore, important factors in designing UHF amplifier tubes, particularly of the miniature type.

Amplifier Input Impedance

A better method for determining amplifier stability is to measure the input impedance variations when detuning the plate circuit Figure 12 shows the input impedance of a grounded-grid amplifier tube consisting of a lead inductance L_K in the cathode, an input capacitance C_i, and two resistances. R_k is the input resistance at low
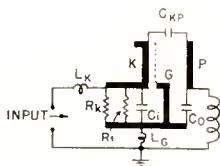
R_k = INPUT RESISTANCE AT LOW FREQUENCIES
$\doteq \dfrac{1}{g_m} + \dfrac{1}{2\pi \Delta f \mu C_o}$ APPROX

R_t = TRANSIT TIME EFFECT
$\doteq \dfrac{15}{f^2} \times 10^{20}$ APPROX

$R_i = \dfrac{R_k R_t}{R_k + R_t}$ = TUBE INPUT RESISTANCE AT UHF

$C_i = C_{KG} + K\, C_{KP}$

Fig. 12—Input impedance of pencil triode.

frequencies. It consists of the low-frequency input resistance of the tube when the plate is short-circuited (this is approximately equal to the reciprocal of tube transconductance g_m) and an added resistance to take into account the effect of the plate-load impedance when the plate is tuned. The added resistance component of R_k is a function of the bandwidth of the amplifier selective circuit, the output capacitance, and the tube amplification factor μ.

In addition to the low-frequency resistance R_k, the transit-time effect at UHF can be simulated by adding a resistance R_t across the cathode and grid. The tube input resistance R_i at UHF is the equiva-
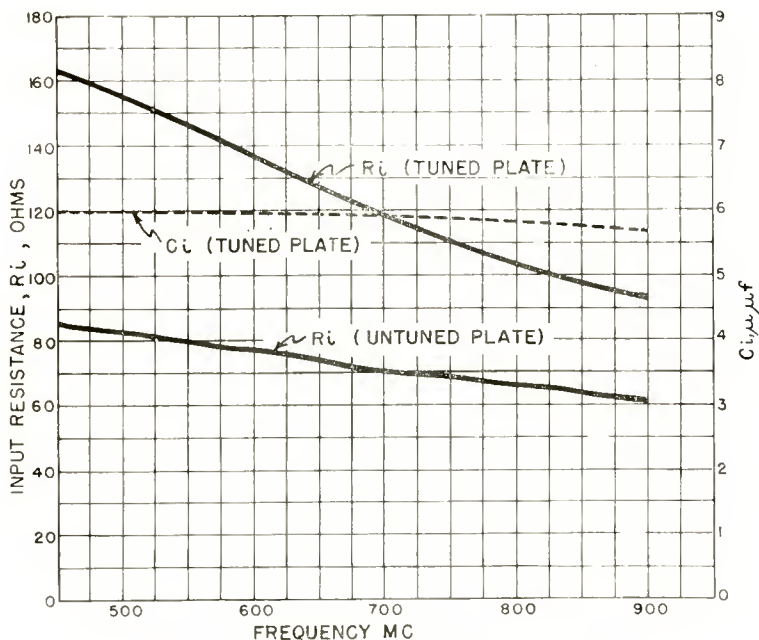
Fig. 13—Input parameters of pencil triode.

lent resistance of R_k and R_t. This equivalent resistance R_i therefore changes with plate tuning. It is higher with a tuned plate unless excessive feedback is taking place in the tube so that a negative resistance is reflected to the input circuit. A stable amplifier and an unstable amplifier will be discussed to illustrate the input impedance variations under these conditions.

Pencil Triode Input Impedance—In the case of a pencil triode, the curves in Figure 13 show how the tube input resistance varies

with frequency with either a tuned or an untuned plate circuit. The tube input resistance with a tuned plate is greater than that with the plate untuned. The difference between these two curves decreases as the frequency increases since the resistance R_t which simulates the transit time effect is roughly inversely proportional to the square of frequency. The dotted curve represents the equivalent tube input capacitance C_i which is substantially constant throughout the UHF television band. Judging from these results, the tube is operating normally. No excessive feedback is taking place in the tube under these operating conditions.

The tube input resistance R_i and capacitance C_i can be presented in a different form. The Smith chart of Figure 14 shows the series
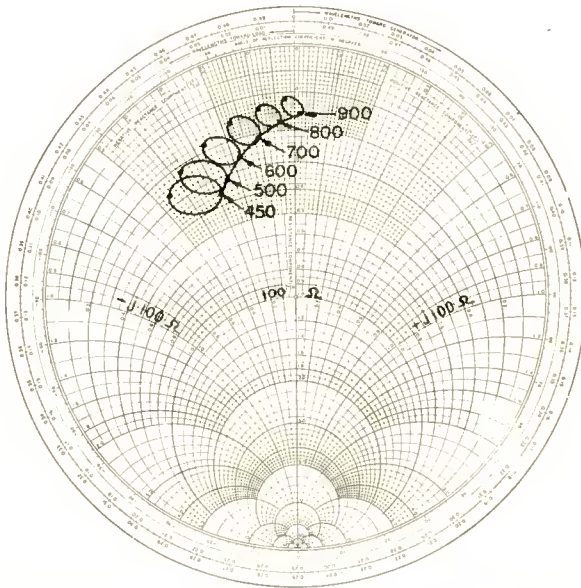
Fig. 14—Input impedance of pencil triode, Smith chart.

input impedance of a pencil triode which is mounted in a special tube socket. The inherent inductance of this socket and the chassis return path shifted the input impedance curve in the clockwise direction by a substantial amount, indicating one of the disadvantages of using conventional circuits with the planar or cylindrical types of tubes. The cross-over point from capacitance to inductive reactance under the untuned output condition occurs at about 850 megacycles. This point should be well over 1000 megacycles if no external inductance is added to the tube.

The continuous curve represents the input impedance when the plate load is negligibly small. By tuning the output from one side of resonance, through resonance, and beyond, the input impedance at any particular frequency varies in the form of a nearly closed loop. The size and the direction of such loops depend primarily upon the Q of the output circuit and the type of tube being used. With a passband of 12 megacycles, the variation of input impedance due to detuning in the plate circuit is relatively small in the case of the pencil triode. The tube is considered to be stable. The input impedance curves of the 416A, L29, and the rocket tube 5768 are similar to that of the pencil triode. The total inductance L_K in the cathode of the pencil triode is
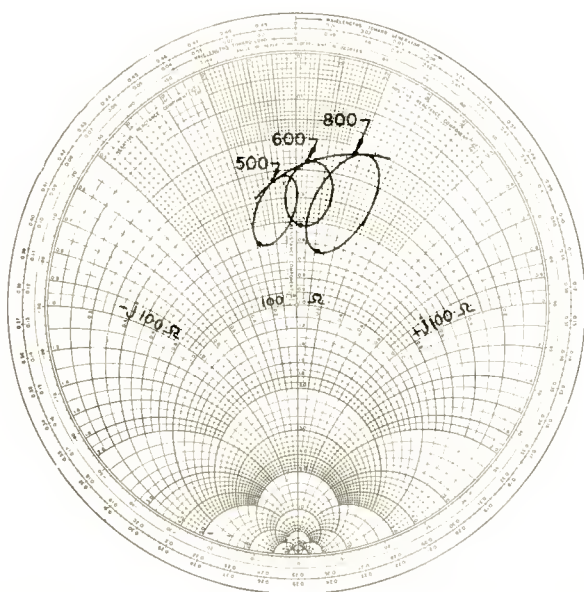
Fig. 15—Input impedance of a commercial miniature tube, Smith chart.

0.005 microhenry. The equivalent series input impedance, including the cathode lead inductance, is measured directly by an admittance meter. The loops are above the curve, indicating no excessive negative resistance being reflected to the input circuit.

Miniature Tube Input Impedance—The input impedance of a typical miniature-type tube behaves quite differently, as shown in Figure 15. The input impedance curve under the untuned plate condition is more inductive and its resistive component is greater than the

corresponding pencil triode curve. Also, a tuned plate makes the input impedance more capacitive, and the resistive component greater. The size of the nearly closed loops is larger, indicating greater variation in tube input impedance between tuned and untuned plate. Such loops are located below the untuned plate curve indicating negative resistance being reflected to the input circuit under these operating conditions.

The corresponding tube input resistance R_i and capacitance C_i shown in Figure 16 reveal a clearer picture of what is taking place in the miniature-type tube. The input resistance with the plate circuit tuned at a certain frequency is almost equal to the input resistance
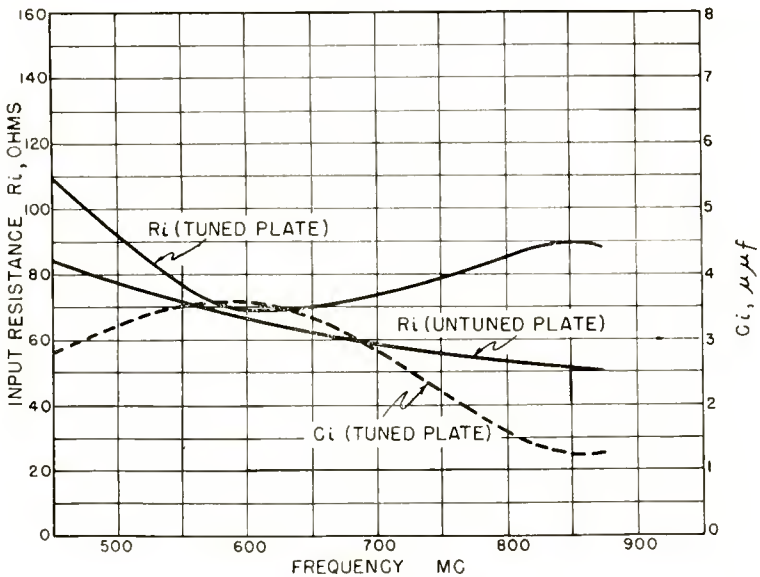
Fig. 16—Input impedance of a commercial miniature tube.

with the plate circuit untuned. At that particular frequency, the amplifier is quite regenerative, though it is still not oscillatory. The considerable variation in input capacitance is another sign of unstable operation. It makes the tracking of the input tuned circuit very difficult. The irregular magnitude of the input resistance R_i introduces mismatch between the receiving antenna and the r-f amplifier resulting in loss of signal power. If the same miniature tube is operated at reduced gain, then the input impedance variations would approach stable conditions. Insofar as stability is concerned, a reduction in amplifier gain makes the amplifier more stable.

Effect of Radio-Frequency Amplifier on other Tuner Characteristics

Because of relatively unstable operation, a UHF amplifier using a miniature-type tube is usually operated at reduced gain, thus degrading its noise factor to some extent. The over-all tuner noise factor under these conditions is not substantially improved over the good commercial television receivers on the market. The planar-type tubes do better, but they may not be good enough to justify their high cost. The present cylindrical-type tubes are less expensive, but they are not quite as good. Television designers may question the advisability of using an r-f stage unless new tubes are developed or unless there are other advantages for the use of a UHF amplifier in a television receiver.

Automatic Gain Control—The operating point of a crystal diode mixer is usually determined by the amount of excitation supplied by the local oscillator. In extremely strong signal areas, the mixer might be overloaded, which would degrade the picture quality in many ways. By applying automatic gain control (a-g-c) to the UHF amplifier stage the overloading effect might be reduced.

When both the heater and plate power supplies are cut off, the UHF amplifier stage has a loss of 10 to 20 decibels, measured from the cathode to the plate circuit. Since the frequency is high, the forward isolation is rather poor due to coupling through the tube. The use of an a-g-c controlled r-f amplifier stage extends the overloading level about 3 to 1 in signal field strength. This improvement is obtained at the expense of some complications to the amplifier operation, because any circuit component inserted in the grid of the amplifier tube may lead to undesired effects on amplifier stability. The question of how serious the overloading problem is in the present UHF commercial receivers has yet to be answered.

According to FCC ruling, the effective radiated power is to be measured in the horizontal plane. In the case of tilted-beam antennas, it has been found that as much as 2000 kilowatts e.r.p. on the main lobe is possible. The free-space line-of-sight fields shown in Figure 17 were calculated for differences in elevation of 100 and 1000 feet for a typical tilted-beam antenna at short distances. Ground reflection may double the field strength shown. Examination of the curves reveals the fact that fields higher than 10 volts per meter will practically never be encountered; fields up to 1.0 volt per meter can be expected as far as 5 miles from the transmitter. High transmitting antennas are desirable to keep down overload and interference on nearby receivers.

With a field of 1.0 volt per meter, the signal voltage developed across the tuner input impedance is about 0.5 volt or less. This would not badly overload the present commercial receivers using a crystal diode mixer. Therefore, the overloading problem does not seem to be serious at UHF unless the receiving antenna gain is high or the FCC should increase the maximum permissible e.r.p.

Oscillator Radiation—The Radio Electronic Television Manufacturers Association recommended that receiver oscillator radiation be limited to 500 microvolts per meter at 100 feet on all UHF channels.
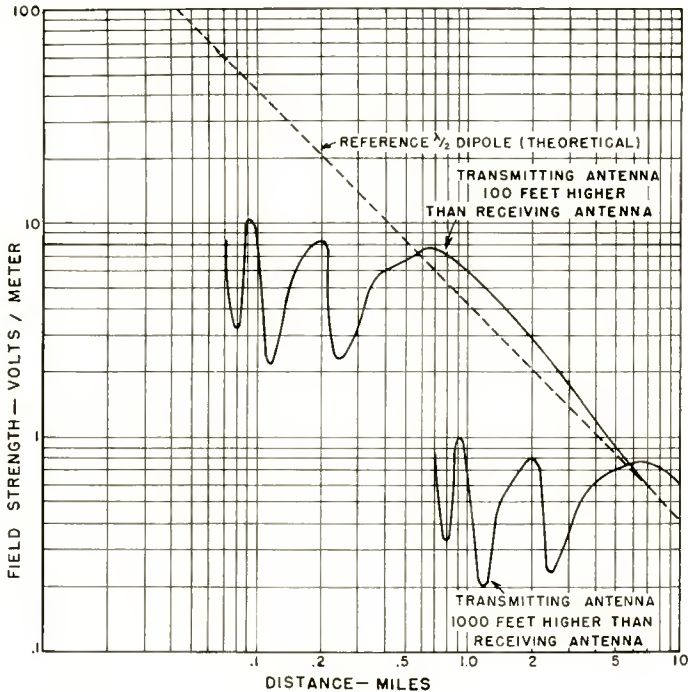
Fig. 17—Field strength from UHF television transmitter with tilted-beam antenna. The e.r.p. in the horizontal plane is 1000 kilowatts.

Most UHF receivers on the market today fail to fulfill this requirement. Oscillator radiation consists of two major components—(a) radiation directly from the receiver or tuner chassis, and (b) radiation through the signal frequency circuits and the receiving antenna. At the present time each component of the radiation generally exceeds the limit. The use of an r-f amplifier stage preceding the mixer helps reduce the oscillator radiation through the signal frequency circuit

and the receiving antenna. With the anticipated improvement in receiver noise factor and future lowering of the UHF oscillator radiation limit, additional isolation between oscillator and antenna may become essential. While the backward attenuation of a grounded-grid amplifier, from the plate to the cathode circuit, varies with the type of tube, with the type of circuitry, and with frequency, an attenuation of 20 decibels is readily obtainable.

ACKNOWLEDGMENT

REFERENCES

Alvin B. Glen, "Study of Noise Reduction by Feedback in Ultra-High-Frequency Amplifiers," Technical Information Series, Report No. 52-E-301, General Electric Company, April, 1952.

H. W. A. Chalberg, "R-F Performance of a UHF Triode," *Proc. I.R.E.*, Vol. 41, p. 46, January, 1953.

G. M. Rose, D. W. Power, and W. A. Harris, "Pencil-Type UHF Triodes," *RCA Review*, Vol. X, p. 321, September, 1949.

T. Murakami, "A Study of Grounded-Grid, Ultra-High-Freqency Amplifiers," *RCA Review*, Vol. XII, p. 682, December, 1951.

CERAMIC–METAL SEALS OF
THE TUNGSTEN–IRON TYPE*

By

D. G. Burnside

Research Department, RCA Laboratories
Princeton, N. J.

Summary—A method of preparing ceramic–metal seals is described. The method is one that is relatively simple and noncritical in processing. The area of the ceramic to be metalized is brush or spray coated with a thin layer of mixed tungsten and iron powders and fired to a suitable temperature in a diluted reducing atmosphere. A homogeneous and dense metal film is produced which is strongly adherent to the ceramic. Tests indicate that the bond may be stronger than the ceramic body itself.

Some other ceramic–metal seal processes are briefly reviewed, and a discussion of ceramics and sealing metals is included.

INTRODUCTION

THE advantages of higher permissible temperatures and better dielectric properties have made ceramic materials attractive for use in vacuum tube construction, particularly in high-power microwave tubes, and have been an incentive to the development of successful methods of sealing metals to ceramics.

Coating of ceramics with glazes and metals for ornamental purposes is an ancient art. There is, however, little similarity between the ornamental coating and that required for vacuum-tube envelopes.

Historically, the development of hermetic seals between ceramic bodies and metals began some fifteen or sixteen years ago. During the ensuing period numerous techniques have been discovered by several individuals and some commercially useful seals have become available. The short descriptions that follow indicate the nature of some of the seals that have been studied.

1. Metallic Oxide Seal

If a metallic oxide, such as that of copper, is applied to a ceramic and suitably fired, a diffusion occurs to form a physical-chemical union. By subjecting this impregnated surface to the action of a reducing atmosphere in a furnace, a pure metal film is left which is thin and adherent.

2. Pressed-Powder Seal

The pressed-powder method of combining a ceramic and a metal

---

* Decimal Classification: R331.

consists in applying, under pressure, a powdered layer of nickel, iron, molybdenum, etc. to a suitable ceramic raw material in powder form and sintering to solidification. A dense compact is possible if the raw material is of a type to permit bonding, and if the expansion properties are compatible. Differences of thermal expansion may be matched somewhat by using adjusted layers of ceramic–metal mixture.

3. The High-Pressure Seal

A bond can be formed between certain metals and ceramics by the application of pressure of the order of 3000 pounds per square inch, at a temperature of around 1000° C, in vacuum or pure nitrogen.

4. The Titanium- or Zirconium-Hydride Process

In this method the ceramic is coated with the hydride of an active metal, and assembled with the metal part to which it is to be attached, along with the brazing material. The assembly is then heated in vacuum, or in a pure inert gas, to the melting temperature of the brazing material. The reaction is such that a strong vacuum-tight bond is formed simultaneously with the brazing. This method has been extended experimentally to include materials other than ceramics.

5. Active-Metal Seal

The presence of hydrogen, as in a metal hydride, is not necessary in the formation of a ceramic–metal bond. An active metal, such as titanium, zirconium, etc., preferably alloyed with silver, will wet and bond ceramics, or bond a ceramic to a metal. A useful composition is 15 per cent zirconium, or titanium, with 85 per cent silver.

6. Ceramic-Glaze Seal

Simple and effective seals between ceramic parts can be made using suitable glaze materials. Similarly, metal-to-ceramic seals are made if means are taken to control oxidation of the metal, and the metal has properties such that a bond can be formed.

7. Glaze and Metal Powder Seals

Ceramic metalizing can be effected by firing on its surface a mixture of a suitable glaze and metal powder. A useful mixture is 8 parts of nickel powder and 2 parts glaze, made into a suspension for brushing or spraying. The vehicle may, for example, be nitrocellulose dissolved in ethyl acetate. Firing is carried out in a protective atmosphere, such as 15 per cent forming gas (15 per cent hydrogen, 85 per cent nitrogen), with the temperature being dependent on the type of glaze and ceramic used.

8. *The Molybdenum–Manganese Process*

The molybdenum–manganese method, one currently of considerable interest in that it is useful in metalizing high-temperature ceramic bodies of the alumina type, consists in applying mixed powders of manganese and molybdenum to the ceramic and firing at a high temperature in a reducing atmosphere nearly saturated with water vapor. Sintering on a layer of electroplated nickel or copper, or a nickel powder, is desirable to facilitate hard soldering.

9. *Sintered Seals*

Seals of the sintered type, made with the refractory metals in powder form, are of importance. Molybdenum, rhenium, and tungsten have been used, generally with additions such as nickel, iron, or cobalt to improve the properties of the seal. The tungsten–iron seal is a seal of this type, an important feature of which is that a rigid schedule of processing is not required to produce successful seals. Considerable variations in metal powder composition, firing rate, temperature and atmosphere can be tolerated.

CERAMIC-TO-METAL SEALS

Forming a bond between a ceramic and a metal involves two fundamentally different materials. The chemical and physical natures of such materials must be considered in attempting to join them in the intimate relationship necessary for a strong, permanent, and gas-tight seal. If silver or copper is heated until molten on a ceramic surface and kept in that condition for a few minutes before cooling, spheres of metal form like droplets of mercury. These spheres neither wet nor stick to the ceramic. If the spheres are kept molten for a much longer period of time the spherical shape remains but the spheres adhere to the ceramic. This phenomenon may be explained by the fact that the molten metal slowly reacts with the ceramic at the point of contact to form an interface which facilitates bonding.

Several theories have been advanced to explain why a firmly adhering layer of metal on a ceramic can be obtained. The reactions that occur are complex, and it is believed that none of the explanations is complete enough to satisfy the several conditions encountered.

One plausible, but not very revealing, assumption is that in the case of a refractory metal powder, the bond consists of metal and ceramic which, by chemical action, has resulted in the formation of a bonding material at the interface. Another hypothesis holds that the metal diffuses into the ceramic, and, possibly by a peculiar arrangement

or rearrangement of the crystals at the interface, a bond is created. Still another belief is that certain constituents in the ceramic promote crystallizations and prevent the separation of a glass phase, and that by a type of slag formation, the metal is firmly and intimately joined to the ceramic. It is also believed that solid reactions take place because of loosening of the atomic bonds by thermal agitation, permitting mutual diffusion of the different atoms into adjacent parts of the structure. In this case it is possible that large crystals grow from smaller ones, or a new type of crystal grows from two dissimilar ones. Some knowledge of the formation of the interface, its composition and its properties, is important to an understanding of the bonding processes between ceramics and metals.

TUNGSTEN–IRON TYPE OF SEAL

To form an adherent coating of metal, such as tungsten and iron, on a ceramic it is desirable that the metals be pure and in finely divided form. Suitable metal powders are commercially available. The metals, preferably of one to four microns particle size, are mixed in the approximate proportions of one part of iron and nine parts of tungsten by weight. The metal powders in liquid suspension are applied, by brushing or by spraying, in uniform thickness of one to two mils, to the area of the ceramic to be metalized.

A suitable vehicle is added to the combined metal powders to provide a metalizing mixture having a consistency to suit the method of application to a ceramic surface. The vehicle may be nitrocellulose and ethyl acetate. Ball-milling the metal powders and organic binder makes a more thoroughly mixed metalizing material and, consequently, a more uniform metal coating. Metalizing, or the formation of an adherent metal layer on the ceramic, is carried out in a furnace capable of operation up to 1350° or 1400°C, and of such construction that the atmosphere in it can be controlled.

Because most ceramic bodies are subject to heat shock to some extent, depending on the type, a period of preheating is necessary before being introduced to the hot zone of the furnace.

The coated ceramic is fired at a temperature of 1300° to 1400°C, for 15 to 30 minutes, depending on the type of ceramic body. Forsterite and zircon are fired at 1340° to 1360°C, while the high alumina bodies require higher temperatures.

The tungsten–iron type of seal is not critically dependent on the atmosphere in which the coated ceramic is fired. Pure hydrogen has been satisfactory, although a slight impurity in the form of oxygen appears to be desirable. Forming gas (a mixture of hydrogen and

nitrogen) of from 15 to 30 per cent hydrogen has given equally good results.

CERAMIC BODIES FOR CERAMIC–METAL SEALS

While practically all types of ceramics can be metalized, and uses found for them, only certain ones are useful for electron-tube or high-frequency applications.

Properties of ceramics that must be considered for electron tube use are porosity, strength, thermal expansion, thermal conductivity, thermal shock resistance, softening temperature, and radio-frequency losses. For the creation of a strong bond between a ceramic and a metal, the chemical composition and physical structure of the ceramic body must be such that the necessary reactions may occur.

The properties of ceramic bodies are functions of the materials used and their processing into ceramics. Very often relatively small variations in either composition or processing at any stage of the ceramic making will cause undesirable characteristics.

For tube envelope use, dense, impervious bodies are required to assure vacuum tightness, which must be retained up to 600°C or more. Strong and stable ceramic compositions have approximately straight thermal expansion curves. The expansion characteristics of both metal and ceramic should match sufficiently well to prevent excessive strain at the interfaces or in one of the components of an assembly.

Tensile and compressive strength of ceramics are important since the ceramic can be subjected to considerable strain if the ceramic-metal bond is strong. Some bodies, particularly forsterite and zircon, have failed when put under stress by the metal on cooling because the metal–ceramic bond was stronger than the body of the ceramic. The ceramics that have low expansion properties have high thermal shock resistance and, conversely, the high expansion ceramics have in general poorer thermal shock properties. High mechanical strength and good thermal conductivity may, however, act as compensating factors to improve the resistance to thermal shock.

The methods of applying adherent coatings of metals, such as tungsten, molybdenum, iron, manganese, cobalt, etc., to ceramic bodies employ relatively high temperatures. There is danger of causing deformation of some ceramic bodies by reason of the high temperature. In forming ceramic–metal seals, however, the time of firing is generally short and the proper application of the metalizing techniques should cause little or no distortion.

It is known that ceramic bodies of a similar type made by different manufacturers may have dissimilar properties. This is understandable

when it is considered that ceramic raw materials are of commercial grades, therefore not chemically pure, and that impurities as well as differences in processing produce ceramics having different characteristics.

The electrical properties of ceramic bodies are of importance for use in electron tubes, as well as in circuit components. Certain ceramics have electrical losses that are sufficiently low at temperatures high enough to permit increased operating efficiencies of electron tubes. At the same temperatures tube envelopes of glass construction would have prohibitive losses.

The thermal expansion characteristics of four ceramic bodies are shown by the curves in Figure 1. Ceramic body 243* is a forsterite, 228* is a steatite, 4462** is a high alumina body, and 475* is zircon.

Figure 2 shows the electrical losses, expressed as power factor, of three ceramic bodies, designated as above. Measurements of power factor were made in the Laboratory for Insulation Research, Massachusetts Institute of Technology.

A composite tabulation of the properties of some ceramic bodies is that shown by Table I.

For some applications it may be necessary that the ceramic parts received from the supplier be altered in size or shape before metalizing. In production work such alterations would usually be accomplished with diamond tools—drills and grinding wheels. In experimental work ceramic bodies of the forsterite, zircon and steatite types can be more or less satisfactorily machined with the usually available shop tools. For example, holes have been drilled through ceramic parts with carbide tipped drills, and more safely but more slowly by using copper tubes with silicon carbide grit. In addition, drilling and cutting have been accomplished with suitable sand blast equipment, using an alumina abrasive instead of sand. In the case of the very-hard high-alumina ceramic bodies, machining is much more difficult and diamond tools are generally necessary.

Before metalizing, ceramic parts are usually given a cleaning or surface conditioning operation. To form an adherent layer of metal on a ceramic surface, the ceramic must be free of any contaminating material. Since the contaminants are ordinarily unknown, a single specific cleaning procedure may be insufficient. Usually, suitable cleaning may be obtained by firing the ceramic parts to 800°-1000° C in air. Alternatively, a suitable alkaline cleaning solution is often

---

* American Lava Corp.
** Frenchtown Porcelain Co.

used, followed by immersion in dilute nitric acid for a period of two to five minutes. Chromic acid or other glass-cleaning materials and methods are often satisfactory.

METALS FOR BRAZING TO CERAMICS

Where two materials of widely different properties are rigidly attached to each other, it is evident that one or both must be ductile,
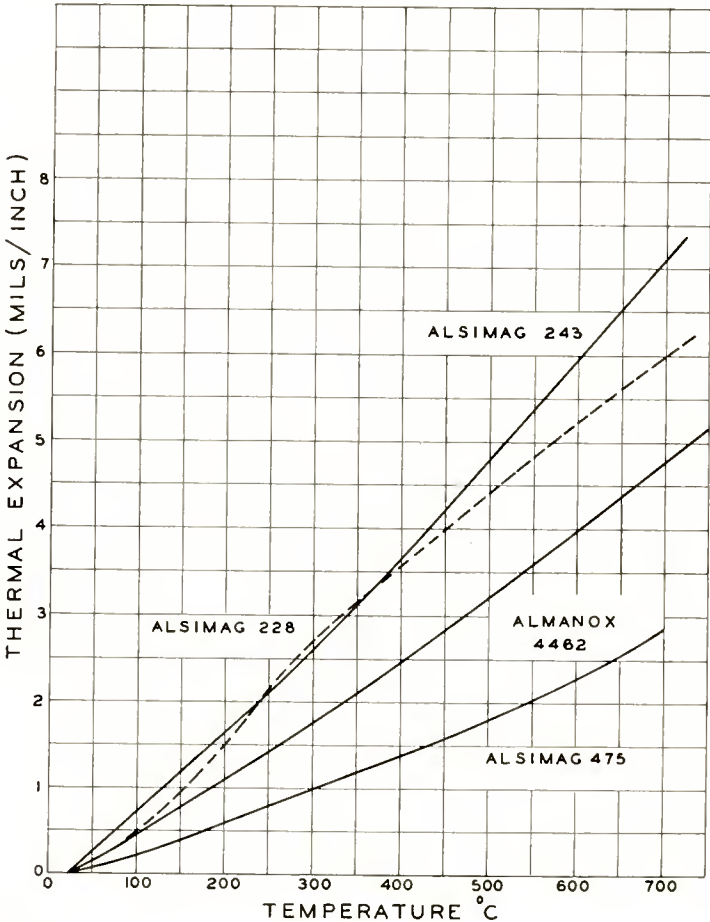

Fig. 1—Thermal expansion curves of some ceramic bodies. Forsterite (243), Steatite (228), Zircon (475), high alumina (4462).

or have sufficient "give" to avoid stresses that would cause failure. Ceramics are, by their nature, relatively unyielding materials. Hence, should a permanent joint between a ceramic and a metal be desired,

it is necessary that the metal be capable of yielding to any dimensional changes imposed by the ceramic.

There are a few pure metals and a few alloys having properties that make them suitable for brazing to ceramics. In addition some composite or "clad" metals have practical value to complete metal–ceramic parts.

Even though the expansion properties do not match perfectly, there are several combinations of metals and ceramics which result in very successful assemblies. All of the most useful metals are capable of being annealed so that they are ductile or "soft" enough to be permanently attached to ceramics.

The pure metals generally have straight thermal expansion curves, and of these copper, nickel, iron, and platinum have been soldered to ceramics. Molybdenum has been attached to zircon, but it has some objectionable features. Titanium and zirconium are other possible
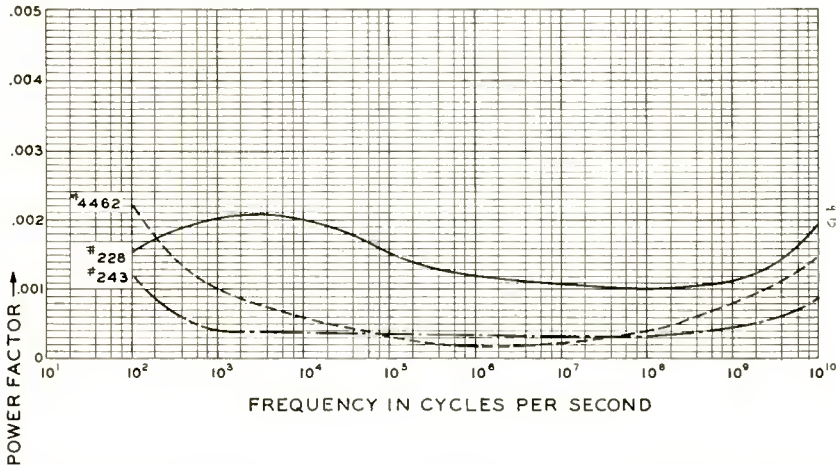

Fig. 2—Power factor curves of ceramics. Alsimag 243 at 22°C, Alsimag 228 at 25°C, Almanox 4462 at 25°C.

metals, but would require treatment, such as nickel plating, to permit of brazing, which would have to be carried out in an inert atmosphere or in vacuum.

Some of the alloys which were developed for glass-to-metal seals are useful for brazing to ceramics. Most of these are nickel-iron alloys, having 40-50 per cent nickel content. Some of the nickel–iron alloys have their properties modified to advantage by the addition of chromium or cobalt.

The dilation behavior of the nickel–iron base alloys is a function of the nickel content. For a nickel–iron alloy with 36 per cent nickel

Table I — Composite Tabulation of the Properties of Some Ceramic Bodies

Ceramic Body	Steatite	Forsterite	Zircon Porcelain	Alumina
Specific gravity	2.7	2.8	3.1	3.5
Porosity (per cent)	0–0.01	0–0.02	0–0.02	0–0.01
Tensile strength (p s i)	8500	10,000	10,000– 15,000	18,000
Compressive strength (p s i)	80,000	85,000	80,000–150,000	175,000
Modulus of rupture (p s i)	20,000	20,000	23,000	40,000
Hardness (Mohs scale)	7.5	7.5	8.0	9
Thermal conductivity (c g s units)	0.006	0.008	0.008	0.02
Coefficient of expansion $\times 10^{-6}$ 20 —100° C	6.4	9.0	3.2	5.6
20 —700° C	8.3	10.0	4.5	7.2
Thermal shock resistance			Good	Good
Softening temperature (°C)	1400	1440	1450	1800
Safe temperature (°C)	1100	1100	1000–1300	1500
T e Value (°C)	700	1000	690	800
Dielectric strength (volts/mil)	240	240	250	240
Dielectric constant (at 1 megacycle)	6.2	6.3	7.2	8
Power factor (at 1 megacycle)	.0013	.0004	.0009	.001–.003

(Invar), the thermal expansion coefficient is low and fairly constant up to a temperature of around 200°C. In this region a magnetic inversion or Curie temperature occurs and a change to a higher expansion coefficient begins.

The expansion curves of some alloys showing inflection points are seen in Figure 3. Expansion curves of some other commercially available alloys are given in Figures 4 and 5. The properties of a few metals are shown in Table II. The properties of other metals are available
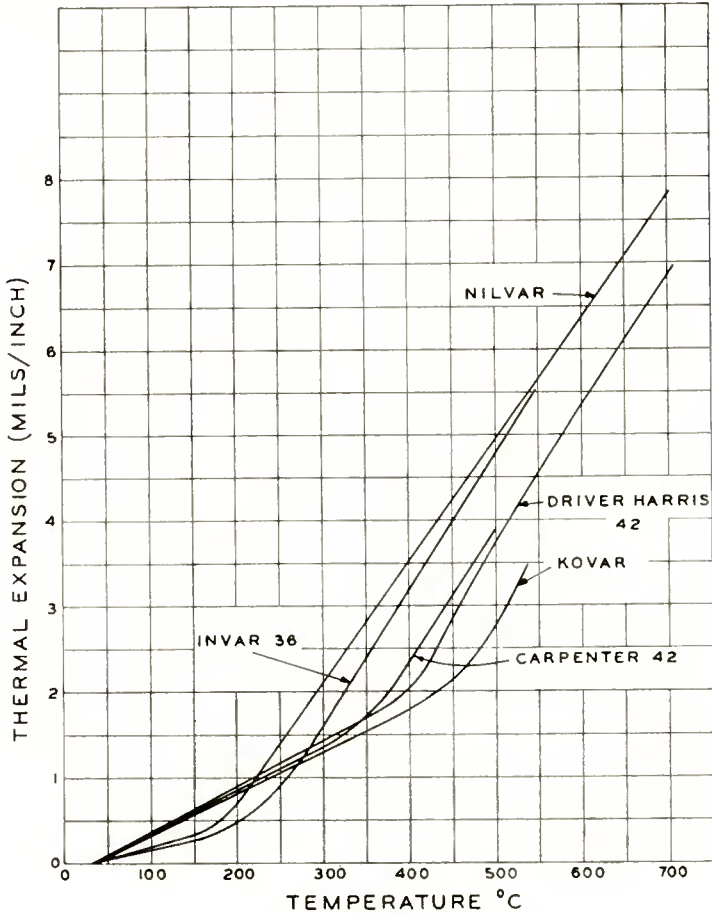

Fig. 3—Thermal expansion curves of some alloys having pronounced inflection temperature regions.

from the manufacturers and some are found in the literature.

A metal for an "outside seal" is one that has a slightly higher thermal expansion than that of the ceramic. When the metal part

embraces the ceramic part, the joint remains under compression and dangerous tensile stresses are avoided. Thin metal, of the order of five to fifteen mils thickness, is preferred for brazing to a ceramic. The thin metal parts should be sufficiently elastic so that the tensions caused by rapid temperature changes do not damage the seals.

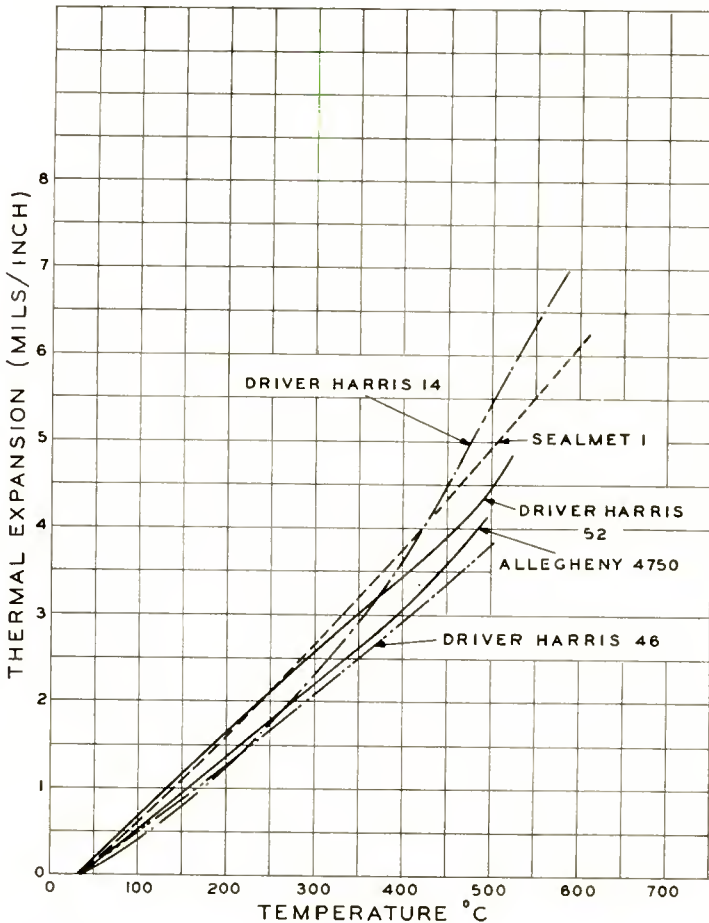Figure 6 compares the thermal expansion of alloys #42 and #46

Fig. 4—Thermal expansion curves of some sealing alloys.

with ceramic #4462. Figure 7 compares forsterite with alloys #4 and #49. Also, kovar and zircon are shown.

Several of the forms that ceramic–metal seals and assemblies may take are illustrated in Figure 8.

Figure 9 is a view of ceramic–metal tube 6181, an air-cooled power tetrode designed for television and CW applications.[1]

CERAMIC–METAL BRAZING

Ceramic–metal units are completed by soldering. Solders that have been found useful include those of the low melting temperature tin
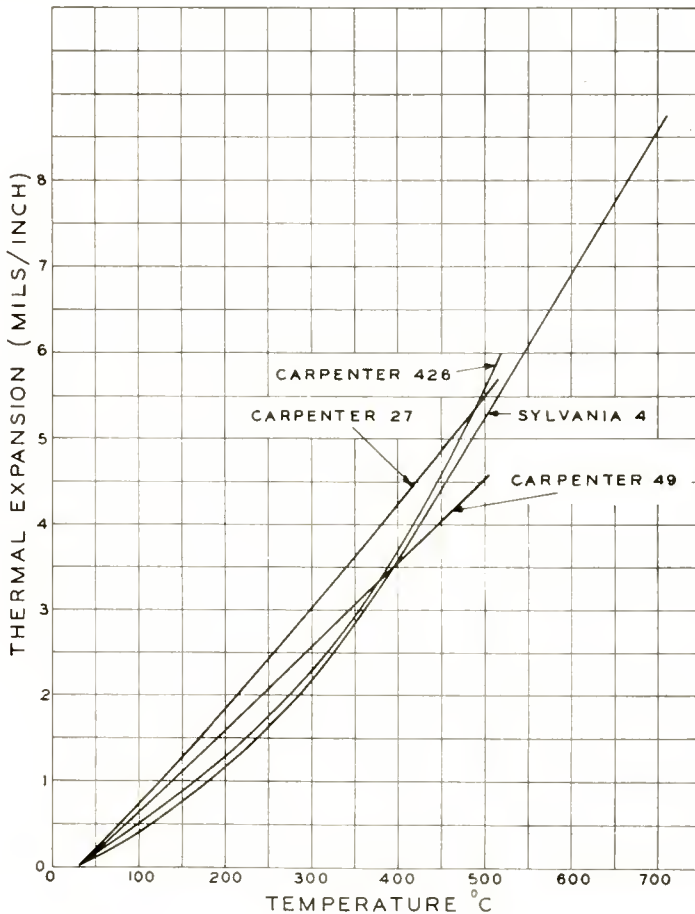

Fig. 5—Thermal expansion curves of sealing alloys.

or tin–lead alloy group, as well as high temperature brazing alloys of the silver–copper class, and pure metals, such as silver, gold, and

[1] W. P. Bennett and H. F. Kazanowski, "One-Kilowatt Tetrode for UHF Transmitters," *Proc. I.R.E.*, Vol. 41, p. 13, January, 1953.

Table II — Properties of Some Metals Useful for Ceramic–Metal Seals

|	Copper	Alloy #4	Alloy #14	Alloy #46	Alloy #52	Alloy #430
Composition	OFHC	Ni 42% Cr 5.6% Fe 52.3%	Ni 42% Cr 5.5% Fe 52.5%	Ni 46% Fe 54%	Ni 51% Fe 49%	Cr 16-18% Mn 1% max Si 1% max Ni 0.5 max Fe bal.
Melting point (°C)	1083	1425	1425	1425	1425	1480
Coefficient of expansion × 10^{-6}						
20°C	16.6					
20–400°C		9.6–10.2				
20–425°C	17.4	11.1	10.8	8.0	9.5	11.2
20–500°C						
20–800°C						11.8
Thermal conductivity (c g s units)	0.928	0.032	0.032	0.0365	0.04	0.054
Heat treatment (°C)	700	1050	1050	1050	1050	1000
Anneal in atmosphere	H_2	dry H_2	dry H_2	H_2	H_2	dry H_2
Specific resistance (microhm-centimeter at 20°C)	1.724	34	93	45.7	43.2	60
Magnetic	No	Yes	Yes	Yes	Yes	Yes
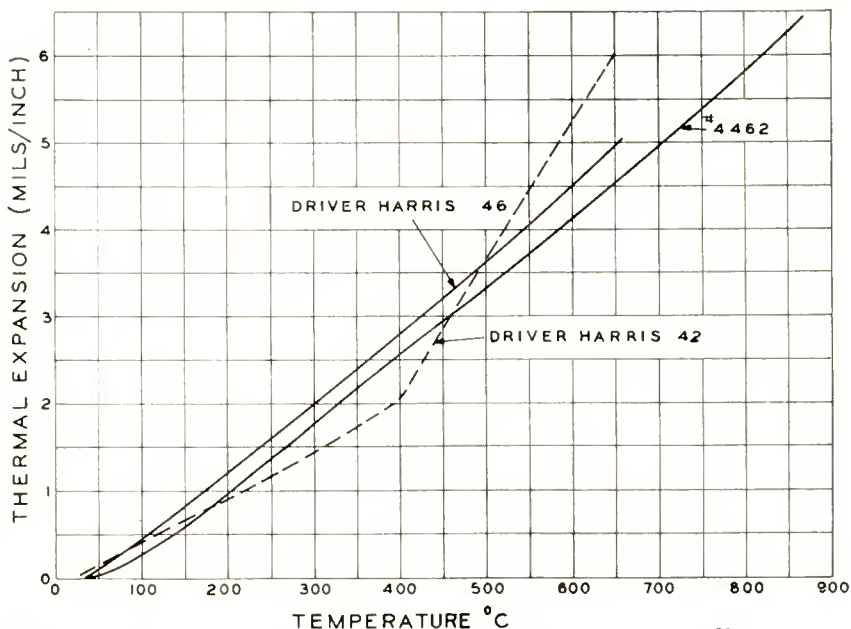
Fig. 6—Thermal expansion comparison between ceramic 4462 and alloys
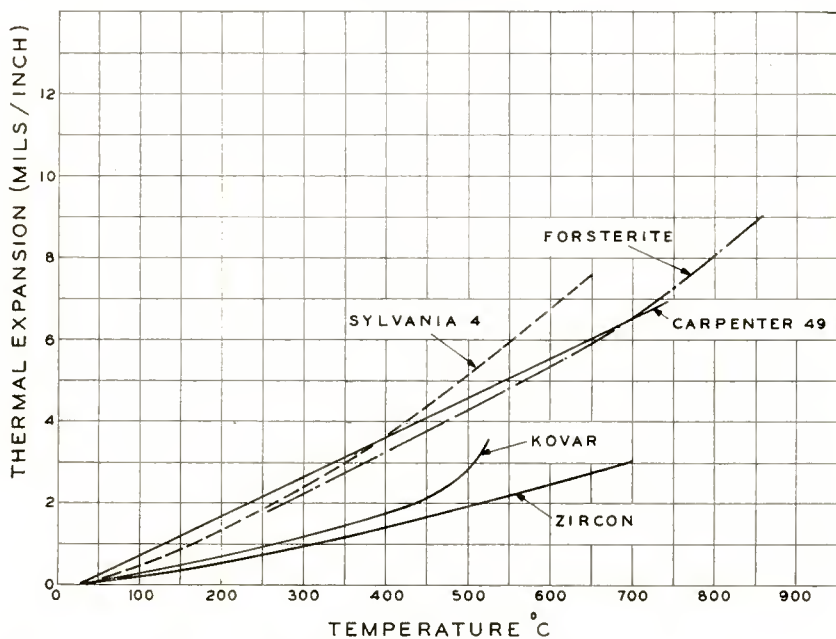46 and 42.

Fig. 7—Graph showing expansion comparisons of Forsterite and alloys #4
and #49, also, zircon and kovar.

copper. For electron tube use, solders that may be exposed internally should have no high vapor pressure constituents.

Silver–copper alloys are generally used for ceramic–metal brazing, and the brazing operation carried out in a protective atmosphere, usually in a hydrogen furnace, in much the same way as metal to metal brazing is done. Brazing can be done directly to the tungsten–
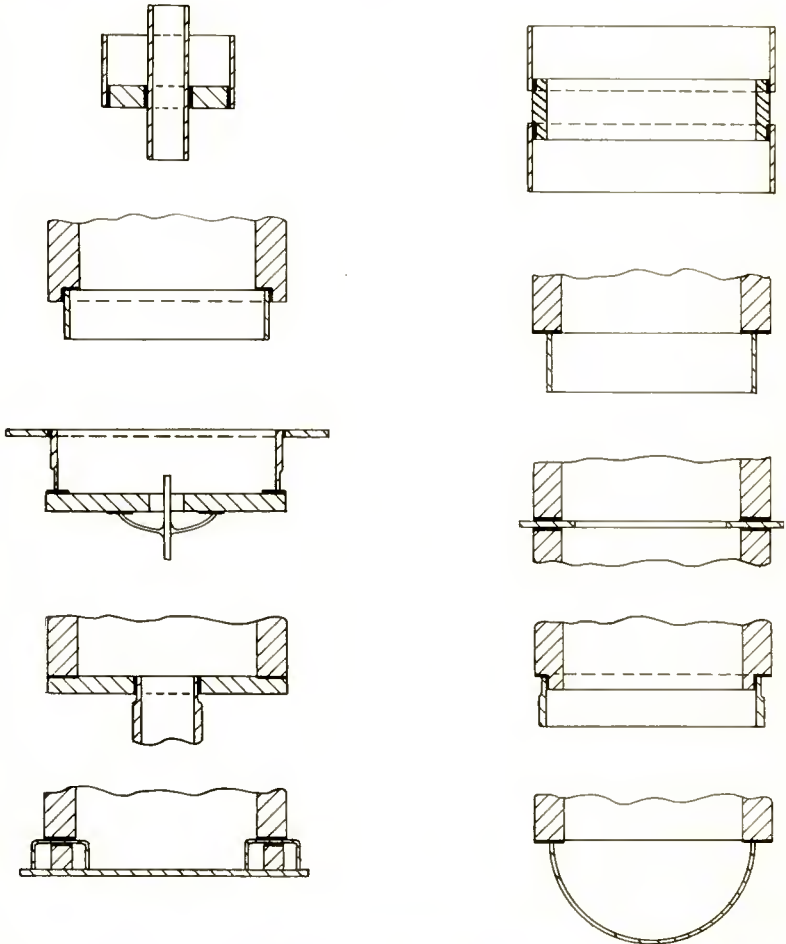

Fig. 8—Several of the forms that ceramic-metal seals and assemblies may take.

iron coating on a ceramic without any intermediate treatment being necessary. However, for best results a treatment, such as nickel plating and/or copper plating, with or without sintering, produces better and more certain results.

If the metal to be brazed to a ceramic is an alloy of the chromium bearing type, brazing cannot be effected in ordinary moist or tank hydrogen because of the chromium oxide that forms. In dry hydrogen, however, brazing of chromium alloys can be done effectively. Alternatively, a protective layer of metal such as nickel, applied by electroplating is readily wetted by the brazing metal in tank or "line" hydrogen, and brazing to a metalized ceramic is readily accomplished. In all brazing operations involving high-temperature solders, the ceramic parts should be preheated to avoid stresses, the heating rate and temperature depending on the thermal shock properties of the particular ceramic body. On the other hand, use of the low-temperature solders such as tin and lead generally does not require preheating of
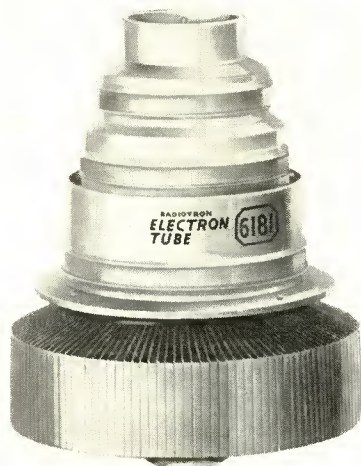
Fig. 9—Ceramic–metal envelope tube 6181.

the ceramic, although it is advisable as a precaution.

In brazing a metal to a ceramic, the metal part should snugly fit the ceramic, and the expansion match be reasonably good. If the ceramic–metal fit is unsuitable, or the metal at the intended soldering area expands too fast or too far, a gap may develop which would require an excess of solder to fill. Too much solder or too large a fillet may cause failure of the bond by fracture of the ceramic or stripping. On the other hand too little solder may cause a weak joint and a leaky one. Too high a temperature in brazing may cause a loss of solder, or alloying, or intergranular penetration, depending on the metal involved since certain metals are particularly susceptible to attack by silver and its alloys.

FILTER USING COAXIAL TRANSMISSION LINE AS ELEMENTS*

By

H. B. Yin and T. U. Foley

RCA Victor Engineering Products Division,
Camden, N. J.

Summary—A new approach towards the design of filters using transmission-line sections is presented. Equations derived for filters are expressed in exact form. The discontinuity capacities due to the steps along the transmission line are taken into consideration. An example is worked out to show the accuracy of the developed equations. Considerations in the design of low-pass filters are discussed.

INTRODUCTION

THE technique of using coaxial-transmission-line sections as filter elements has been used before.[1-5] A number of approximations were assumed in deriving lumped constants for transmission-line sections. Fairly reasonable agreement was obtained between theoretical and experimental values.[6]

In this paper exact equivalent circuits are first developed for individual sections of transmission line. The effect of step capacity at the discontinuity[7] is included in the equivalent circuits. By applying the equivalent circuits and these equations to filters made up of cascade

---

* Decimal Classification: R386.2.

[1] W. P. Mason and R. A. Sykes, "The Use of Coaxial and Balanced Transmission Lines in Filters and Wide-Band Transformers for High Radio Frequencies," *Bell Sys. Tech. Jour.*, Vol. 16, pp. 275-302, July, 1937.

[2] L. R. Quarles, "Transmission Lines as Filters," *Communications*, Vol. 26, pp. 34-38, June, 1946.

[3] C. L. Cuccia and H. R. Hegbar, "An Ultra-High-Frequency Low-Pass Filter of Coaxial Construction," *RCA Review*, Vol. 8, pp. 743-750, December, 1947.

[4] Radio Research Laboratory, Harvard University, *Very-High Frequency Technique*, McGraw-Hill Book Co., Inc., New York, N. Y., 1947, Chapters 26 & 27.

[5] D. E. Mode, "Low-pass Filters Using Coaxial Transmission Lines as Elements," *Proc. I.R.E.*, pp. 1376-1383, November, 1948.

[6] George L. Ragan, *Microwave Transmission Circuits*, M. I. T. Series, Vol. 9, McGraw-Hill Book Co., Inc., New York, N. Y., 1946, p. 626.

[7] J. R. Whinnery and H. W. Jamieson, "Equivalent Circuits for Discontinuities in Transmission Lines," *Proc. I.R.E.*, Vol. 32, pp. 98-114, February, 1944.

or single sections of transmission line, it is possible to predict accurately the performance in terms of image impedance, cutoff frequency, attenuation, and band limits. This technique is rigorous for any frequencies where only TEM wave is present.

Notation

$Y_1, Z_1 =$ Characteristic admittance and impedance, respectively, of the main transmission line.

$Y_2, Z_2 =$ Normalized admittance and impedance, respectively, of sleeve or undercut section.

$Y'_2, Z'_2 =$ Normalized equivalent admittance and impedance, respectively, of sleeve or undercut section.

$B_d =$ Normalized susceptance due to step discontinuity.

$B, X =$ Normalized equivalent shunt susceptance and series reactance, respectively.

$l_1, l_2, l''_2, l'_2, l =$ Physical lengths or equivalent physical length of transmission line sections as noted in appropriate figures.

$\alpha_0 =$ Image attenuation constant of filter section.

$\beta_0 =$ Image phase constant of filter section.

$\theta =$ Image transfer constant of full filter section.

$= \alpha_0 + j\,\beta_0.$

$$\left.\begin{aligned}Z_{11N} &= \frac{z_{11}}{Z_1} \\[2mm] Z_{22N} &= \frac{z_{22}}{Z_1}\end{aligned}\right\} \text{Normalized image impedance as shown in appropriate figures.}$$

Equivalent Circuits of Transmission-Line Sections

A section of transmission line with characteristic impedance or admittance different from the main transmission line could be used as an impedance matching device.[8] It is a sleeve section when $Y_2 > Y_1$ or $Z_2 < Z_1$; otherwise it is an undercut section. The sleeve or undercut section introduces a shunt capacity or a series inductance respectively in a coaxial transmission line. Its value has been derived.[9] An exact

---

[8] T. Moreno, *Microwave Transmission Design Data*, McGraw-Hill Book Co., Inc., New York, N. Y., 1948, Chapter 6.

[9] R. W. Klopfenstein, "Impedance Matching with Transformer Sections," *RCA Review*, Vol. XIV, pp. 64-71, March, 1953.

and simplified equivalent circuit could be developed as follows:
The input admittance looking towards the right at $a\,a$ *and* $a'a'$ as
shown in Figure 1 a and 1b must be equal. Therefore

$$\frac{Y_2 + j\,Y_2\,(B_d + Y_2 \tan \beta l_2)}{(Y_2 - B_d \tan \beta l_2) + j \tan \beta l_2} + jB_d = Y'_2 \frac{\dfrac{1}{Y'_2} + j \tan \beta l'_2}{1 + j\,\dfrac{\tan \beta l'_2}{Y'_2}}. \qquad (1)$$

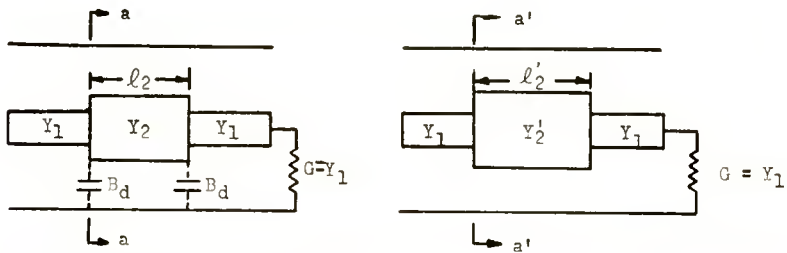By equating real and imaginary components,

Fig. 1—(a) Actual transmission-line section, (b) Equivalent transmission-line section without step capacities.

$$Y'_2 = \sqrt{\; Y_2{}^2 + B_d \left[\frac{2\,Y_2}{\tan \beta l_2} - B_d \right]}$$

$$\tan \beta l'_2 = \frac{Y'_2 \tan \beta l_2}{Y_2 - B_d \tan \beta l_2}. \qquad (2)$$

Equation (2) shows the effect of step susceptance on Y_2 and l_2. From
circuit symmetry it is evident that the equivalent circuit is true for
two-way transmission for any values of terminating admittance or
impedance.[10] Since the equations shown are general, the value of Y_2
could be larger or smaller than Y_1. Simplified and exact equivalent
circuits for sleeve and undercut sections will proceed separately from
Figure 1b in the following manner.

Sleeve Section $(Y_2 > Y_1$ or $Z_2 < Z_1)$

A sleeve section (Figure 2a) can be represented by a length of line
with a shunt susceptance (Figure 2b). The value of equivalent B and

---

[10] T. E. Shea, *Transmission Networks & Wave Filters*, D. Van Nostrand
Co., Inc., New York, N. Y., 1935, Chapter 3, pp. 64-99.

l''_2 can be obtained by equating the input admittance using transmission line equations,

$$Y'_2 \frac{\dfrac{1}{Y'_2} + j \tan \beta l'_2}{1 + j \dfrac{\tan \beta l'_2}{Y'_2}} = \frac{1 + j \left(B + \tan \dfrac{1}{2} \beta l''_2 \right)}{1 - B \tan \dfrac{1}{2} \beta l''_2 + j \tan \dfrac{1}{2} \beta l''_2} \tag{3}$$

from which

$$B = \left(Y'_2 - \frac{1}{Y'_2} \right) \sin \beta l'_2 \tag{4}$$

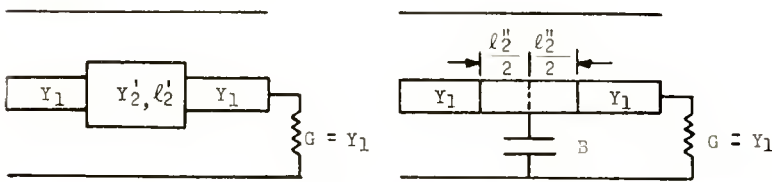$$\tan \frac{1}{2} \beta l''_2 = \frac{\tan \dfrac{1}{2} \beta l'_2}{Y'_2} .$$

Fig. 2—(a) Cross section of sleeve section, (b) Its exact equivalent.

It is apparent that a sleeve section is equivalent to a piece of transmission line of the same characteristic admittance as the main transmission line, with a shunt susceptance at its center. By substituting Equations (2) into Equations (4), the equivalent B and length could be expressed in terms of actual constants of transmission line section as shown in Figure 1a. Then

$$B = \left(Y_2 - \frac{B_d^2 + 1}{Y_2} \right) \sin \beta l_2 + 2 B_d \cos \beta l_2 \tag{5}$$

$$\tan \frac{1}{2} \beta l''_2 = \frac{\tan \dfrac{1}{2} \beta l_2}{Y_2 - B_d \tan \dfrac{1}{2} \beta l_2} .$$

Undercut Section ($Y_2 < Y_1$ or $Z_2 > Z_1$)

An undercut section can be represented on an impedance basis by a series inductance as shown in Figures 3a and 3b.

By the same reasoning as used above, the input impedances must be equal:

$$Z'_2 \frac{\dfrac{1}{Z'_2} + j \tan \beta l'_2}{1 + j \dfrac{\tan \beta l'_2}{Z'_2}} = \frac{1 + j\left(X + \tan \dfrac{1}{2}\beta l''_2\right)}{1 - X \tan \dfrac{1}{2}\beta l''_2 + j \tan \dfrac{1}{2}\beta l''_2} \tag{6}$$

from which

$$X = \left(Z'_2 - \frac{1}{Z'_2}\right) \sin \beta l'_2$$

$$\tag{7}$$

$$\tan \frac{1}{2}\beta l''_2 = \frac{\tan \dfrac{1}{2}\beta l'_2}{Z'_2}.$$

Considering the actual circuit constants, then Equation (7) becomes

$$X = -\left\{\left[\frac{1}{Z_2} - (B_d^2 + 1) Z_2\right] \sin \beta l_2 + 2 B_d \cos \beta l_2\right\}$$

$$\text{or} \quad -X = \left[Y_2 - \frac{B_d^2 + 1}{Y_2}\right] \sin \beta l_2 + 2 B_d \cos \beta l_2$$

$$\tag{8}$$

$$\text{and} \quad \tan \frac{1}{2}\beta l''_2 = \frac{\left(\dfrac{1}{Z_2^2} - B_d^2\right) \sin \beta l_2 + \dfrac{2 B_d}{Z_2} \cos \beta l_2}{\dfrac{1}{Z_2}(1 + \cos \beta l_2) - B_d \sin \beta l_2}$$

$$\text{or} \quad \tan \frac{1}{2}\beta l''_2 = \frac{(Y_2^2 - B_d^2) \sin \beta l_2 + 2 B_d Y_2 \cos \beta l_2}{Y_2(1 + \cos \beta l_2) - B_d \sin \beta l_2}.$$

It is noted that an undercut section is equivalent to a piece of transmission line of characteristic impedance same as the main transmission line, with a series inductance at its center.
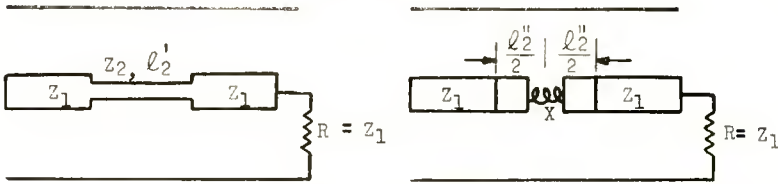
Fig. 3—(a) Cross section of undercut section, (b) Its exact equivalent.

From Equations (5) and (8) or Equations (4) and (7), it is evident that the absolute value of X is the same as B, but of opposite sign.

Low-Pass Filter

As mentioned above, a filter can be built with many sections in cascade. For purpose of analysis, it is convenient to use only one section. This is similar in treatment to conventional lumped-constant filters.

The equivalent circuits developed above for either sleeve or undercut transmission line sections are equally applicable in design of filters. The development that follows is based upon sleeve sections. However, a similar approach could have been chosen using undercut sections as filter elements.

Suppose a filter is made as shown in Figure 4a. Then by means of equivalence, it can be shown as in Figure 4b.

The relation between l_2 and l''_2, and Y_2 and B are shown by Equations (4) and (5). Application of four-terminal network theory to the equivalent network of Figure 4b leads to formulas for image impedance and transfer constant. For convenience in calculation, the full symmetrical section may be split into two half sections. The image impedance for the half section will be the same as for a full section. The transfer constant for a half section will be half of that for a full section. The half section is shown in Figure 5a, and its four-terminal network equivalent is shown in Figure 5b. The application of four-terminal network theory to low-pass filters follows.
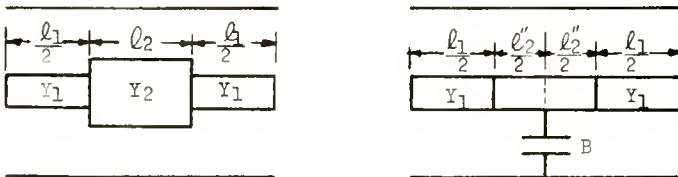

Fig. 4—(a) Low-pass filter, (b) Its equivalent.

In a four-terminal network, the following relationship exists between sending and receiving voltage and current:[11]

$$E_1 = A'E_3 + B'I_3$$

$$I_1 = C'E_3 + D'I_3 . \tag{9}$$

The image impedances are

$$z_{11} = \sqrt{\frac{B'A'}{C'D'}} \tag{10}$$

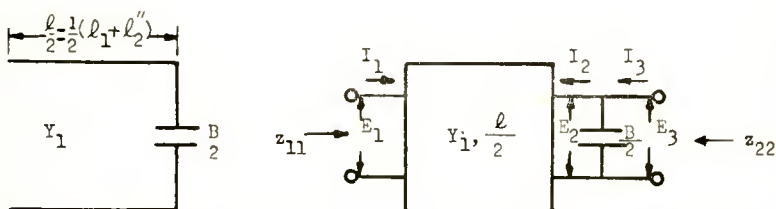and

$$z_{22} = \sqrt{\frac{B'D'}{A'C'}} . \tag{11}$$

Fig. 5—(a) Half section of low-pass filter, (b) Four-terminal network equivalent.

The transfer constant for half section is

$$\cosh \frac{\theta}{2} = \sqrt{A'D'}. \tag{12}$$

By transmission line relations,

$$E_1 = E_2 \cos \frac{1}{2}\beta l + j\, I_2 Z_1 \sin \frac{1}{2}\beta l$$

$$\tag{13}$$

$$I_1 = j\, \frac{E_2}{Z_1} \sin \frac{1}{2}\beta l + I_2 \cos \frac{1}{2}\beta l.$$

[11] E. Guillemin, *Communication Network*, Vol. II, John Wiley & Sons, New York, N. Y., Chapter V.

Since $\quad E_2 = E_3,$

$$(14)$$

$$I_2 = j\,\frac{B}{2}\,E_3 + I_3$$

then $\quad E_1 = \left[\cos\frac{1}{2}\beta l - \frac{B}{2}\,Z_1\sin\frac{1}{2}\beta l\right]E_3 + j\,Z_1\,I_3\sin\frac{1}{2}\beta l$

$$(15)$$

$$I_1 = j\left\{\frac{\sin\dfrac{1}{2}\beta l}{Z_1} + \frac{B}{2}\cos\frac{1}{2}\beta l\right\}E_3 + I_3\cos\frac{1}{2}\beta l.$$

Therefore

$$A' = \cos\frac{1}{2}\beta l - \frac{B}{2}\,Z_1\sin\frac{1}{2}\beta l,\ \ B' = j\,Z_1\sin\frac{1}{2}\beta l$$

$$(16)$$

$$C' = j\left\{\frac{\sin\dfrac{1}{2}\beta l}{Z_1} + \frac{B}{2}\cos\frac{1}{2}\beta l\right\},\ \ D' = \cos\frac{1}{2}\beta l$$

and

$$Z_{11N} = \frac{z_{11}}{Z_1} = \left\{\frac{1 - \dfrac{B}{2}\tan\dfrac{1}{2}\beta l}{1 + \dfrac{B}{2}\cot\dfrac{1}{2}\beta l}\right\}^{\frac{1}{2}}$$

$$(17)$$

$$Z_{22N} = \frac{z_{22}}{Z_1} = \left\{\frac{1}{1 - \dfrac{B^2}{4} + B\cot\beta l}\right\}^{\frac{1}{2}}$$

$$(18)$$

$$\cosh\frac{\theta}{2} = \sqrt{\cos^2\frac{1}{2}\beta l - \frac{B}{4}\sin\beta l}$$

$$(19)$$

or $\quad \cosh\theta = \pm\left(\cos\beta l - \frac{B}{2}\sin\beta l\right)$

$$(20)$$

A low-pass filter with transmission-line sections is very well described by Equations (17), (18), and (20). In pass bands, $\theta = j\beta_0$, and in stop bands, $\theta = \alpha_0$.

The choice of sign for Equations (20) depends upon the value of βl. If βl is in the first or second quadrants, the sign is negative; if it is in the third or fourth quadrants, the sign is positive. When $\beta l = 90°$ or 270°, maximum attenuation depends upon the equivalent value of B. However, there are some other limiting factors which govern the design of the filter. Required image impedance in the pass band, width of reject band, and maximum attenuation are all interrelated functions of Y_1, Y_2, l_1, and l_2 as shown by the equations. In other words the performance of a filter depends upon the geometry of the actual transmission-line sections. All of these factors should be taken into consideration in choosing appropriate configuration for a given filter application.

The shape of the image impedance curve in the first pass band is relatively insensitive to modification of the geometrical configuration. Primarily, the configuration establishes the impedance level and
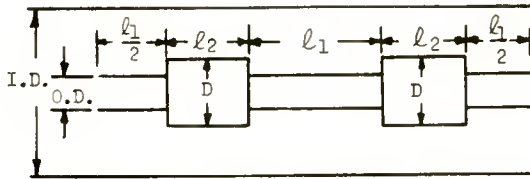

Fig. 6—A typical low-pass filter.

locates the cutoff frequency for the first pass band. The width of the first stop band is very sensitive to configuration. In order to obtain wide stop band width, it is necessary to make the ratio Y_2/Y_1 fairly large. This same ratio, Y_2/Y_1 determines the maximum amount of rejection obtainable in a single-section filter, large ratios giving large attenuation. The maximum amount of attenuation per section is relatively unimportant since more sections can be added until required attenuation is realized.

EXPERIMENTAL VERIFICATION

A two-section low-pass filter designed according to the above equations is shown in Figure 6. The standard $3\frac{1}{8}$-inch, 50-ohm, ultra-high-frequency transmission line is used for the main section of this filter. The value of discontinuity susceptance B_d is plotted in Figure 7 for either a sleeve or an undercut section for this kind of transmission

line. For instance, $B_d = .107 \times 10^{-3} \times f_{mc}$ for this particular value of $Y_2 = 2.01$.

$$Y_2 = 2.01$$
$$I.D. = 3.027''$$
$$O.D. = 1.315''$$
$$D = 2.000''$$
$$l_1 = 4.540'' \text{ or } \beta l_1 = .1387° \times f_{mc}$$
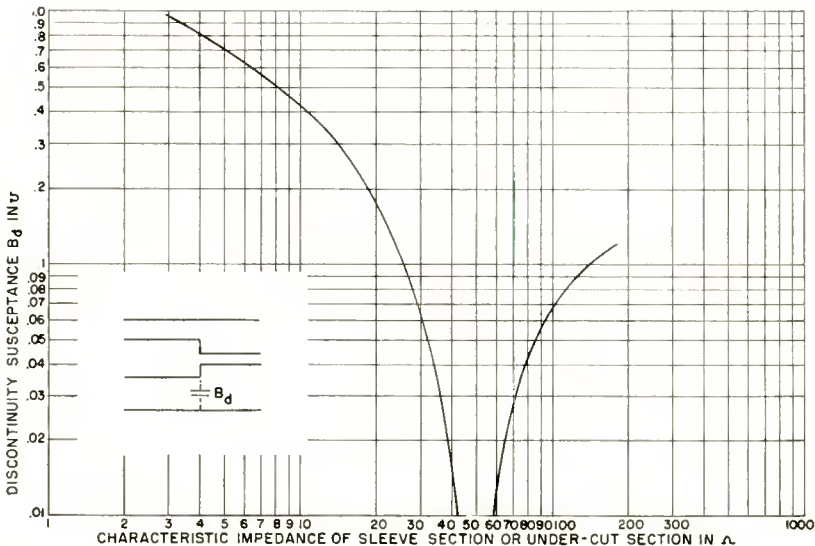$$l_2 = .875'' \text{ or } \beta l_2 = .0267° \times f_{mc}.$$

Fig. 7—Discontinuity susceptance (normalized to $(1/50)\, \mho$) in a 50-ohm 3⅛-inch coaxial transmission line at $f = 1000$ megacycles.

Equations (5), (17), and (20) were used to calculate the image impedance and attenuation. The results are plotted in Figure 8 together with experimental data points. The effect of the step capacity is obvious and cannot be neglected. Even the small value of the step capacitive susceptance for this filter will lead to considerable error in evaluation of the filter performance if it is neglected.

The sample chosen illustrates the importance of geometrical configuration as cited above. The reject band width is very narrow and is followed by a wide second pass band.

Conclusion

Throughout the analysis, there is only one limiting factor, namely the assumption of lossless line. However, the length of the transmission line dealt with in practice is very short and the materials used are of high conductivity. This assumption, therefore, will leave no serious error in evaluation of the performance of the filter.

The validity and exactness of the equivalent circuits and of the equations developed therefrom has been confirmed by laboratory measurements. As a result, low-pass filters using transmission-line sections as elements can be designed explicitly and their performance predicted accurately by the equations presented. Use of these equations will simplify design procedures.
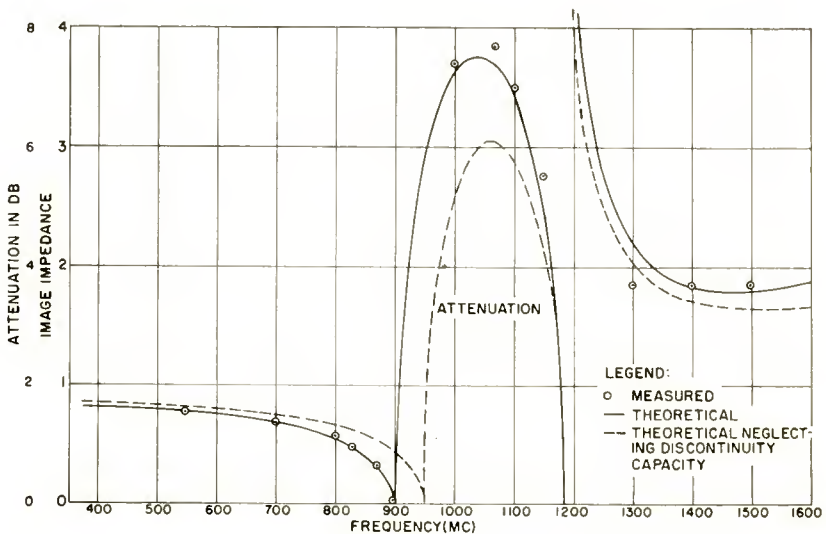
Fig. 8—Attenuation and image impedance versus frequency.

While the above example represents a low-pass filter design, it is important to note that the equivalent circuit equations for individual sections are perfectly general and apply to any coaxial transmission line with discontinuities, such as impedance matching transformer, power dividing networks, step lines, etc.

Acknowledgment

The authors wish to express their appreciation to J. Z. Grayum for obtaining and evaluating all laboratory data.

Appendix—Practical Evaluation of Equivalent Susceptance

The result for equivalent susceptance B obtained in Equation (5) could be rewritten as follows:

$$B = \sqrt{Y_2{}^2 + 2\,(B_d{}^2 - 1) + \frac{(B_d{}^2 + 1)^2}{Y_2{}^2} \sin\,(\beta l_2 + \phi)}$$

where (21)

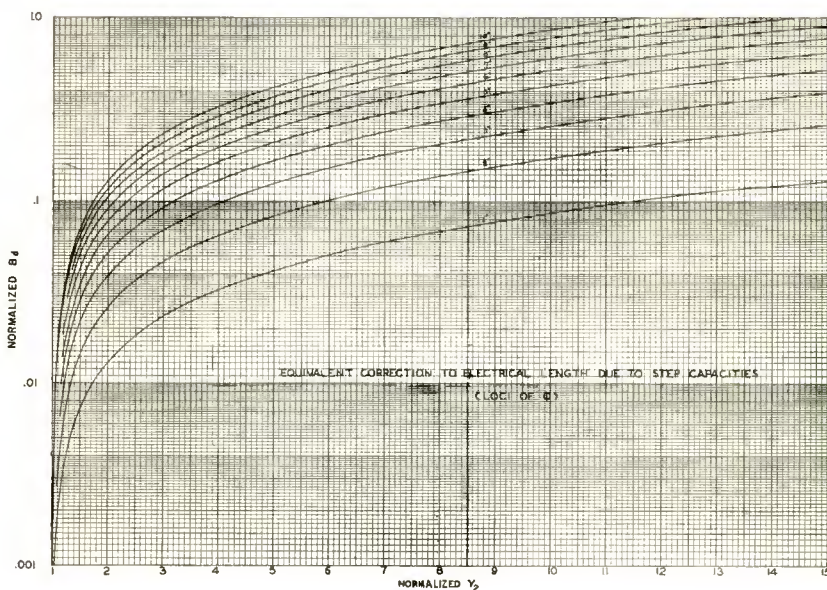$$\phi = \tan^{-1} \frac{2B_d}{Y_2 - \dfrac{B_d{}^2 + 1}{Y_2}} \cdot$$

Fig. 9—Equivalent correction to electrical length due to step capacities.

This represents a change of electrical length due to the presence of B_d. The loci of ϕ from $1°$ to $10°$ has been plotted in Figure 9 for different values of B_d and Y_2. Any angle ϕ which does not fall on the locus could be interpolated from the curve. The spacing between the loci of ϕ follows the logarithmic scale when the value of Y_2 is greater than 3.

The value of B_d can be neglected under the radical for any value of ϕ from $0°$ to $10°$. The maximum error introduced by omitting B_d

within this range is only 1 per cent. However, the effect on the electrical length is severe. Therefore, the equivalent value, B, for any sleeve section or undercut section becomes

$$B = \left(Y_2 - \frac{1}{Y_2} \right) \sin \left(\beta l_2 + \phi \right). \tag{22}$$

The reasons for plotting the loci of ϕ from $1°$ to $10°$ are arbitrary. However, this range will satisfy most applications.

RECRYSTALLIZATION OF GERMANIUM FROM INDIUM SOLUTION*

By

Jacques I. Pankove

Research Department, RCA Laboratories
Princeton, N. J.

Summary—Upon cooling a germanium-in-indium solution in contact with solid germanium, germanium from the supersaturated solution recrystallized onto the solid crystal in epitaxial fashion. The growth forms a group of separate [100] needles consisting of a stack of (111) plates, many of which are hollow. Although the outer portion of the recrystallized region may be rich in defects, there is a relatively perfect continuous recrystallized layer or overgrowth region adjacent to the p-n junction. This overgrowth region is a single crystal p-type semiconductor which continues the lattice of the n-type seed. The overgrowth is thinnest in the (100) direction.

There is some indication that the alloy front, and hence the p-n junction, tend to be flattest in (111) planes. The p-n junction seems to coincide with the alloy front at least within the limits of the present experimental resolution.

INTRODUCTION

THIS paper discusses work done on the recrystallization of germanium from its solution in indium. The purpose of the experiment was to obtain a large-scale recrystallized region in the germanium–indium system so that a better insight in the process of making alloy-junction devices would result. In particular, it was sought to examine whether the progress of the alloying front, i.e., the liquid–solid interface, is affected by crystallographic orientation, whether a uniform junction can be obtained, and how perfect a recrystallized region can be produced.

The penetration of the alloy front into germanium determines the geometry of the region between the two junctions of a transistor. Both the current-amplification factor and the transit-time dispersion of minority carriers are affected by this geometry.

Uniformity of the junction is desirable in order to obtain a high and sharp breakdown voltage. The breakdown voltage of a junction is shown by the V–I characteristic which presents the sum of the current contribution from every region of the junction. Hence a "soft" breakdown voltage may be attributed to a nonuniform junction.

The homogeneous recrystallized p-type region forms a single crystal

---

75

with the underlying n-type germanium as in the grown junction. However, the transition between the n and p regions is very abrupt in contrast to the more gradual transition of the usual grown junction. Also, the recrystallized region is of very low resistivity. This is desirable for the emitter of a p-n-p transistor.

THE EXPERIMENT

A single crystal of germanium originally grown in the [111] direction was cut into a cylinder with its axis in nearly the [110] direction. This particular orientation was selected because a cross section of the cylinder normal to this direction exposes the three major axes (see Figure 1).
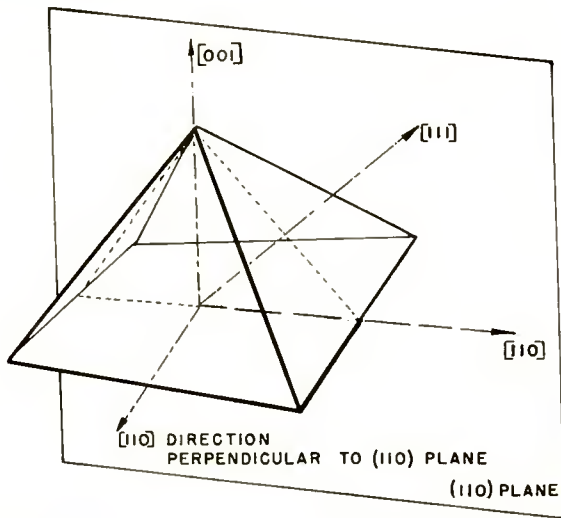
Fig. 1—Half of octahedral unit cell showing how the (110) plane contains the three major axes.

After etching, the crystal was dipped into a pot of indium which was brought to 600°C in an inert atmosphere in a manually regulated furnace. The crystal was clamped by a carbon ring supported by the pot as shown in Figure 2, so that the immersed surface was spaced from the surrounding walls. The phase diagram for the indium–germanium system[1] shows that at 600°C the equilibrium concentra-

---

[1] W. Klem, et al, "The Behavior of the Elements of Group III with One Another and with the Elements of Group IV," *Z. Anorg. Chem.*, Vol. 256, p. 239, 1948.

tion of germanium dissolved in indium is 20 atomic per cent. The temperature was reduced from 600° to 100°C in about two hours. Initially, the temperature was lowered at an even slower rate than the above average of 250 degrees per hour.

The indium was dissolved away by immersion in mercury followed by a short nitric acid etch which removed the last visible traces of indium and mercury without attacking the germanium.

EXTERNAL OBSERVATIONS

The cleaned crystal exhibited the spectacular array of needles shown in Figures 3, 4, and 5.

As the temperature was lowered, germanium atoms from the supersaturated solution grew back onto the original crystal in epitaxial
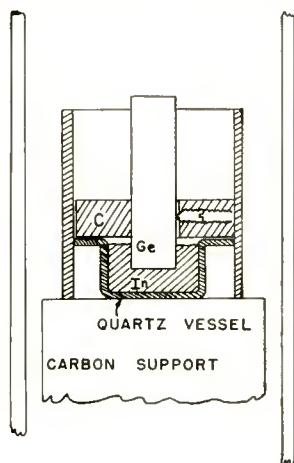
Fig. 2—Setup in the furnace. The germanium crystal descends into the indium as soon as the indium melts, and assumes the position shown.

fashion. The greatest crystal growth was in the [100] direction, forming needles which grew up to the walls of the container, and leaving voids between the needles and holes within their structure. These [100] needles are made up of sets of four octahedron facets stacked up like hollow pyramids. These are (111) facets with triangular boundaries about 1 millimeter on the side. Many of these facets are incomplete, i.e., only their edges have formed. These are 110 edges which usually make (111) facets grow faster along their plane than in thickness.

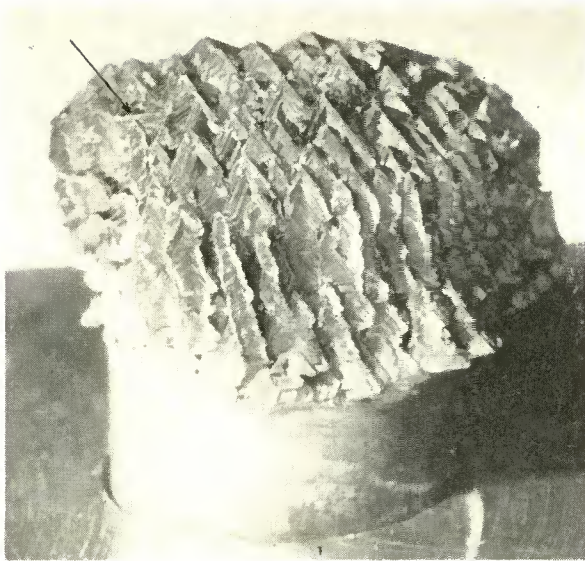A few twins have been found (horizontal facet at upper left of

Fig. 3—A view of the recrystallized germanium. The arrow points to the twin. Note the stacked-up needle formation.

Fig. 4—Another view of the recrystallized germanium showing the hollow (111) facets.

Figure 3 and triangles at left and right of Figure 5).

Figure 5 is a view along the [100] axis. Since most terminal (111) facets are incomplete, one can see only the 110 edges meeting at the apex of the needles and forming a pattern of crosses except for occasional twins which show up as triangles. Recrystallization proceeded up to the walls of the container; the noncylindrical appearance of the specimen is due to the fact that some of the needles broke off.

INTERNAL OBSERVATIONS

The specimen was cut in the plane of the three major axes, the
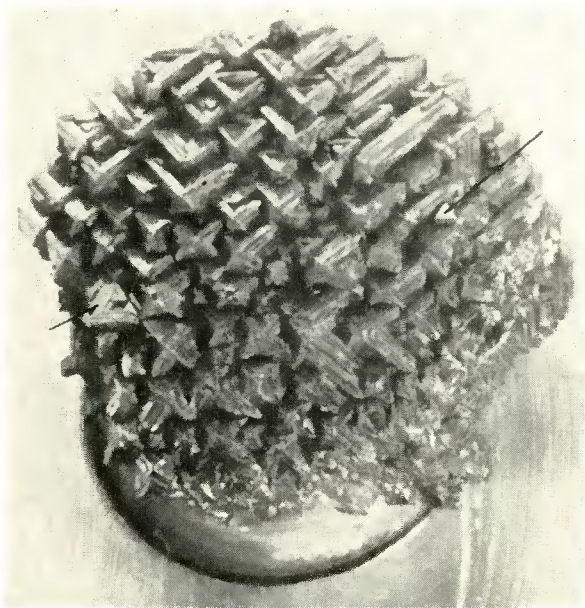
Fig. 5—A third view of the recrystallized germanium looking down the [100] axis. The arrows point to the twins.

(110) plane. After lapping, the exposed surface was etched to reveal the p-n junction. This is shown in the composite photograph of Figure 6 as a white line at the base of the recrystallized region. From etching studies there is evidence that the region outside the p-n junction consists of recrystallized germanium. Hence it may be concluded that the junction runs very close to what was the liquid–solid interface at 600°C. Initially, the recrystallization forms an overgrowth or continuous layer which includes numerous large pits. X-ray dif-

fractions confirmed that the overgrowth region is a crystallographic continuation of the underlying seed crystal. The overgrowth region appears to be thinnest in the [100] direction but can be as thick as 100 microns in other directions. In this (110) plane no correlation could be found between penetration of the alloy front and crystallographic orientation. The interpretation is hindered by the fact that
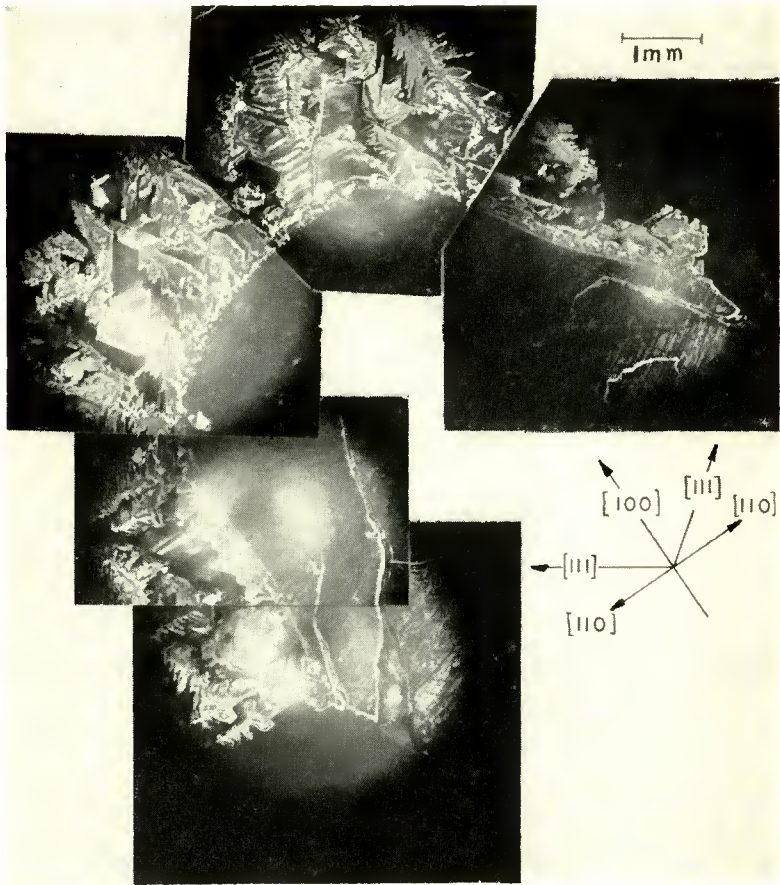

Fig. 6—Cross section of the specimen in a (100) plane. The p-n junction is the fine line, mostly white, at the base of the recrystallized region.

the initial boundary condition consisted of a flat plane intersecting a cylinder. A better resolution would have been obtained had a spherical surface been chosen instead of a cylinder.

A cut in the (100) plane, across one of the needles is shown in
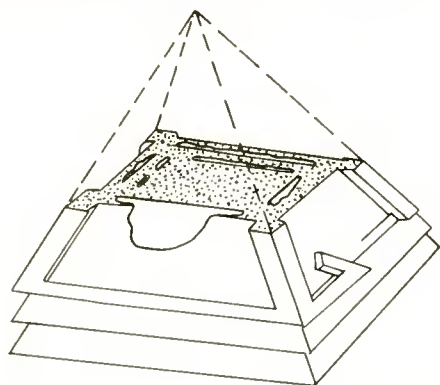
Fig. 7—Illustrating the internal appearance of a [100] needle.

Figures 7 and 8. These show how (111) facets are separated by empty spaces, the outer side of the (111) plate being more perfect than the inner side. As the solution is cooled, the concentration of germanium in solution increases radially away from the center of the crystalline needle so that the needle tends to grow towards those regions of the
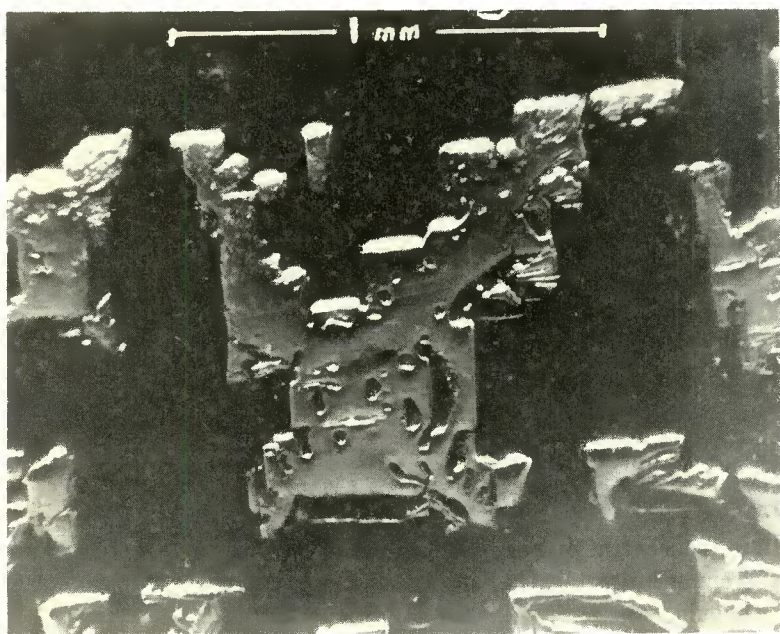

Fig. 8—Cross section of a [100] needle in a (100) plane. Note the increased pitting due to the acid etch at the extremities remote from the center of the needle.

solution which are richest in germanium. As crystallization proceeds, more indium atoms get trapped in the newly formed layers. As shown in Figure 8, the extremities of the recrystallized region exhibit more pits due to acid etching than the center. This suggests a faster etching rate, which would confirm the hypothesis of greater defect concentration in the last material to crystallize. S. M. Christian of these Laboratories has observed that there is a limit to the number of indium atoms which can be included in the germanium lattice, and that for maximum
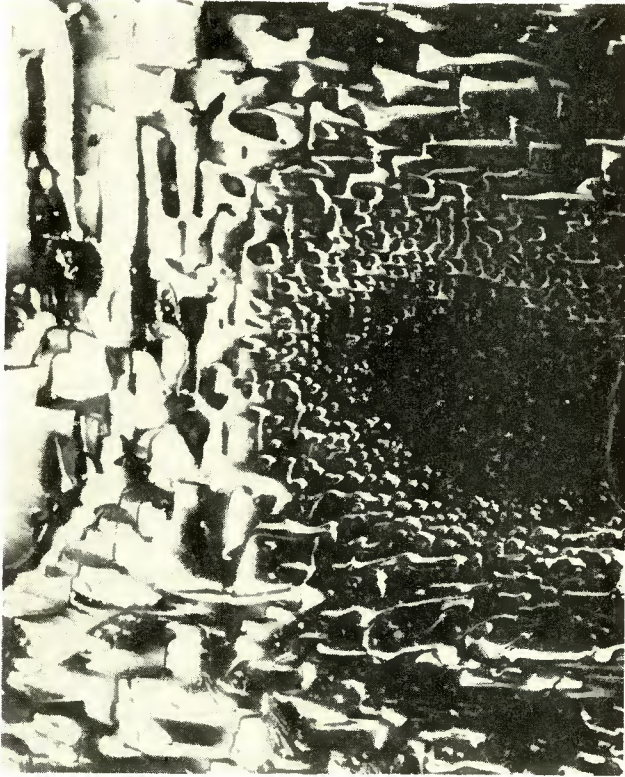
Fig. 9—Cross section of most of the crystal in the (100) plane. The dark oval shaped region is the parent crystal. The pitted region is the recrystallized germanium.

indium concentration the specific resistivity of the material is about 0.003 ohm-centimeter, the material remaining a semiconductor. Hence one should expect that in the present experiment the recrystallized germanium is still a semiconductor and has a resistivity of about 0.003 ohm-centimeter.

Figure 9 shows a cross-section of the whole crystalline system in

the (100) plane after a light etch which was sufficient to reveal the junction. The original crystal is the lightly pitted oval shaped region. The size and number of pits increases radially. The p-n junction, not visible on the photograph, runs along the inside of the inner ring of coarse pits.

Figures 10 and 11 show long etch lines which wave about the |100] axis. At 45 degrees to the [100] axis, a fine structure of line spreads on either side of the central etch line and coincides with (111) planes.

Figure 12 is a cross section in the (100) plane. It shows that the recrystallization is more homogeneous and thicker in the |110| direc-
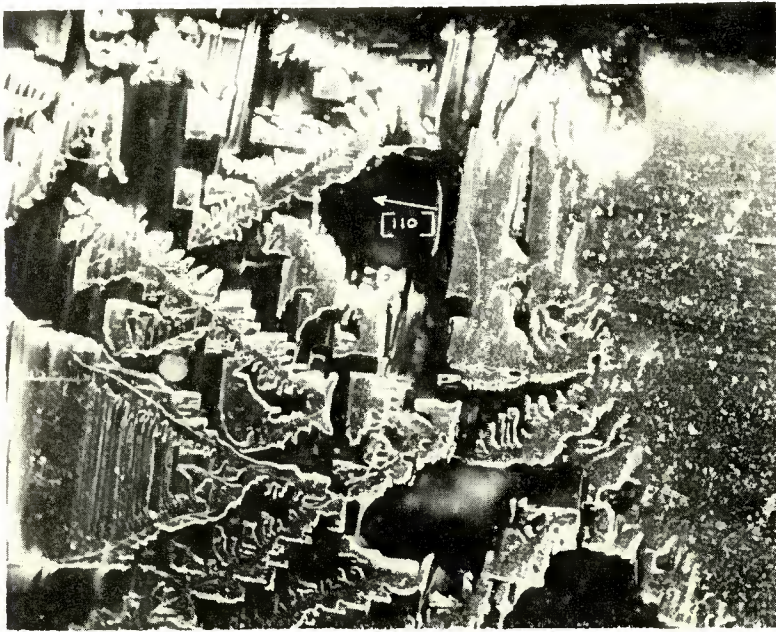
Fig. 10—Cross section of a recrystallized region in the (100) plane. The parent crystal is at the right. Note the thick overgrowth region in the [110] direction (arrow), and at the lower left-hand corner the stack of (111) facets appearing in cross section.

tion than in the [100] direction. This photograph also shows that the p-n junction is nearly a straight line in the (110) plane.

THE PRACTICAL CASE

In making alloy-type junctions, a pellet of indium is fused to the flat surface of a germanium wafer. The liquid–solid interface assumes
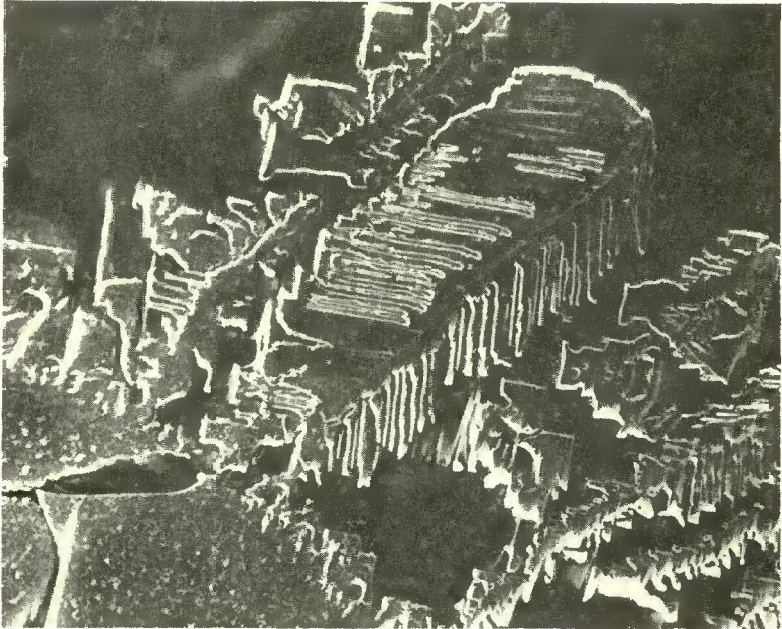
Fig. 11—Cross section of another recrystallized region in the (100) plane showing cross section through a [100] needle. Note the long etch line, the line structure at 45 degrees to it, and the stack of (111) plates.

Fig. 12—Cross section of still another recrystallized region in the (100) plane. The arrow points to the p-n junction. Note that the overgrowth layer is thicker in the [110] direction than in the [100] direction.

a concave configuration. Now, recrystallization can take place from the seed surface inward (instead of outward as in the case described above). Germanium from the supersaturated solution condenses into well-ordered overlapping plates lying in (111) planes (see Figure 13). Regions which have not been wetted properly remain at the original level of the crystal surface or protrude from the concave bottom and are seeds for bulkier recrystallization, i.e., the recrystallized material in these regions forms an assemblage of octahedrons instead of (111)
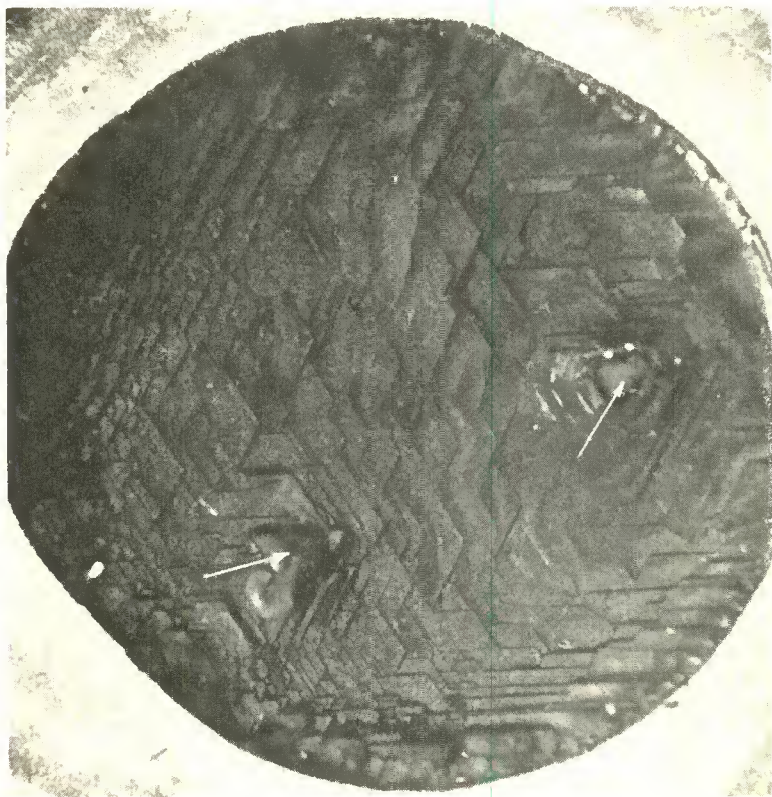
Fig. 13—Photograph of the recrystallized region at the collector of a p-n-p transistor. The zig-zagging pattern is formed by the exposed edges of overlapping (111) plates. The arrows point to poorly wetted regions.

plates. When the indium wets uniformly a germanium surface which has been exposed as a (111) plane, the recrystallized (111) plates tend to grow together to form a homogeneous recrystallized region.

A DEMOUNTABLE VACUUM SYSTEM FOR ELECTRON-TUBE DEVELOPMENT*

By

T. M. SHRADER

Tube Division, Radio Corporation of America,
Harrison, N. J.

Summary—This paper describes a demountable vacuum system for use in the development of electron tubes, particularly those requiring associated external circuit elements. In this system, the experimental tube and circuit elements are mounted on circular metal disks and sealed into circular openings in five sides of a cubical metal test chamber. This arrangement provides unusual flexibility in concentration of equipment in and around the test chamber. The chamber is connected through its remaining side to a high-speed exhaust system consisting of an oil pump, an oil-diffusion pump, and a liquid-air trap. Low vacuum pressures are very rapidly attained by "freezing out" the condensible gases on surfaces at liquid-air temperature. Savings of up to 50 per cent can be effected in the time and the cost required for tube development by the use of this system.

INTRODUCTION

THE time and cost required for electron-tube development has increased in recent years in about the same proportion as the complexity of tube operation. Such development, however, could be accomplished in less time and at much lower cost with the use of improved demountable vacuum equipment, or "bell-jar" equipment, as it is commonly called. The following disadvantages were common to most of the demountable systems used in the past:

(1) Lack of flexibility in the concentration of proper tube and circuit elements in and around the vacuum chamber.
(2) The extreme cleanliness required in the preparation and handling of parts to be placed in the vacuum chamber.
(3) The length of time required to start and stop operation of the exhaust system between experiments.
(4) The difficulty in obtaining a vacuum pressure low enough for electron emitters to be activated and operated for periods of time without deterioration of emission.

The demountable vacuum unit described in this paper retains all of the desirable features of previous systems, but eliminates the unde-

---

* Decimal Classification: 533.85.

86

sirable features listed above. This system provides unusual flexibility for the arrangement of tube elements and equipment in and around the test chamber. Vacuum pressures of 5×10^{-7} millimeter can be attained in 10 minutes even under very unfavorable conditions. Electron emitters can be activated, excellent emission obtained, and tubes operated for prolonged periods of time without deterioration of emission.
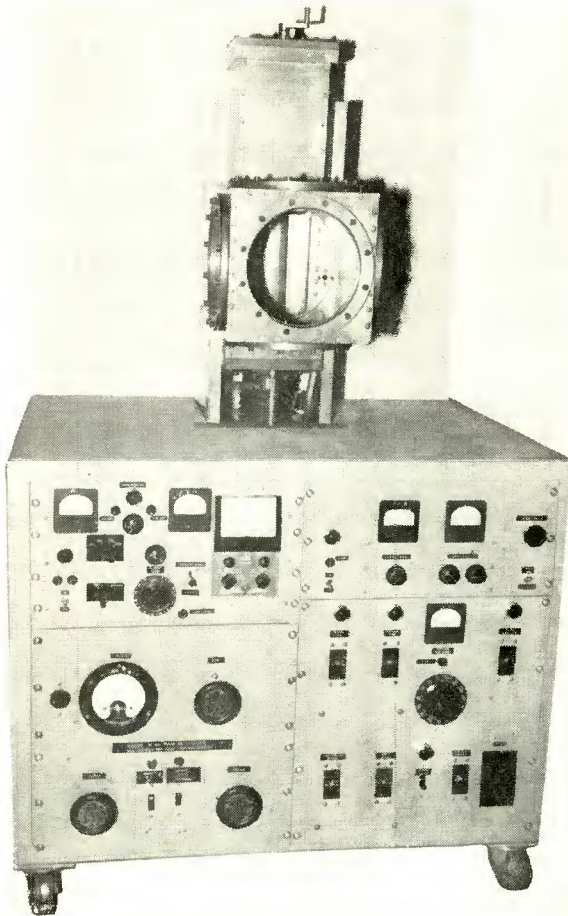

Fig. 1—Photograph of demountable vacuum unit showing test chamber and control panel.

New Demountable System

A front-view photograph of the new demountable vacuum unit is shown in Figure 1. The front panel of the cabinet contains the elec-

trical controls for a Pirani gauge, an ionization gauge, a magnet, and a power source. Two upright support guides on top of the cabinet hold a cubical box toward the front of the cabinet and a long box toward the rear. The cubical box toward the front of the cabinet is the test chamber in which the tube elements are inserted for experimental tests. The long box toward the rear of the cabinet is the pump manifold. This long box supports a number of small valves and interconnecting pipes, a pressure wheel, and a small crank. An oil-diffusion pump is located below the manifold. All of the equipment supported on the upright guides can be raised or lowered by means of the jack screw below the test chamber.

TEST CHAMBER

The cubical test chamber and the pump manifold are shown in Figure 2. The test chamber is demountable with respect to the pump manifold. During operation, the test chamber is sealed to the manifold with a rubber gasket and held in place with bolts through its flange. A large opening in the side of the cubical box attached to the vacuum unit provides for unimpeded flow of gases from test chamber to pump manifold. The remaining sides of the cubical test chamber have circular openings which comprise most of each face area. Into these openings are sealed round plates upon which the tube and circuit elements required for a particular development have been mounted. Such parts as the tube elements, power leads, input circuits, magnet pole pieces, and tuning or adjusting mechanisms are bolted to or inserted through the plates. Vacuum-tight seals are made between the parts and the plates with the aid of soft solder or rubber gaskets.

Typical examples of assemblies mounted on plates for insertion in the test chamber are shown in Figure 3. The plates are sealed to the openings in the sides of the test chamber. If desired, a plateglass viewing window can be sealed in any of the openings. Typical setups for operating a magnetron in the test chamber are shown in Figure 4. In the setup shown in Figure 4, the tube elements, the power-output waveguide, the magnet pole pieces, the tuning mechanism, and the water-cooling pipe are mounted on the plate at the right. The magnetic field for the magnetron is supplied through the top and bottom plates. A tuning shaft is inserted through the plate to the left, and a plateglass viewing window is sealed in the front opening.

With this system, there is no tendency to accumulate a large amount of fixed equipment. Blank plates are supplied for each major development and, upon completion of the experiments, the plate assemblies are stored as part of the particular program. Setup time and cost

for such programs is substantially reduced by the use of accessories such as universal mounting plates, tuning mechanisms, micrometer-screw movements, and power leads.

The test chamber can be removed from the pump manifold if it is more convenient to assemble equipment at another location. If desired, a different chamber may also be substituted for the test chamber for use with the pump system. The test chamber, manifold, plates, and
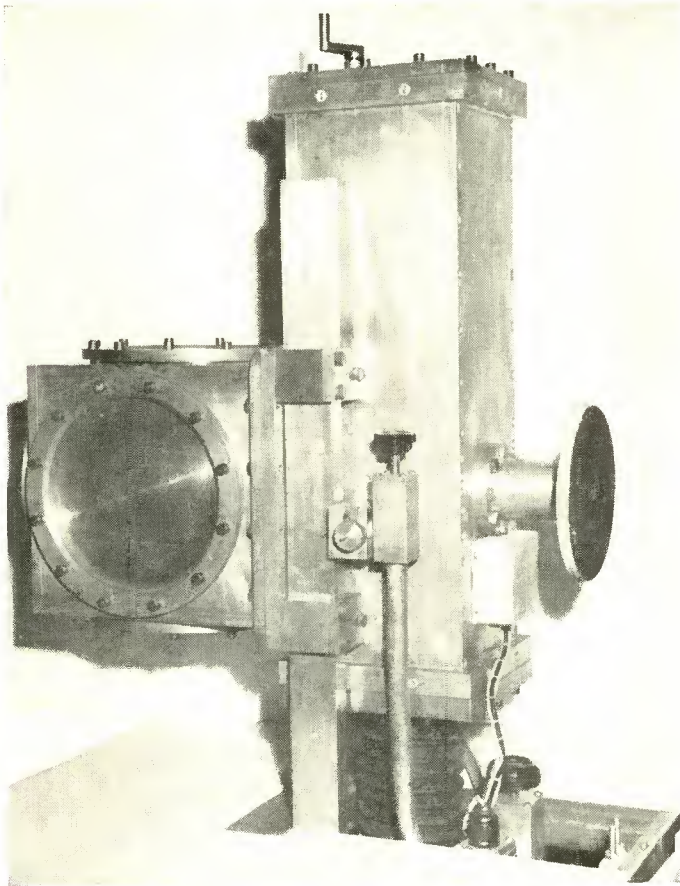

Fig. 2—Top part of demountable unit showing pump manifold at the right and test chamber at the left.

supports are made of brass to prevent distortion of magnetic fields and to facilitate soldering.

ACCESSORIES

A number of accessories developed for use with the demountable

vacuum system are shown in Figure 5. These accessories are identified below:

1. A useful, adjustable stand for holding the blank plates or universal plates while equipment is being mounted.
2. A heat-insulating cylinder which converts the test chamber into a high-temperature oven. The cylinder is water-cooled on
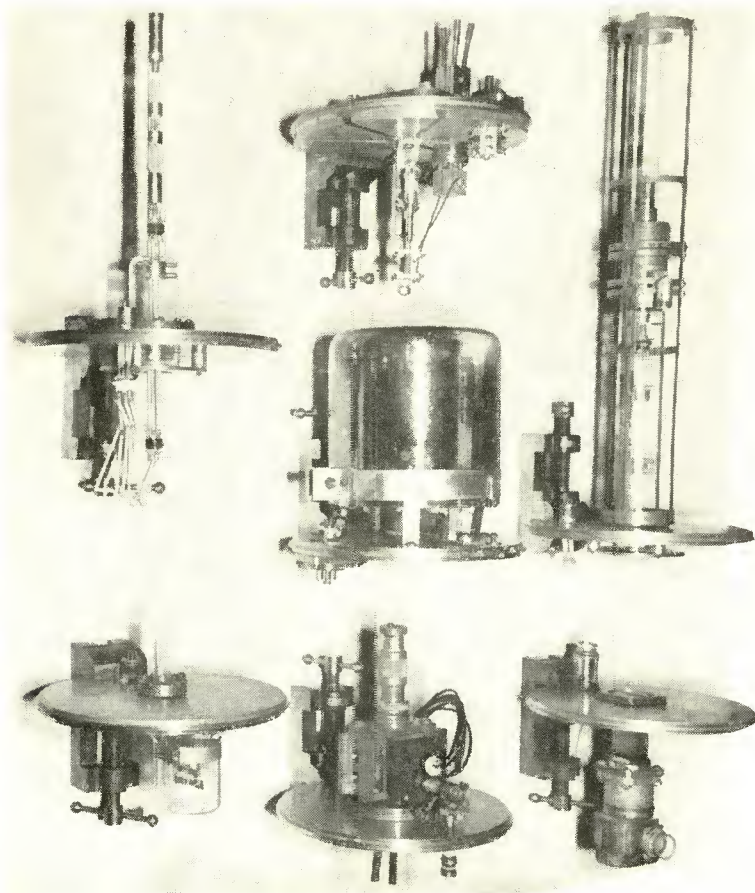

Fig. 3—Typical test assemblies mounted on plates.

the outside and contains a series of heat-reflecting cylinders on the inside. Heat insulation at the end is provided by reflecting disks mounted on the universal plates sealed in the test chamber near the ends of the cylinder. The heating coils and holding fixtures are mounted on the same universal plates.
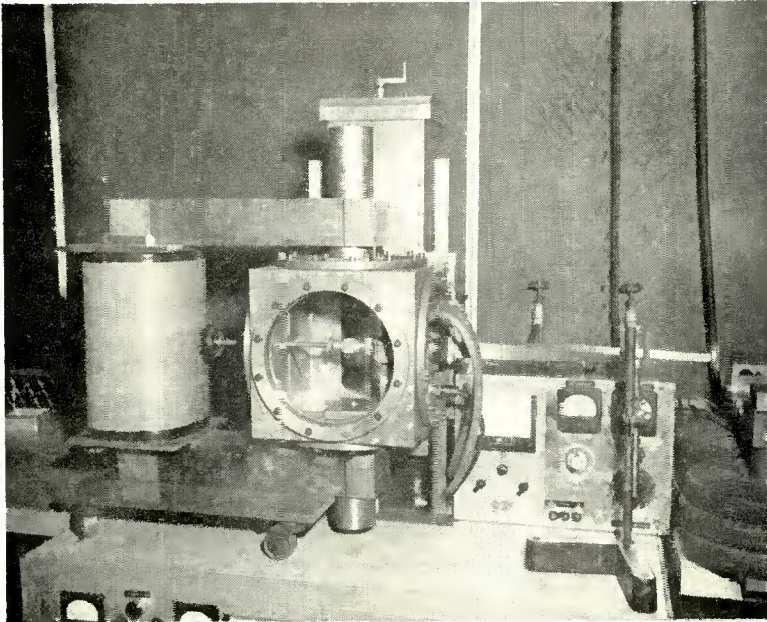
Fig. 4—Typical setup for operating magnetron in test chamber.
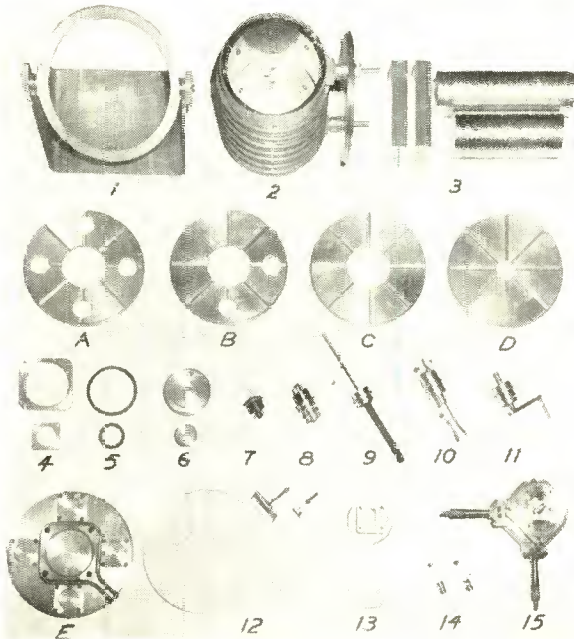

Fig. 5—Accessories for use with demountable system.

3. Pole pieces for use with the large magnet accessory shown in Figure 4. The pole pieces seal into universal plates and carry the magnetic field inside the test chamber.

A, B, C, and D. Universal mounting plates. T-grooves for holding mounting screws radiate from the center of the plates. Various hole combinations are provided for the insertion of smaller accessories.

E. The reverse side of an A-type plate showing blank disks (6) sealed in with rubber gaskets (5) and compression plates (4). A rectangular formed pipe for water-cooling the plate is also shown.

4. Compression plates for use in sealing disks or tube parts to blank plates or universal plates.

5. Rubber gasket for use in sealing components to plates.

6. Blank disk on which tube and circuit components can be mounted for sealing in the holes in plates.

7. A standard metal-type receiving-tube stem and base which seals into the universal plates in a manner similar to the blank disks. This stem-and-base assembly provides an expendable unit having eight leads for use in assembling and testing many small tube elements.

8. A similar stem and base which provides convenient terminals inside the test chamber and a tube-base terminal outside the chamber.

9. A useful devise for moving elements inside the test chamber during testing. The rubber tubing over the portion of rod outside the test chamber provides the vacuum seal. The portion of rod outside the chamber can be twisted, pulled, pushed, or moved from side to side, giving a corresponding motion to the portion of rod inside the test chamber.

10. Two water-cooled 500-ampere leads having heavy terminals inside and outside the test chamber.

11. A shaft which provides continuous rotation or in-and-out movement, useful for tuning and adjusting.

12. Glass disks which can be sealed in as viewing windows, and mirrors which can be mounted inside the test chamber.

13. Microwave power-output windows.

14. A pair of small micrometer-screw drive units which can be mounted in any position inside the test chamber and operated by flexible shaft from the outside.

15. A positioning device which seals into the large center hole of the universal plates. The center post extending from the device

can be positioned anywhere within a square-inch area by means of the two micrometer screws extending at right angles from it. Tube elements mounted on the center post, therefore, can be adjusted with micrometer accuracy with respect to other stationary elements.

VACUUM-PUMP SYSTEM

The pump system, shown in Figure 6, consists of a cylindrical liquid-air container in the center of the manifold and, below it, an oil-diffusion pump backed by a mechanical oil pump. The cone-shaped shield at the lower end of the liquid-air container serves as a condensing baffle which prevents diffusion-pump oil from entering the test chamber. The ionization gauge is mounted at the back of the
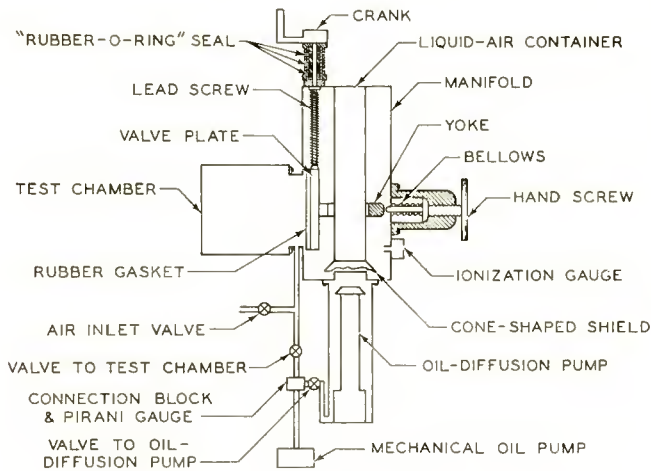
Fig. 6—Diagram of unit showing pump system.

manifold, and the Pirani gauge in the connection block to the backing pump. There is a small valve between the Pirani gauge and the diffusion pump and another between the Pirani gauge and the test chamber. An air-inlet valve is mounted on the connection between the Pirani gauge and the test chamber. The crank outside and at the top of the manifold turns a lead screw which raises or lowers a large valve plate over the opening between the manifold and the test chamber.

A rubber sealing gasket is imbedded in the face of the manifold valve plate. When changes in setup are desired, the test chamber is sealed off from the manifold by lowering the manifold valve plate over the opening and applying pressure with the hand-operated screw out-

side and to the rear of the manifold. The pressure is transmitted through a bellows, which maintains a vacuum seal, and a yoke around the liquid-air cylinder.

The operation of the pump system is unusual. Approximately 90 per cent of the gases evolved from the test chamber are not pumped out, but are frozen out on the surface of the liquid-air cylinder. It has been discovered that practically all of the gas given off in the test chamber from a typical setup is condensable and can be frozen out at a very high rate. The average "freezing-out" rate for the area exposed to the test chamber is about 2000 liters per second. Experience has shown that these condensable gases, such as water vapor, oil vapor, perspiration, and carbon dioxide, are the most damaging to electron-emitting surfaces.

The remaining, noncondensable gases are removed by the relatively small oil-diffusion pump. A pressure of 5×10^{-6} millimeter has been found adequate to activate electron emitters, obtain excellent emission, and operate tubes for prolonged periods of time without deterioration of emission. This pressure is probably that of the noncondensable gases; the pressure for the condensable gases must be much lower.

When it is desired to make changes in the experimental setup, the test chamber is opened by closing the manifold valve and opening the air-inlet valve. After the changes have been made and the plates sealed in the test chamber, the air-inlet valve is closed, the small valve to the diffusion pump is closed, the small valve to the test chamber is opened, and the test chamber is given a rough exhaust with the mechanical oil pump. The small valve to the diffusion pump is then opened, the manifold valve is opened, the small valve to the test chamber is closed, and final exhaust is completed. The pressure indications on the Pirani gauge determine the timing for these operations. A pressure of 5×10^{-6} can be attained in the test chamber in about 2 minutes. The final pressure, which is much lower and averages 5×10^{-7}, can usually be attained within 10 minutes.

No special precautions are required in the cleaning and handling of parts placed in the test chamber. Parts made in the shop can be cleaned once in an oil solvent, assembled in the chamber, and tested. Small quantities of rubber, bakelite, or spaghetti insulation used in the chamber have little effect when the chamber is pumped to a pressure of 5×10^{-6}; the pumping time required to attain a pressure of 5×10^{-7}, however, is increased.

TRANSMISSION-LINE ANALOG OF A MODULATED ELECTRON BEAM*†

By

S. BLOOM AND R. W. PETER

Research Department, RCA Laboratories,
Princeton, N. J.

Summary—The differential equations describing the amplitude of the space-charge waves propagating along a laminar-flow, single-velocity electron beam are found to be identical with those describing electromagnetic wave propagation along a transmission line. Thus the investigation of wave propagation along such beams can be replaced by a study of the equivalent transmission line. Since line theory has been developed so extensively, this analogy provides convenient conceptual aids. Many well-established characteristics of transmission lines, such as impedance transformation, filter behavior, and matching properties can be applied directly to the study of beams.

Furthermore, knowing the d-c voltage and current, beam diameter, and metal-boundary geometry, one can construct a transmission-line model of the beam. The standing wave experimentally measured along the line then represents the amplitude pattern of the beam waves. In this way the line model serves as an analog computer for the solution of complicated wave-propagation problems.

The example chosen for testing the practical usefulness and accuracy of such a computer was that of space-charge-wave propagation through a planar diode, including the effects of an average initial d-c electron velocity. The agreement between the computed and measured standing-wave patterns was within the measuring accuracy.

The transmission-line terminology allows us to put the matrix equations of the planar diode into a particularly simple form. It is shown that under usual conditions of operation the diode is an essentially exponential impedance transformer.

INTRODUCTION

THE propagation of small perturbations along a uniform cylindrical electron beam moving in a field-free concentric drift tube has been described by Hahn[1] and Ramo.[2] Their analyses show that in each mode of space-charge-wave propagation, two waves are possible, one traveling slightly faster and one traveling slightly slower than the average beam current. Interference of the two waves along

---

[1] W. C. Hahn, "Small Signal Theory of Velocity-Modulated Electron Beams," *Gen. Elec. Rev.*, Vol. 42, p. 258, June, 1939.
[2] S. Ramo, "Space Charge and Field Waves in an Electron Beam," *Phys. Rev.*, Vol. 56, p. 276, 1939.

a modulated beam may result in standing space-charge waves. The properties of wave propagation along a uniform drifting beam can be described by a matrix[3] which is similar in form to the wave-propagation matrix for a uniform transmission line. L. J. Chu,[*] of MIT, suggested the substitution of an a-c potential V for the a-c velocity component in the beam to make the two matrices formally identical.

The present study shows that such a formal analogy also holds for the general cases of nonuniform lines and beams. It is found that the differential equations governing the wave propagation along an arbitrary laminar-flow electron beam and along a lossless nonuniform transmission line are identical within certain limits.

The study of space-charge waves, therefore, can be placed within the more familiar and better established framework of standard transmission-line theory. Thus, the concepts of impedance, reflection coefficient, matching, etc., can be applied directly to beams. Also, the band structure of transmission-line filters is entirely analogous to the amplification or de-amplification regions of an electron beam with periodically varying impedance.[4]

Furthermore, in those cases in which the beam parameters vary in too complicated a way to permit an analytical attack, the transmission-line analogy permits the construction of an equivalent line-model to act as an analog computer. The standing-wave experimentally measured along the line then represents the amplitude pattern of the space-charge wave along the beam.

TRANSMISSION-LINE ANALOG

The system being considered is a simple one, consisting of a laminar-flow single-velocity electron beam upon which is impressed a sinusoidal perturbation. This disturbance excites axial oscillations in the plasma, which, since the beam is moving, appear as space-charge waves. We shall not be concerned with the mechanism of excitation, nor with any external wave-carrying circuits upon which the fluctuating stream might interact. Thus the analysis of this steady-state situation may proceed entirely from the ballistic equations of the beam.

In the usual manner, the equations will be linearized by means of

---

[3] See e.g., p. 23 of: First Quarterly Report (May-July 1951), Contract No. DA36-039-sc-5548.

[*] Paper given at the I.R.E. Conference on Electron Tubes, Durham, N.H., 1951.

[4] R. W. Peter, S. Bloom, and J. A. Ruetz, "Space-Charge-Wave Amplification Along an Electron Beam by Periodic Change of the Beam Impedance," *RCA Review*, Vol. XV, p. 113, March, 1954.

the small a-c signal approximation. For the steady state, all a-c quantities vary with the signal (or noise) perturbation frequency ω, as $e^{j\omega t}$. Finally, a sufficiently strong axial magnetic field is assumed to confine all motion to the z direction.

If the a-c quantities are written in the form

$$v_{ac}(z, t) = v'(z)\, e^{j\omega t}, \quad \text{etc.},$$

then the a-c force equation reads

$$\eta E' = j\omega v' + \frac{d}{dz}\,(v'v_0) \tag{1}$$

where $v_0(z)$ and v' are the d-c and a-c velocities and $\eta = e/m$. Since the beam is assumed to be externally open-circuited to a-c, the total a-c current (convection plus displacement) is zero:

$$I' + j\omega\epsilon_0\sigma E' = 0. \tag{2}$$

Here $I' = \sigma i'$ is the total a-c convection current, σ the cross-sectional area, and ϵ_0 the dielectric constant. The small-signal a-c current density i' is

$$i' = \rho_0 v' + v_0\rho', \tag{3}$$

where ρ_0 and ρ' represent the d-c and the a-c charge density, respectively. Finally, for slow variations of the area $\sigma(z)$ along the beam, the equation of continuity reads

$$\frac{1}{\sigma}\,\frac{dI'}{dz} + j\omega\rho' = 0. \tag{4}$$

This is the same type of approximation as is used, for example, in treating wave propagation in slowly flaring acoustical horns.

Eliminating the electric intensity E' from Equations (1) and (2), and ρ' from Equations (3) and (4) we find

$$\left(\frac{j\eta}{\omega\epsilon_0\sigma}\right) I' = j\omega v' + \frac{d}{dz}\,(v'v_0) \qquad \text{and}$$

$$v_0\,\frac{dI'}{dz} = j\omega\sigma\rho_0 v' - j\omega I'. \tag{5}$$

The usual procedure at this point is to eliminate either I' or v' and to solve the resultant second-order equation for the particular beam being considered. A different procedure will be followed here. To establish the analogy between beam and line, it is necessary to substitute an a-c potential for the a-c velocity. We let

$$v' = v e^{-j\omega \int^z \frac{dz}{v_0}}, \text{ etc.,} \qquad (6)$$

and attribute an a-c potential V to the a-c velocity v, defined on a small-signal a-c energy basis:

$$2\eta \left(V_0 + V \right) = (v_0 + v)^2 = v_0^2 + 2v_0 v$$

or

$$V = \frac{v_0\, v}{\eta}. \qquad (7)$$

Equations (5) then reduce to

$$\frac{dV}{dz} = \left(\frac{j}{\omega\epsilon_0\,\sigma} \right) I$$

$$\qquad (8)$$

$$\frac{dI}{dz} = \left(\frac{j\omega I_0}{2\, v_0 V_0} \right) V$$

where $I_0 = \sigma\, i_0$ is the total d-c current, and V_0 the d-c beam voltage.

So far our treatment holds for a one-dimensional beam only, i.e., a beam in which the electric field has components only in the direction of electron flow.

The equations can be modified, however, to hold for finite diameter beams if we introduce one further approximation. From the work of Hahn and of Ramo it is known that the effect of a finite beam diameter and of a surrounding metal shield is to increase the stray transverse field, thereby decreasing the longitudinal field. This increases the plasma wavelength, or effectively replaces the infinite-beam plasma frequency

$$\omega_{p\infty} = \sqrt{\frac{\eta\,\rho_0}{\epsilon_0}} = \sqrt{\frac{\eta\, I_0}{\epsilon_0 v_0 \sigma}} \qquad (9)$$

by a reduced value

$$\omega_p = p\,\omega_{pz}, \qquad 0 \leqq p \leqq 1. \tag{10}$$

The plasma-frequency reduction factor p is a function of $\omega s/v_0$, the ratio a/s of shield-to-beam radius, and of the radial mode of propagation. Even though p is obtained from Ramo's analysis only for a drifting beam, Parzen[5] has shown that, to a good approximation, this factor may be used in calculating geometric effects upon an accelerated stream, by taking into account the variation of $\omega s/v_0$ along the beam. Thus, according to Equation (9), we introduce the p factor by replacing the dielectric constant ϵ_0 by its effective value ϵ_0/p^2. Then Equations (8) become

$$\frac{dV}{dz} = \left(\frac{jp^2}{\omega\epsilon_0\sigma} \right) I$$

$$\frac{dI}{dz} = \left(\frac{j\omega I_0}{2\,v_0 V_0} \right) V. \tag{11}$$

It is to be noted that Equations (11), as well as (8), describe only the amplitude envelope of the space charge waves, i.e., the amplitude modulation along the z-axis of the electronic wave represented by the factor

$$e^{j\omega t \,-\, j\omega \int \frac{dz}{v_0}}.$$

Equations (11) are of the same form as those describing a lossless nonuniform transmission line:

$$\frac{dV}{dz} = j\,X\,I$$

$$\frac{dI}{dz} = j\,B\,V. \tag{12}$$

In analogy, therefore, one can attribute to the beam a series reactance and a shunt susceptance per unit length

---

[5] P. Parzen, "Space-Charge Wave Propagation in a Cylindrical Electron Beam of Finite Lateral Extension," *Jour. Appl. Phys.*, Vol. 23, p. 215, February, 1952.

$$X \equiv 2 \frac{V_0}{I_0} \frac{\omega}{v_0} \left(\frac{\omega_p}{\omega} \right)^2 = \frac{p^2}{\omega \epsilon_0 \sigma}$$

(13)

$$B \equiv \frac{I_0 \omega}{2 v_0 V_0} = \frac{\omega \epsilon_0 \sigma}{p^2} \left(\frac{2\pi}{\lambda_p} \right)^2$$

where λ_p is the effective plasma wavelength. Figure 1 depicts a general electron beam and its equivalent transmission-line analog. The shunt capacitance/meter, C, is seen to have the form of a capacitance of a parallel-plate capacitor of area σ. The increase in capacitance due to stray fields outside of the finite beam is indicated by the factor ϵ_0/p^2.
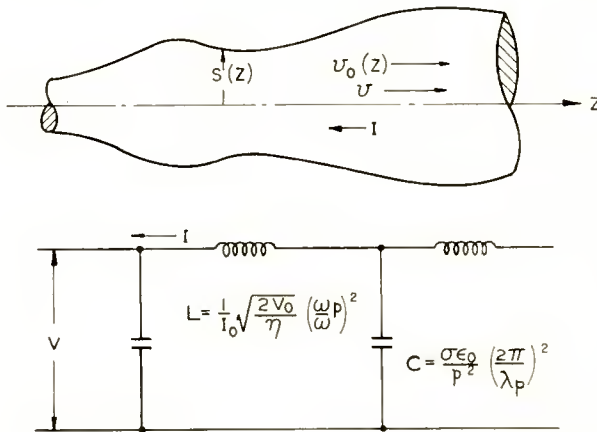
Fig. 1—Transmission-line analog of an electron beam.

In further analogy to practice in transmission line theory, we use an altered form of Equations (12), containing two new parameters: the phase

$$\beta \equiv \sqrt{X B} = \frac{2\pi}{\lambda_p} = \frac{\omega_p}{v_0}$$

(14)

and the characteristic impedance

$$W \equiv \sqrt{\frac{X}{B}} = 2 \frac{V_0}{I_0} \frac{\omega_p}{\omega}.$$

(15)

Thus, on going to the new independent variable

$$\phi \equiv \int \beta(z)\,dz, \tag{16}$$

we find

$$\frac{dV}{d\phi} = j\,W\,I$$

$$\tag{17}$$

$$\frac{dI}{d\phi} = j\,W^{-1}\,V.$$

We see, then, that the equations describing the wave propagation along an electron beam of variable d-c parameters are formally identical with those of a transmission line of variable characteristic impedance $W(\phi)$. The line Equations (17) are not only simpler to handle in many cases but, more importantly, the analog allows us to simulate complicated beams by a constructible transmission line and measure experimentally the standing-wave amplitude patterns excited on it. Thus, for example, a coaxial line, in which the inner conductor slowly changes its diameter in such a way as to correspond to $W(\phi)$ of the beam, can be probed for its standing-wave amplitude.

For computational purposes, the phase and impedance Equations ((14) and (15)) can be written as

$$\frac{\beta}{f I_0^{\frac{1}{2}}} = 5.815 \times 10^4 \left(\frac{p}{\gamma_0 s} \right) V_0^{-\frac{5}{4}} \tag{18}$$

$$W I_0^{\frac{1}{2}} = 1.101 \times 10^4 \left(\frac{p}{\gamma_0 s} \right) V_0^{\frac{1}{4}} \tag{19}$$

where β is in meters^{-1}, W in ohms, V_0 in volts, I_0 in milliamperes, and $f = \omega/(2\pi)$ in kilomegacycles. Figure 2 gives $p/(\gamma_0 s)$ as a function of $\gamma_0 s$ ($\equiv \omega s/v_0$) for various shield-radius to beam-radius ratios a/s and for the first three radial modes of wave propagation along a cylindrical electron beam.

For a specific beam, the radius s and the d-c voltage V_0 are known as functions of the axial position z, the parameters I_0, f, and mode being fixed. Thus $\beta(z)$ and $W(z)$ can be found along the entire elec-

tron beam. The phase angle $\phi(z)$ can also be found analytically or by a graphical integration.

Going now to the line analog, it is convenient to hold the phase velocity on the line fixed; thus $\beta_0 = \omega'/c$ where ω' is the signal frequency used on the line and c is the speed of light. The axial distance along the line, z', is thus related to that along the beam z, by

$$\phi(z) = \beta_0 z' = \frac{2\pi z'}{\lambda'}. \tag{20}$$

By means of this correspondence we can compute the impedance $W(z')$. These impedance values are then constructed by, e.g., suitably varying the diameter of the conductors in a coaxial line.
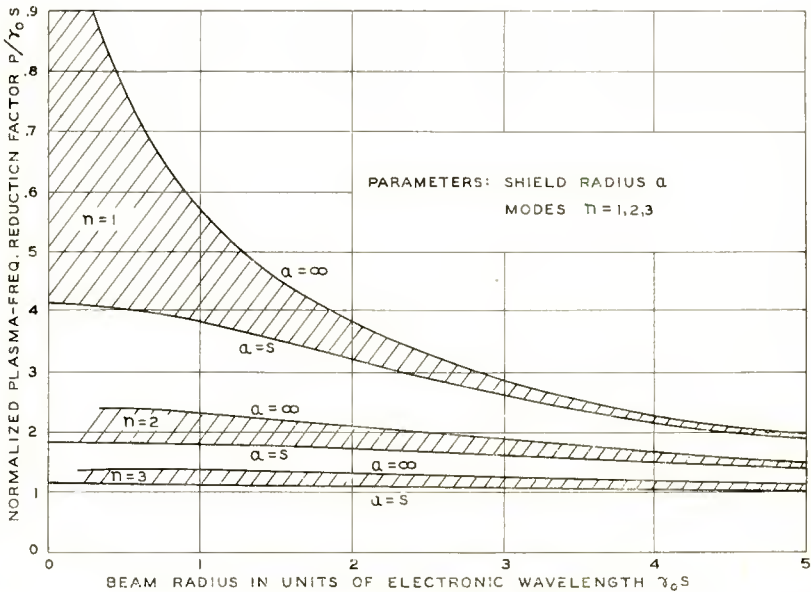
Fig. 2—For a beam of finite radius s, the effective plasma frequency is less than its infinite-beam value: $0 \leqslant p = \omega_p/\omega_{p\infty} \leqslant 1$. The reduction depends upon the value of the radius in units of the electronic wavelength, $\gamma_0 s$, upon the radial mode, n, and upon the radius of the surrounding metallic tube, a.

APPLICATION TO A PLANAR DIODE

To illustrate and test the accuracy of the transmission-line model as an analog computer, we study the propagation of space-charge waves

along the electron stream in a planar diode. This particular system is chosen since an exact analytical treatment is possible. We shall, therefore, first compute the amplitudes of the a-c current and voltage through an infinitely extended beam flowing between plane parallel electrodes; then the beam impedance, W, is computed as a function of the phase angle ϕ. From this, the analog line is constructed. Finally, the measured standing-wave amplitudes are compared with those calculated for assumed simple initial conditions.

Wave Propagation in the Planar Diode with an Initial D-C Velocity

The infinite planar diode is taken to be radio-frequency open-circuited so that the total a-c current density is zero. The analysis of the preceding section is therefore applicable. The space charge gives rise to the following equations of motion:

$$v_0 = \frac{kt^2}{2} + v_{01}$$

$$(21)$$

$$z = \frac{kt^3}{6} + v_{01}t$$

where $k \equiv \eta I_0/\epsilon_0$, I_0 being now defined as the total d-c current in a unit cross section of the beam, t is the transit time from $z = 0$ to z, and v_{01} is the average initial d-c (thermal) velocity. The origin is taken at the plane of the potential minimum, so that the entrant d-c acceleration is zero.

Since the beam is assumed to be infinite, $p = 1$ and by Equation (13) the beam reactance becomes simply $1/(\omega \epsilon_0)$, the area σ being now unity. Thus the line Equations (12) reduce to

$$\frac{d^2V}{dz^2} + \frac{kV}{v_0^3} = 0,$$

or, in terms of t, by Equations (21),

$$\frac{d^2V}{dt^2} - \frac{kt}{v_{01} + \dfrac{kt^2}{2}} \frac{dV}{dt} + \frac{k}{v_{01} + \dfrac{kt^2}{2}} V = 0.$$

This has the solution

$$V = At + B \left(\frac{kt^2}{2} - v_{01} \right)$$

and therefore, from Equation (12), the a-c current per unit area is

$$I = \frac{\omega \, \epsilon_0}{jv_0} \, (A + B \, kt).$$

Denoting values at $z = 0$ by subscript 1, the general solutions for the a-c current and a-c voltage are

$$I = \left(\frac{v_{01}}{v_0} \right) I_1 + \left(j\omega I_0 \frac{\eta t}{v_0 \, v_{01}} \right) V_1$$

$$(22)$$

$$V = \left(\frac{j \, v_{01} \, t}{\omega \epsilon_0} \right) I_1 + \left(1 - \frac{\eta I_0}{2\epsilon_0} \frac{t^2}{v_{01}} \right) V_1.$$

When written in terms of the a-c velocity, Equations (22) become identical with those of Llewellyn and Peterson[6] and of Smullin.[7]

It is convenient to write these equations in terms of the usual space-charge factor

$$\zeta = 3 \left(1 - \frac{T_0}{T} \right),\qquad (23)$$

where T is the transit time through the diode. In the absence of space charge ($\zeta = 0$), T becomes

$$T_0 = \frac{2D}{v_{01} + v_{02}},$$

D being the distance from virtual cathode to anode. Then, on denoting values at the anode by subscript 2, we obtain from Equations (21) the

[6] F. B. Llewellyn and L. C. Peterson, "Vacuum Tube Networks," *Proc. I.R.E.*, Vol. 32, p. 144, March, 1944.

[7] L. D. Smullin, "Propagation of Disturbances in One-Dimensional Accelerated Electron Streams," *Jour. Appl. Phys.*, Vol. 22, p. 1496, December, 1951.

following useful d-c relations:

$$v_{01} = v_{02} \frac{1 - \zeta}{1 + \zeta}$$

$$v_0 = \frac{v_{02}}{1 + \zeta} \left[2 \zeta \left(\frac{t}{T} \right)^2 + 1 - \zeta \right]$$

$$z = v_{02} \frac{t}{1 + \zeta} \left[\frac{2}{3} \zeta \left(\frac{t}{T} \right)^2 + 1 - \zeta \right] \qquad (24)$$

$$D = v_{02} T \frac{1 - \dfrac{\zeta}{3}}{1 + \zeta}, \qquad\qquad I_0 = \frac{4 \epsilon_0 v_{02}}{\eta T^2} \frac{\zeta}{1 + \zeta}.$$

With these inserted into Equations (22), there results

$$I = \left[\frac{1 - \zeta}{2 \zeta \left(\dfrac{t}{T} \right)^2 + 1 - \zeta} \right] I_1 + \left(\frac{4 j \omega \epsilon_0}{D} \right) \left[\frac{t}{T} \zeta \frac{\left(1 - \dfrac{\zeta}{3} \right) \dfrac{1}{1 - \zeta}}{2 \zeta \left(\dfrac{t}{T} \right)^2 + 1 - \zeta} \right] V_1$$

$$(25)$$

$$V = \left(\frac{jD}{\omega \epsilon_0} \right) \left[\left(\frac{t}{T} \right) \frac{1 - \zeta}{1 - \dfrac{\zeta}{3}} \right] I_1 + \left[\frac{1 - \zeta - 2 \zeta \left(\dfrac{t}{T} \right)^2}{1 - \zeta} \right] V_1.$$

Since the present discussion is for a beam of unit area, the characteristic impedance (Equation 15) has now the dimensions ohms/meter². By Equations (24), this impedance becomes

$$W = \frac{D}{2 \omega \epsilon_0} \frac{\left[1 - \zeta + 2 \zeta \left(\dfrac{t}{T} \right)^2 \right]^{\frac{3}{2}}}{\left(1 - \dfrac{\zeta}{3} \right) \sqrt{\zeta}}, \qquad (26)$$

or normalized to its value W_1 at the virtual cathode $(t = 0)$,

$$\frac{W}{W_1} = (1 + \tau^2)^{\frac{3}{2}} = \left(\frac{v_0}{v_{01}}\right)^{\frac{3}{2}}, \tag{27}$$

where

$$\tau \equiv \frac{t}{T}\sqrt{\frac{2\zeta}{1-\zeta}} = \frac{t}{T}\sqrt{\frac{v_{02}}{v_{01}} - 1}. \tag{28}$$

In terms of this new variable τ, the matrix Equations (25) for the planar diode take on a particularly simple form:

$$I = \left(\frac{1}{1+\tau^2}\right)I_1 + j\sqrt{2}\left(\frac{\tau}{1+\tau^2}\right)\frac{V_1}{W_1}$$

$$ \tag{29}$$

$$V = j\sqrt{2}\,\tau\,W_1\,I_1 + (1 - \tau^2)\,V_1.$$

To have convenient initial conditions, we choose the entrant a-c current I_1 to be zero. Then the a-c voltage has a zero at $\tau = 1$, which corresponds to the position along the beam

$$\left(\frac{z}{D}\right)_0 = 4\,\frac{1-\zeta}{3-\zeta}\sqrt{\frac{1-\zeta}{2\zeta}}. \tag{30}$$

The a-c current is a maximum at this point. For customary values of ζ (≈ 0.9) the voltage zero lies very close to the virtual cathode; when $\zeta = 1/3$ the zero is at the anode and when $\zeta < 1/3$ it falls beyond the anode. This is seen in Figure 3 where $|V/V_1|$ and $|I\,W_1/V_1|$ are plotted versus the relative diode position z/D. Because of the rapid increase in d-c velocity, it is seen that the a-c convection current can never reach zero again within the diode.

Design of a Line Analog of the Planar Diode

To construct the transmission-line model of the diode we need to know the beam impedance W as a function of the phase angle ϕ. This is, from Equations (14), (16), and (24),

$$\phi = \int_0^z \frac{\omega_{px}}{v_0}\,dz = 2\sqrt{\zeta}\int_0^{\frac{t}{T}}\left[1 - \zeta + 2\zeta\left(\frac{t}{T}\right)^2\right]^{-\frac{1}{2}}d\left(\frac{t}{T}\right)$$

or
$$\phi(\tau) = \sqrt{2} \ln (\tau + \sqrt{1 + \tau^2}). \tag{31}$$

With this ϕ, distances along the model, z', are correlated with those along the beam, z, by means of Equation (20). Thus the relative impedance, Equation (27), has the values along the line model shown in Figure 4. Only a finite portion of this curve, from $z'/\lambda' = 0$ to a maximum value of z'/λ', corresponds to the actual virtual cathode–anode distance of the diode. For different values of the space-charge factor ζ, this distance is indicated along the curve. For example, the impedance-
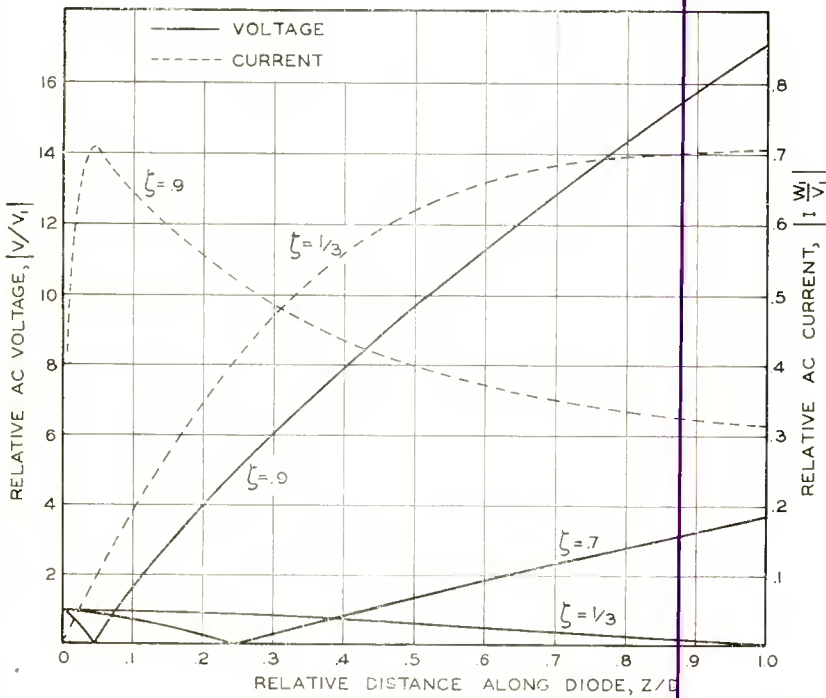
Fig. 3—The relative a-c voltage $|V/V_1|$ and a-c current $|IW_1/V_1|$ at relative positions z/D along a planar diode, for various space-charge factors ζ. The a-c current at the virtual cathode, I_0, is assumed to be zero.

characteristic along the line model of a $\zeta = .8$ diode is shown by the portion of the curve terminated by the point $\zeta = .8$. The relative distance along the model corresponding to the cathode–anode distance in the beam is then $z'/\lambda' = .395$.

Furthermore, for relative distances $z'/\lambda' \tilde{>} .4$, the planar diode represents an essentially exponential impedance transformer. This is evidenced by the dashed exponential curve in Figure 4.
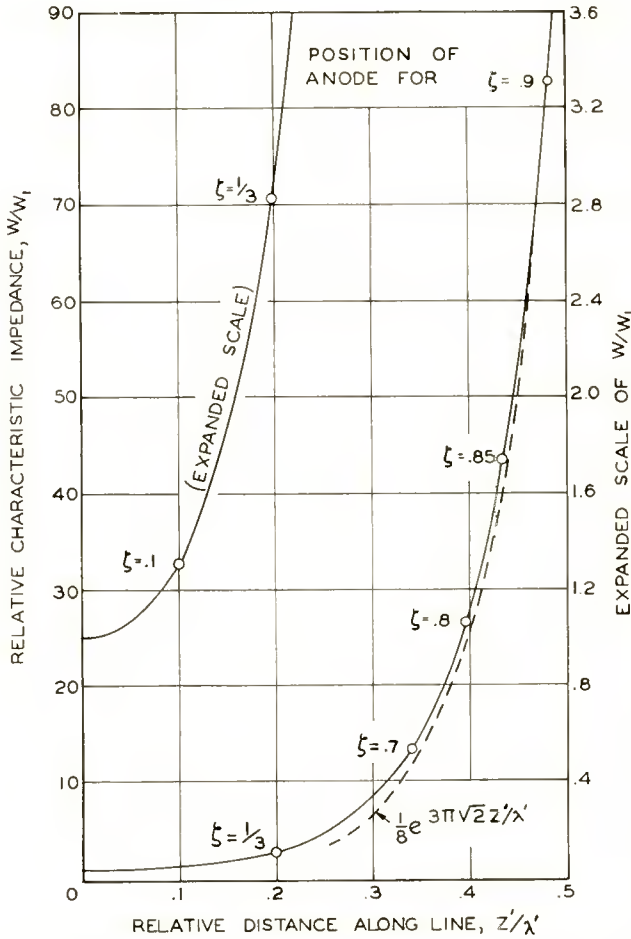
Fig. 4—The characteristic impedance W (in units of its value W_1 at the virtual cathode), versus the position z' (in units of the line wavelength λ') along the transmission line analog of a planar diode. The circles indicate the position of the anode for various space-charge factors ζ.

The relative a-c voltage and current standing waves along the line, as given by Equations (29) and (31), are shown in Figure 5.

It is interesting to note that the phase angle from the virtual

cathode to the position of the a-c voltage zero (current maximum) is
not 90 degress but rather

$$\phi_{(\tau=1)} = \sqrt{2}\,\ln\,(1 + \sqrt{2}) = 71.4 \text{ degrees.}$$
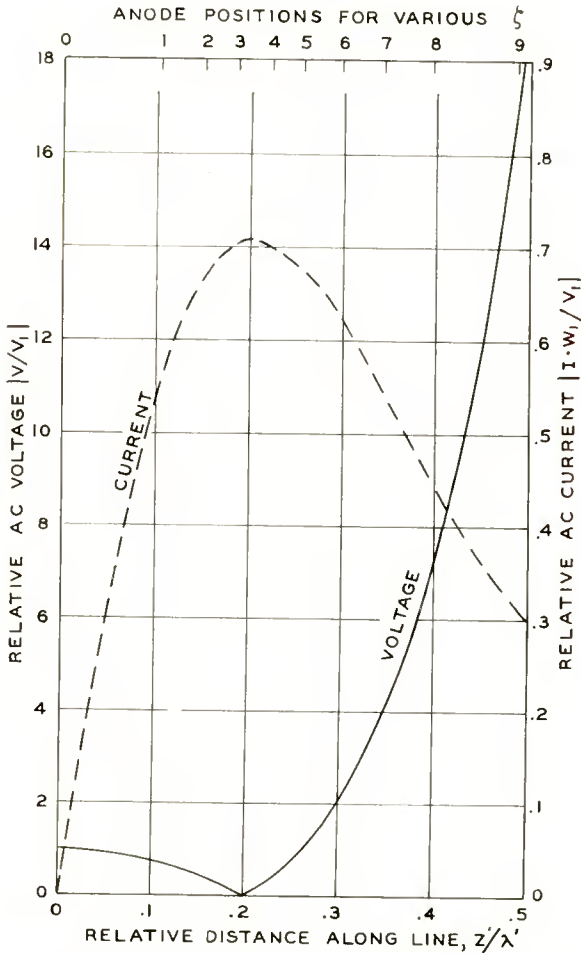
Fig. 5—Relative voltage and current standing waves along a line with the
relative impedances shown in Figure 4. Planar diodes with various space-
charge factors, ζ, are represented by different relative lengths of this
tapered line. A voltage maximum and a current zero were chosen as initial
conditions.

In other words, the varying impedance gives rise to reflections along
every point of the line which add up to produce a total phase loss of
18.6 degrees compared with a uniform line.

Construction of the Analog and Measurement

As a model, a coaxial transmission line with a tapered inner conductor was chosen. The impedance of such a line is proportional to log (b/a) where b is the radius of the outer, and a of the inner conductor. Since we are interested only in the relative a-c potential, V/V_1, the value of the constant of proportionality is chosen such as to effect a compromise between a value of a at the cathode (low impedance end of the diode) which is not too large, and a value at the anode which is not too small. Because of the assumed initial conditions, a sliding short-circuiting plunger is used to put an a-c current zero at the
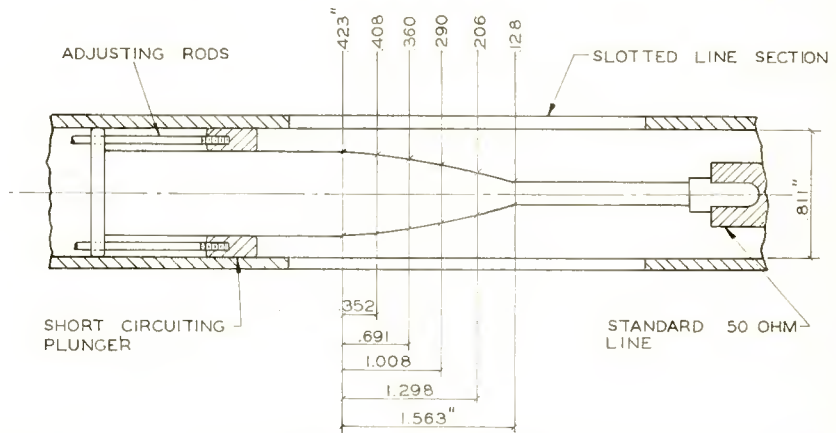
Fig. 6—Design of a coaxial-line model of a planar diode with space-charge factor $\xi = 1/3$.

cathode. The analog line is then probed for its voltage-standing-wave pattern, the measured electric field intensity, E, being converted to potential, V, by means of the known impedance values:

$$\frac{V}{V_1} = \left(\frac{E}{E_1} \right) \left(\frac{W}{W_1} \right)$$

The coaxial transmission line is an accurate analog of the electron beam only if the electric field in the line is purely transverse. Diameter changes of the conductors along the line cause local longitudinal fields. Their effect can be represented by local discontinuity susceptances.[8] To avoid disturbing effects from these susceptances the impedance gradient along the beam should not be too great. For this reason we

---

[8] Ramo and Whinnery, *Fields and Waves in Modern Radio*, John Wiley and Sons, New York, N. Y., p. 374.
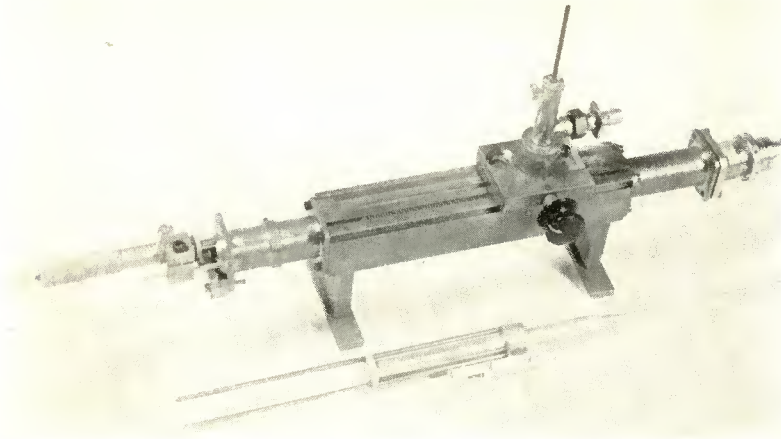
Fig. 7—Tapered inner conductor of line model and short-circuiting plunger, together with slotted line.

have chosen the case of space-charge factor $\zeta = 1/3$. Steeper beam-impedance gradients can, however, be represented in line models by the use of long line wavelengths and correspondingly long models.

Figure 6 shows the design of the diode analog; Figure 7 is a photograph of the tapered inner conductor and plunger together with the slotted line used in the experiments.
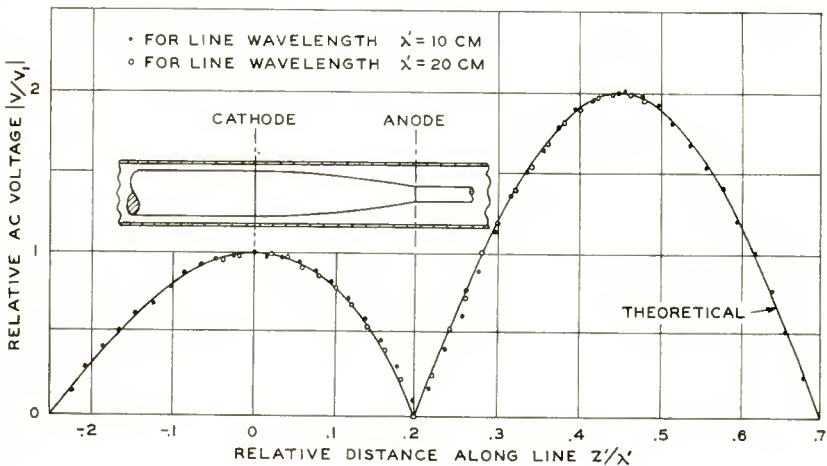
Fig. 8—Experimental values of the relative a-c voltage $|V/V_1|$ measured along two transmission-line models of a $\zeta = 1/3$ planar diode. Better agreement with the theoretical curve is obtained with the longer wavelength, i.e. shallower taper.

The experimental values of V/V_1 for the chosen case of $\zeta = 1/3$, are shown in Figure 8. For a line wavelength of $\lambda' = 10$ centimeters, the observed values are too high toward the anode end of the diode region and too low in the anode end of the following drift space. This discrepancy can be attributed to the curvature of the wavefronts arising from too steep a taper on the inner conductor; at a given probe position the field actually measured is that of an electric-intensity line originating from a point closer to the cathode. These geometrical effects were remedied by use of a longer line wavelength, $\lambda' = 20$ centimeters, and a correspondingly longer model. The agreement between measured and theoretical voltage-standing-wave ratios along the line was within measuring accuracy.

SPACE-CHARGE-WAVE AMPLIFICATION ALONG AN ELECTRON BEAM BY PERIODIC CHANGE OF THE BEAM IMPEDANCE*

By

R. W. Peter†, S. Bloom†, and J. A. Ruetz‡

Summary—The transmission-line analogy of an electron beam is used to show the common basis of all single-velocity space-charge-wave amplifiers (or dc-amplifiers). It is found that the "velocity-jump" amplifier, for example, is only one particular case of a whole group of amplifiers which operate by a periodic change of the "beam impedance." The impedance of a given beam can be altered by changing (a) the beam voltage, (b) the diameter of the surrounding drift tube or (c) the beam diameter. Consequently, there exist three basic types of space-charge-wave amplifiers and combinations thereof.

By relating periodic beams to periodic transmission lines, it is found that amplification or dc-amplification occurs wherever the filter-line analog would have a stop band. Existing data on the cutoff regions of filter lines can be used, therefore, to compute the amplification bands of alternating impedance-beam amplifiers.

Introduction

THE excitation of space-charge standing waves by an alternating perturbation on a moving electron stream has been first analyzed by Hahn[1] and Ramo.[2] Field, Tien, and Watkins[3] have shown that the amplitude of the space-charge waves can be increased step by step if such a stream is decelerated at a velocity maximum of the standing-wave pattern and accelerated again to the original voltage at a velocity minimum. Similarly, a step-wise decrease of the amplitude

---

¹ W. C. Hahn, "Small-Signal Theory of Velocity-Modulated Electron Beams," *Gen. Elec. Rev.*, Vol. 42, pp. 258-270, June, 1939.

² S. Ramo, "Space-Charge and Field-Waves in an Electron Beam," *Phys. Rev.*, Vol. 56, p. 276, 1939. S. Ramo, "The Electronic-Wave Theory of Velocity-Modulation Tubes," *Proc. I.R.E.*, Vol. 27, pp. 757-763, December, 1939.

³ L. M. Field, P. K. Tien, and D. A. Watkins, "Amplification by Acceleration of a Single-Velocity Stream," *Proc. I.R.E.*, Vol. 39, p. 194, February, 1951.

may be obtained which can be used for beam noise reductions.[4,5] This cycle may be cascaded. Lately, Birdsall and Whinnery[6] have found that a periodic change of the drift-tube diameter has the same effect on the amplitude of a perturbation. The present study is intended to show that these possibilities for signal amplification in an electron beam are only two special cases of a more general group. By applying the transmission-line analog[7] to this problem, it is found that any alternating change of the "beam-impedance" at space-charge standing-wave maxima and minima results in a step-wise amplification or de-amplification of a signal on the beam.#

PRINCIPLE OF SPACE-CHARGE-WAVE AMPLIFICATION

Consider a space-charge wave of a-c velocity v and a-c convection current I in a stream of total d-c current I_0 drifting in laminar flow with d-c velocity v_0 at voltage V_0, and let an a-c potential V be attributed to the a-c velocity v defined on an energy basis as shown in detail in a previous paper:[7]

$$V = \frac{v_0\, v}{\eta} \tag{1}$$

where

$$\eta = \frac{e}{m}.$$

Considering the special case of a uniform beam for which the a-c current I and the a-c voltage V are given at a plane n normal to a uniform beam (or normal to the equivalent transmission line), the corresponding quantities at another plane, $n + 1$, as computed from the differential Equation (17) of Ref. (7), become:

$$V_{n+1} = V_n \cos \theta + j\, W\, I_n \sin \theta$$
$$I_{n+1} = j\, W^{-1}\, V_n \sin \theta + I_n \cos \theta. \tag{2}$$

[4] D. A. Watkins, "Noise Reduction in Beam Type Amplifiers," *Proc. I.R.E.*, Vol. 40, pp. 65-70, January, 1952.

[5] R. W. Peter, "Low-Noise Traveling-Wave Amplifier," *RCA Review*, Vol. XIII, pp. 344-368, September, 1952.

[6] C. K. Birdsall and J. R. Whinnery, "Waves in an Electron Stream with General Admittance Walls," *Jour. Appl. Phys.*, Vol. 24, p. 314, March, 1953.

[7] S. Bloom and R. W. Peter, "Transmission-Line Analog of a Modulated Electron Beam," *RCA Review*, Vol. 15, p. 95, March, 1954.

This material was presented at the I.R.E. Conference on Electron-Tube Research at Stanford University, Stanford, Cal., 1953.

W is defined as the beam impedance,[7]

$$W \equiv 2 \frac{V_0}{I_0} \frac{\omega_p}{\omega},$$ (3)

where ω is the perturbation or signal frequency and ω_p is the effective plasma frequency,

$$\omega_p \equiv p\,\omega_{p\infty} = p \sqrt{\frac{\eta\,I_0}{\pi\epsilon_0 v_0 s^2}}.$$ (4)

The factor p $(0 \leq p \leq 1)$ represents the reduction of the plasma frequency from the Langmuir-Tonks value due to the finite transverse
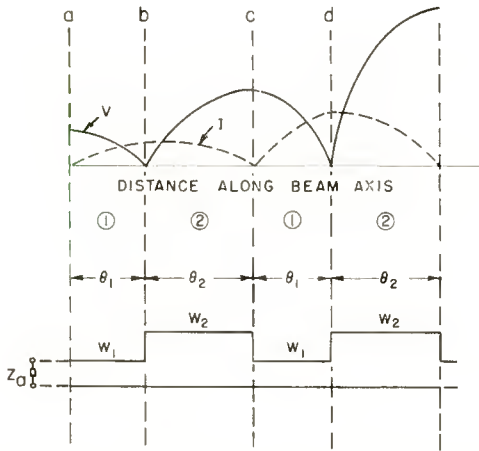
Fig. 1—The space-charge-wave amplitude is increased step-wise by periodically alternating the beam impedance along an electron beam. Z_a represents an open circuit in this case.

dimensions of the beam of radius s, and the influence of the surrounding shields. (See e.g., Ref. (4) or Ref. (7), Figure 2, for curves showing this dependence). The angle $\theta = \omega_p z/v_0 = 2\pi s/\lambda_p$ is the distance between planes n and $n+1$, measured in plasma wave lengths λ_p.

Referring to Figure 1 and taking for example the reference plane at the current minimum a, we have at plane b:

$$V_b = V_a \cos \theta_1$$

$$I_b = j \frac{V_a}{W_1} \sin \theta_1 \tag{5}$$

and for the special case $\theta_1 = \pi/2$,

$$V_b = 0$$
$$I_b = \frac{j V_a}{W_1}. \tag{6}$$

At b the beam impedance is changed to W_2. The a-c potential V and the a-c current I, remaining unchanged at b, produce at c

$$V_c = -\frac{W_2}{W_1} V_a \sin \theta_2$$
$$I_c = j \frac{V_a}{W_1} \cos \theta_2 \tag{7}$$

which becomes, for $\theta_2 = \pi/2$,

$$V_c = -\frac{W_2}{W_1} V_a$$
$$I_c = 0. \tag{8}$$

At this point, we close the cycle by returning to the first beam impedance value W_1. The cycle consists, therefore, of two discontinuities or "jumps" in beam impedance. Theoretically, it may be repeated any number of times, i.e., cascaded.

The signal amplification obtained in a *double impedance-jump*, consisting of two quarter-wave drift regions of impedance W_1 and W_2, follows from Equation (8):

$$\left| \frac{V_c}{V_a} \right| = \frac{W_2}{W_1}. \tag{9}$$

The electron flow is assumed to be laminar, the d-c current, therefore, stays constant. With Equation (4) this can be written

$$\left| \frac{V_c}{V_a} \right| = \frac{V_{02}}{V_{01}} \cdot \frac{\omega_{p2}}{\omega_{p1}} = \left(\frac{V_{02}}{V_{01}} \right)^{3/4} \left(\frac{p_2}{p_1} \right) \left(\frac{s_1}{s_2} \right) \tag{10}$$

From Equation (9) one concludes, therefore, that step-wise amplification of space-charge waves is obtained by periodically decreasing and increasing the beam impedance at a-c velocity maxima and minima. Conversely, de-amplification or reduction of space-charge waves results if the beam impedance is increased at a-c velocity maxima and decreased at minima. According to Equation (10), there exist three basically different ways of changing the beam impedance, namely:

1) Changing the beam voltage, V_0;

2) Changing the surrounding metal boundaries, and thereby the plasma-frequency reduction factor p;

3) Changing the beam radius, s.

There exist, therefore, three different practical methods leading to space-charge wave amplification (or de-amplification):

1. By changing the d-c voltage V_0, and leaving the beam radius constant,

$$\left| \frac{V_c}{V_a} \right| = \left(\frac{V_{02}}{V_{01}} \right)^{3/4} \left(\frac{p_2}{p_1} \right) \quad (s = \text{const.}) \tag{11}$$

This is the Field-Tien-Watkins amplifier.

2. By changing only the plasma-frequency reduction factor, p, and leaving voltage and radius constant,

$$\left| \frac{V_c}{V_a} \right| = \frac{p_2}{p_1} \quad (V_0 = \text{const.,} \ s = \text{const.}) \tag{12}$$

This is the Birdsall-Whinnery amplifier where the diameter of the surrounding metallic shields is periodically changed.

3. By changing the beam radius s and leaving the beam voltage constant,

$$\left| \frac{V_c}{V_a} \right| = \left(\frac{p_2}{p_1} \right) \left(\frac{s_1}{s_2} \right) \quad (V_0 = \text{const.}) \tag{13}$$

Space-charge amplification, therefore, can be obtained by periodi-

cally changing the diameter of the beam. It has been shown[8] that amplification (or de-amplification) exists also if the periodic changes in the beam impedance (e.g., in the beam diameter) are not abrupt, as assumed here for simplicity, but gradual.

A "blooping" beam, for example, is easily obtained by shooting an electron beam under proper conditions into a uniform magnetic field as commonly used for focusing long electron beams. The inner conductors of coaxial transmission-line models of a beam with abrupt impedance changes and of a beam with smooth changes are shown in Figure 2.

According to Equation (9) the most effective space-charge-wave amplifier is the one with the largest impedance jumps. It may be realized by using two or all three possibilities simultaneously. At a-c velocity maxima the beam voltage is stepped down, the cross section is enlarged and the plasma-frequency reduction factor is decreased by
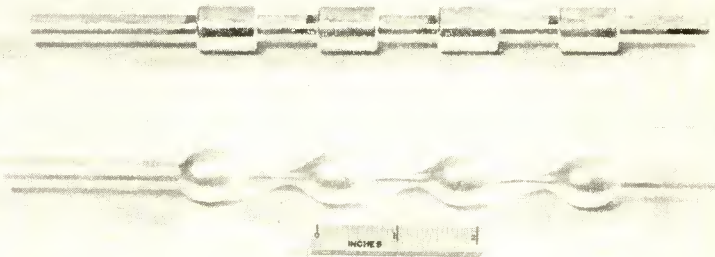
Fig. 2—Transmission-line models of electron beams with abrupt and with smooth periodic impedance changes. This picture shows only the inner conductors of the coaxial lines.

decreasing the distance between beam and metal shields. At a-c current maxima these beam quantities are jumped back to the original values. For noise-fluctuation de-amplification these quantities are changed in the opposite sense.

GENERALIZATION OF THE PRINCIPLE AND RELATIONS TO FILTER THEORY

According to the analogy between wave transmission along an electron beam and along a transmission line, a beam with periodically

---

[8] S. Bloom, "Space-Charge Waves in a Drifting, Scalloped Beam," unpublished report.

changing beam impedance is completely analogous to a line with periodically changing characteristic impedance. Such a periodic beam, therefore, may be thought of as a particular case of a one-dimensional lattice. It will exhibit pass bands and stop bands in the same way as a lattice or a filter line. However, whereas in filter theory one is interested in the regions where real power transfer occurs, for space-charge-wave amplification one looks for the regions where the standing-wave amplitude is increasing along the periodic structure. From this it follows that the regions of space-charge-wave amplification (or de-amplification) correspond to the stop bands of the equivalent filter line, and regions of no change in wave amplitude along the beam correspond to the pass bands of the filter line. This correspondence is shown in Figure 3 which represents an assumed distribution of pass and stop band of a filter line, as a function of the total angle $\theta_1 + \theta_2$ of one period a-c.

TRANSMISSION LINE FILTER	PASS BAND	STOP BAND	PASS BAND	STOP BAND	
PROPAGATION CONSTANT	IMAGINARY	REAL	IMAGINARY	REAL	
ELECTRON BEAM	NO AMPLITUDE CHANGE	AMPLIFICATION OR DE-AMPL.	NO AMPL CHANGE	AMPL. OR DE-AMPL.	NO CHANGE

$$\theta_0 = \theta_1 + \theta_2 \longrightarrow$$

Fig. 3—Relation between an alternating-impedance electron beam and its equivalent transmission-line filter. The wave-amplification (or de-amplification) regions of the beam correspond to the stop bands of the filter. The total angle θ_0 of one structure-period is proportional to the signal frequency in the case of the transmission line, and to the plasma frequency in the case of the beam.

On the basis of this general relation between filter lines and space-charge-wave amplifiers of the variable impedance type, one can apply all results of filter theory to wave amplification. In particular, the filter line of Figure 1 has been extensively studied as a simplified model for filter-helix structures.[9] Defining

$$\theta_1 = \alpha \, \theta_0 \tag{14a}$$

$$\theta_2 = (1 - \alpha) \, \theta_0 \tag{14b}$$

[9] W. J. Dodds and R. W. Peter, "Filter-Helix Traveling-Wave Tube," *RCA Review*, Vol. 14, pp. 502-532, December, 1953.

$$\zeta = \frac{1}{2}\left(\frac{W_1}{W_2} + \frac{W_2}{W_1}\right) \qquad (14c)$$

in correspondence with Figure 9a of Ref. (9), all pass- and stop-band diagrams in Figures 11 to 14 of Ref. (9) can be applied directly to find the conditions for which amplification (or de-amplification) can be obtained. For example, for any given pair

$$\alpha = \frac{\theta_1}{\theta_1 + \theta_2} \quad \text{and} \quad \zeta = 0.5\left(\frac{W_1}{W_2} + \frac{W_2}{W_1}\right),$$

the amplification bandwidth may be read from the graphs.

A more detailed study[8] reveals that inside a stop band (real propagation constant) wave amplification *or* de-amplification prevails. Which of these occurs depends upon the terminating r-f impedance, Z_a. If $Z_a \equiv V_a/I_a = \infty$ as assumed in the case of Figure 1, optimum amplification results; if on the other hand, $Z_a = 0$, the space-charge waves decrease at a maximum rate. The range of amplification as a function of intermediate values of $Z_a = \pm jX$ depends on the product of gain factor and number of cycles. The larger this product the narrower the range of allowed reactance values which lead to de-amplification. If the number of cycles grows very large, the de-amplification range finally converges into a single point, $Z_a = 0$. Thus, along an infinitely long beam, only amplification is possible.

HIGH-FREQUENCY OPERATION OF P-TYPE POINT-CONTACT TRANSISTORS*

By

F. L. HUNTER AND B. N. SLADE

Tube Division, Radio Corporation of America,
Harrison, N. J.

Summary—This paper discusses the characteristics of developmental p-type transistors in radio-frequency-amplifier or oscillator applications. Higher frequencies can be obtained from transistors using p-type germanium rather than n-type germanium because of the greater mobility of the minority carriers (electrons) in the former as compared to the mobility of the minority carriers (holes) in the latter. Short-circuit-stable p-type amplifier transistors have been developed having a current-amplification-factor cutoff frequency of 50 to 60 megacycles. P-type oscillator transistors have been operated at frequencies up to 425 megacycles. Experimental tests have shown that both p-type and n-type oscillator transistors perform satisfactorily at temperatures up to approximately 75° C.

INTRODUCTION

EARLY in the development of point-contact transistors, it was discovered that transistor action could be obtained from p-type as well as n-type germanium.[1] In general, p-type transistors had higher frequency-response characteristics but lower current-amplification factors than n-type units.[1,2] Because a high current-amplification factor is important to point-contact transistor action, n-type germanium has been used predominantly in these devices. P-type transistors can be made, however, having current-amplification factors which are satisfactory for radio-frequency applications. This paper discusses the development of the high-frequency possibilities of p-type point-contact transistors.

ELECTRICAL "FORMING" OF P-TYPE TRANSISTORS

Semiconductor theory[3] ascribes transistor action to the presence

---

* Decimal Classification: R282.12.
[1] W. G. Pfann and J. H. Scaff, "The P-Germanium Transistor," *Phys. Rev.*, Vol. 76, pp. 459, August, 1949.
[2] W. G. Pfann and J. H. Scaff, "The P-Germanium Transistor," *Proc. I.R.E.*, Vol. 38, pp. 1151-1154, October, 1950.
[3] W. Schottky and E. Spenke, *Wiss. Veroffentl. Siemens-Werken*, Vol. 18, pp. 225, 1939.

of an inversion layer, or a change of conductivity type in the barrier layer, of the emitter contact. This layer, believed to be present on the surface of n-type germanium, enables the emitter to inject minority carriers in n-type germanium when the transistor is biased in the forward direction. The injection of minority carriers into p-type germanium by a forward-biased emitter is normally very small because of the poor rectification qualities of p-type germanium. It has been found, however, that electrical "forming" of the emitter of a p-type transistor makes it possible to increase the forward emitter current and thus enhance transistor action.[4]

STABLE RADIO-FREQUENCY AMPLIFIER TRANSISTORS

It can be predicted from theoretical considerations that the frequency response of p-type transistors will be higher than that of n-type units. Shockley[5] has expressed the transit time of electron or hole carriers traveling from the emitter through germanium to the collector as $\tau = \dfrac{S^3 \, \sigma}{\mu \, I_e}$, where τ is the transit time in seconds, S is the spacing in centimeters between the emitter and collector contacts, σ is the conductivity of the germanium in reciprocal ohm-centimeters, μ is the mobility of the electrons or holes in centimeters squared per volt-second, and I_e is the emitter current in amperes. Because the transit time has an approximately inverse relationship to frequency response, the frequency response would be expected to vary directly with the mobility of the minority carriers, other factors remaining constant. The following values for the mobility of electrons and holes were obtained from drift-mobility measurements on single-crystal filaments of n- and p-type germanium.[5]

Hole mobility in n-type germanium, $\mu_p = 1700$ cm^2/volt sec

Electron mobility in p-type germanium, $\mu_n = 3600$ cm^2/volt sec

The ratio of the mobility of electron minority carriers in p-type germanium to that of hole minority carriers in n-type germanium is approximately 2 to 1. Provided all other factors of the transit-time equation remain constant, therefore, a change from n-type germanium

---

[4] J. Bardeen and W. G. Pfann, "Effects of Electrical Forming on the Rectifying Barriers of N and P Germanium Transistors," *Phys. Rev.*, Vol. 77, pp. 401-402, December, 1950.

[5] W. Shockley, *Electrons and Holes in Semiconductors*, D. Van Nostrand Co., Inc., New York, N. Y., 1950.

to p-type germanium should increase the frequency response of a transistor by a factor of approximately 2.

Figure 1 shows the variation of frequency cutoff (3 decibels down in current amplification factor) with point-spacing for p-type and n-type transistors.[6] Although these curves are average curves representing a number of transistors, identical point-spacing intervals and germanium-resistivity values were used. A comparison of these curves shows that higher frequency-cutoff values were achieved by the substitution of p-type germanium for n-type germanium. Variation of the resistivity of the germanium within a range of 1 to 5 ohm-centi-
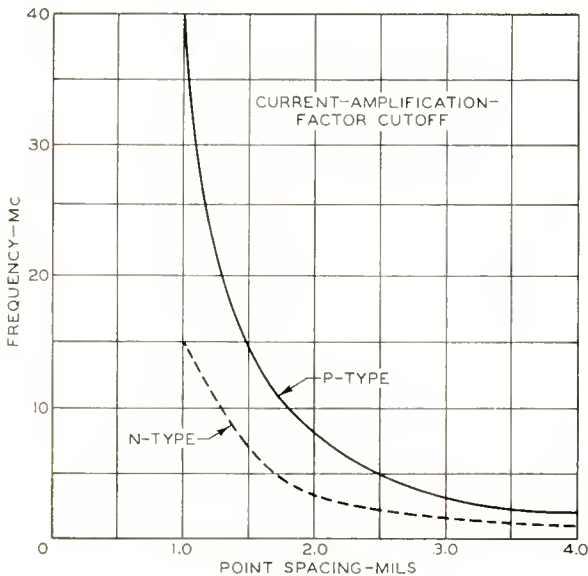
Fig. 1—Effect of variations in point spacing on frequency response of p-type and n-type point-contact transistors.

meters had little effect on the frequency response. The electrical forming treatment, however, affected the frequency response considerably, and extreme care was taken during the forming operation to assure uniform treatment of the transistors. Values of frequency cutoff as high as 25 megacycles at a spacing of 0.002 inch and 50 megacycles at a spacing of 0.001 inch were attained for the p-type transistors, depending on the electrical forming.

One of the factors affecting the stability of point-contact transistors

<hr/>

[6] B. N. Slade, "Factors in the Design of Point-Contact Transistors," *RCA Review*, Vol. XIV, pp. 17-27, March, 1953.

is their equivalent base resistance.[7] Generally, values of equivalent base resistance of approximately 100 ohms or less will assure transistor stability. Figure 2 shows the equivalent base resistance of p-type point-contact transistors as a function of point spacing for various values of germanium resistivity. The curves of Figure 2 resemble similar curves taken on n-type transistors[7] except that the equivalent base resistances are somewhat lower for the p-type transistors for any given resistivity and point spacing. Although the curves in Figures 1 and 2 cannot be used as exact design data, their general shape serves as a guide to transistor design.
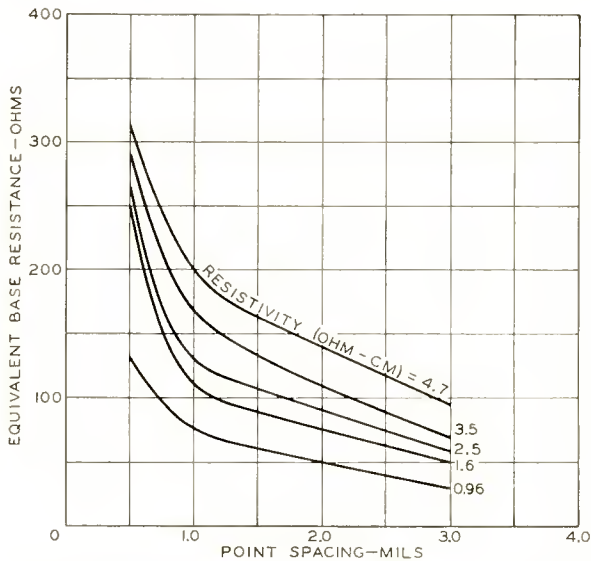
Fig. 2—Effect of variations in point spacing and resistivity on equivalent base resistance of p-type transistors.

By the use of proper control of germanium resistivity and point spacing, a stable point-contact transistor can be designed to operate at high frequencies. Short-circuit-stable transistors using n-type germanium and designed for radio-frequency amplification have been reported previously to have frequency responses up to 30 megacycles.[7] Analogous p-type transistors have been made having frequency responses up to 60 megacycles. Figure 3 shows the current amplification factor, α_{ce}, as a function of frequency for two typical short-circuit-stable radio-frequency-amplifier transistors using p-type germanium.

[7] B. N. Slade, "The Control of Frequency Response and Stability of Point-Contact Transistors," *Proc. I.R.E.*, Vol. 40, pp. 1382-1384, November, 1952.
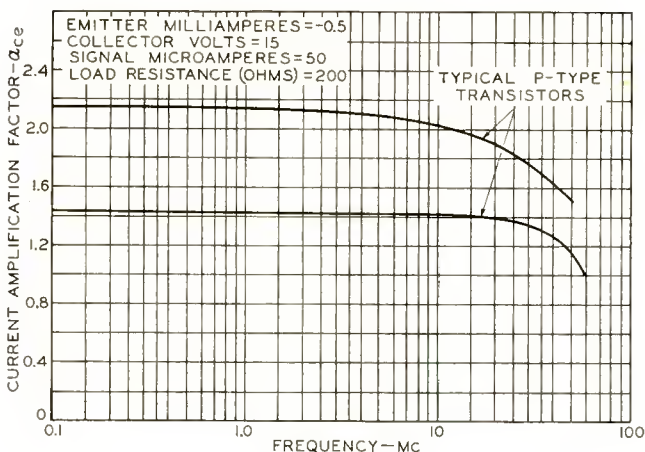
Fig. 3—Frequency-response curves of two typical short-circuit-stable radio-frequency-amplifier p-type transistors.

Oscillator Transistors

A number of p-type point-contact oscillator transistors have also been made having the same point-contact spacings and germanium resistivities as the n-type point-contact oscillator transistors described in a previous paper[8] but differing in the type of impurities predominant in the germanium. Figure 4 shows the output characteristics of both the p-type and the n-type oscillator transistors. The curves of collector voltage versus collector current at constant emitter currents are flatter for the n-type transistors than for the p-type units over the normal

---

[8] G. M. Rose and B. N. Slade, "Transistors Operate at 300 Mc," *Electronics*, Vol. 25, pp. 116, November, 1952.
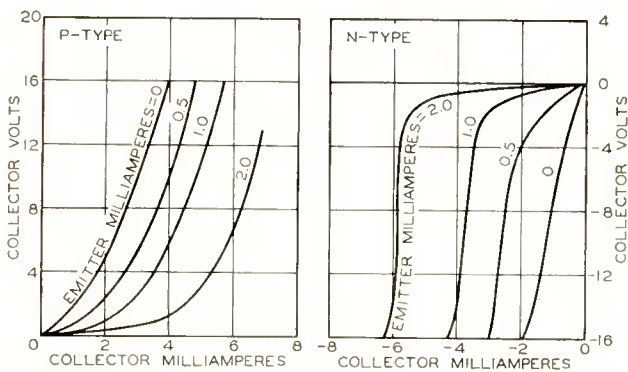
Fig. 4—Output characteristics of point-contact oscillator transistors.

operating range of the transistors, illustrating the better rectification qualities of n-type germanium. The collector resistance in the reverse direction of the n-type transistor, therefore, is greater than that of the p-type transistor. The average collector resistance of a group of 40 p-type oscillator transistors was 6400 ohms; that of a corresponding group of n-type transistors was 10,000 ohms. Comparative values of current amplification factor, which indicate the degree of transistor action, may also be obtained from the output characteristics. If a con-
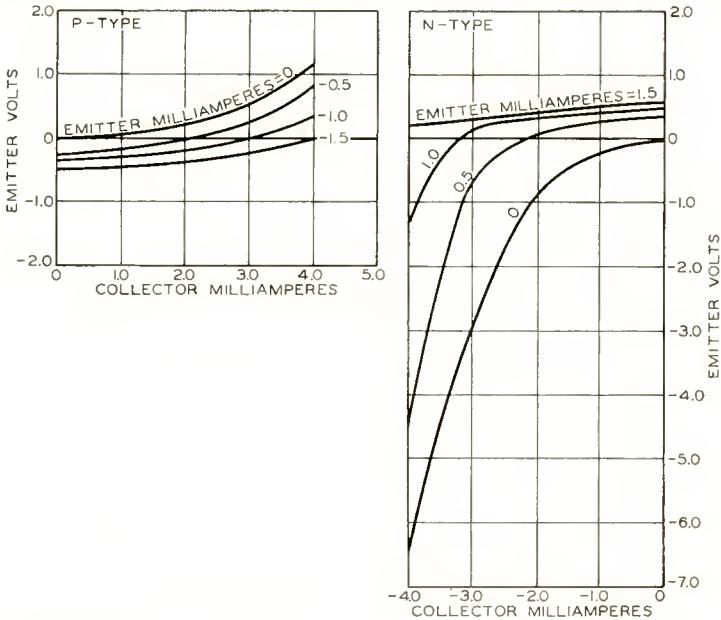
Fig. 5—Feedback characteristics of point-contact oscillator transistors.

stant operating collector voltage is chosen for both types, and the increase of collector current is measured for a given change in emitter current, the current amplification factor of the n-type transistor is found to be somewhat greater than that of the p-type transistor. For the same groups of 40 units mentioned above, the average current-amplification factor of the p-type transistors was 2.0 while that of the n-type transistors was 2.8.

Figure 5 shows the feedback characteristics of both p-type and n-type oscillator transistors. The curves of emitter voltage versus collector current at constant emitter currents are steeper for the n-type transistors than for the p-type units over the operating range. The feedback resistance of the n-type transistors, therefore, is greater than that of the p-type transistors. The group of 40 p-type transistors had

an average feedback resistance of 250 ohms; that of the group of 40 n-type transistors was 400 ohms. Although the emitter of the p-type transistor is negatively biased, the high feedback characteristic causes the emitter voltage to increase and become positive over the main operating range of the transistor. The high feedback characteristic of the n-type transistor, on the other hand, causes the positively biased emitter to become negative over the main operating range of the transistor.
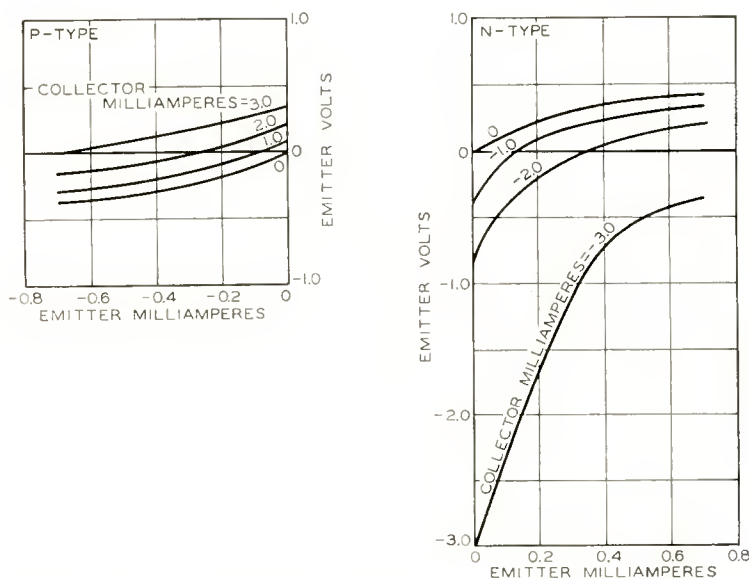
Fig. 6—Input characteristics of point-contact oscillator transistors.

The input characteristics of p-type and n-type oscillator transistors are shown in Figure 6. The effect of the high feedback resistance on the emitter voltage is also evident in the input characteristics of the two transistor types. The decrease of the emitter voltage of the n-type transistor is more pronounced than the increase of the emitter voltage of the p-type transistor because of the higher feedback resistance of the former.

The n-type oscillator transistor has been reported previously to be capable of oscillating readily at frequencies between 100 and 200 mega-cycles.[8] The highest oscillation frequency attained with these units was 302 megacycles. With p-type transistors, however, oscillation frequencies as high as 425 megacycles have been obtained. The oscillator circuit used in the measurement of the frequency of the p-type point-contact oscillator transistors was the same as that used for the n-type
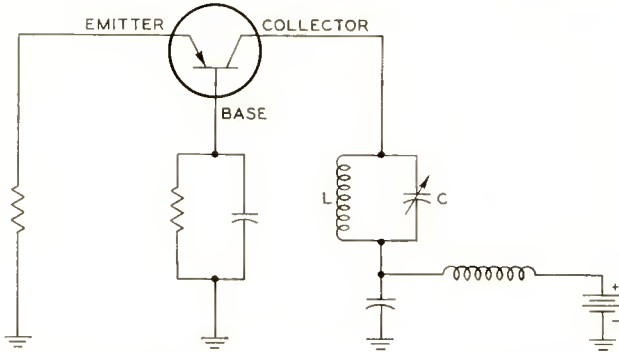
Fig. 7—Oscillator circuit used in measurement of frequency of
point-contact transistors.

transistors except that the polarity of the voltage supply was reversed.
This oscillator circuit is shown in Figure 7. Emitter bias is provided
by the bypassed resistance in the base circuit and the self-biasing
resistance in the emitter circuit. The internal capacitance between
emitter and collector provides a feedback path for oscillation. The
inductance and the capacitance of the parallel resonant circuit in the
collector circuit may be varied to cover an oscillation range from 5 to
425 megacycles. The 40 p-type and 40 n-type point-contact oscillator
transistors mentioned previously were measured in this oscillator cir-
cuit under optimum conditions for maximum oscillation frequency.
Figure 8 shows the percentage of units within given intervals of
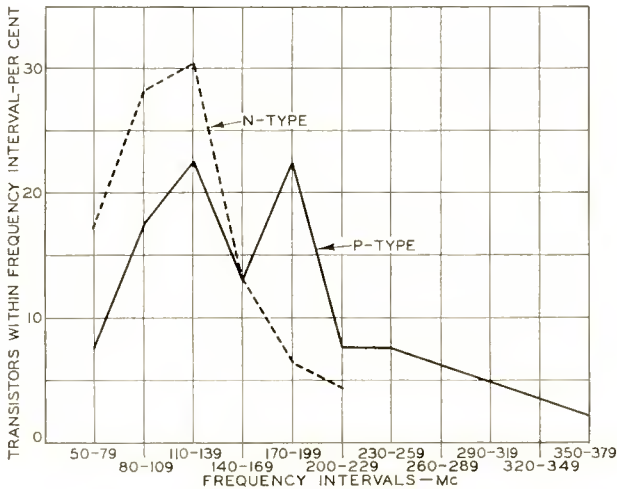
Fig. 8—Distribution of maximum oscillation frequencies of
point-contact oscillator transistors.

maximum oscillation frequency. The median value, or the point at which 50 per cent of the units fall above and 50 per cent below, was found to be 149 megacycles for the p-type oscillator transistors and 112 megacycles for the n-type oscillator transistors.

Effect of Ambient Temperature

The resistivity of p-type and n-type germanium as a function of temperature has been described by Herkart and Kurshan.[9] At resistivities of 16 ohm-centimeters or less, both p-type and n-type germanium have positive temperature coefficients at 25° C (room temperature).
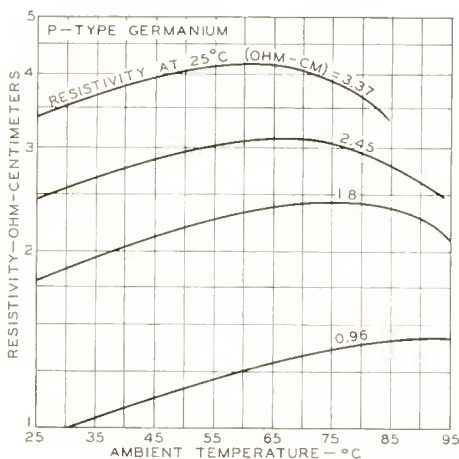
Fig. 9—Effect of variations in ambient temperature on resistivity of p-type germanium.

As the temperature is increased, however, the curve for a given resistivity approaches the negative-slope characteristic of the curve for intrinsic germanium. The resistivity then decreases with increasing temperature. An investigation was made of the effect of ambient temperature on resistivity for both p-type and n-type germanium over the range of resistivities used in making the transistors described above. The results are shown in Figures 9 and 10. For samples having a given resistivity at 25° C, the resistivity of the p-type germanium increases to a higher temperature than that of the n-type germanium before reaching the negative-slope characteristic. For example, the curve for n-type germanium having a resistivity of 1.8 ohm-centimeters

---

[9] P. G. Herkart and J. Kurshan, "Theoretical Resistivity and Hall Coefficient of Impure Germanium Near Room Temperature," *RCA Review*, Vol. XIV, pp. 427-440, September, 1953.

at 25° C reaches a maximum resistivity of 2.1 ohm-centimeters at 65° C before decreasing. The curve for p-type germanium having a resistivity of 1.8 ohm-centimeters at 25° C reaches a maximum resistivity of 2.43 ohm-centimeters at 76° C. P-type transistors, therefore, appear to be capable of operating at higher temperatures than n-type transistors before the change in characteristics becomes sufficient to make the units inoperable.

Ambient-temperature tests were conducted on both p-type and n-type point-contact oscillator transistors. P-type units were operated in the oscillator circuit shown in Figure 7, and a constant collector-supply voltage of 10 volts was applied. The parallel resonant circuit
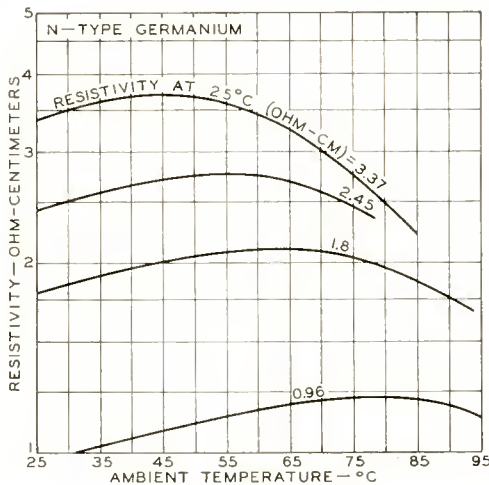
Fig. 10—Effect of variations in ambient temperature on resistivity of n-type germanium.

in the collector was tuned to a resonant frequency of 83 megacycles. The ambient temperature was then allowed to rise from room temperature, and relative radio-frequency power output was measured at intervals of 5 degrees Centigrade. Data for four p-type oscillator transistors are shown in Figure 11(a). The radio-frequency power output for these units gradually decreased as the ambient temperature increased until the transistors failed. As the temperature approached 75° C, all four units were still oscillating satisfactorily at the resonant frequency of 83 megacycles. The transistors failed at temperatures of 77°, 92°, 112° and 129° C. The characteristics of all four units returned to their original values after the transistors cooled to room temperature.

A similar test was conducted on n-type oscillator transistors; the results are shown in Figure 11(b). The collector supply voltage for

these units was —8 volts, and the resonant frequency was 60 megacycles. The radio-frequency power output of n-type transistors also decreased with increasing temperature. The units failed at 64°, 80°, 93° and 122° C. The characteristics of the n-type transistors also returned to their original values when the units cooled to room temperature. Although these results show that the p-type oscillator transistors operated satisfactorily at slightly higher temperatures than the n-type units, definite conclusions cannot be made because of some overlapping of the results.

The effect of ambient temperature on other characteristics of p-type point-contact oscillator transistors was also investigated. Figure 12 shows the small-signal operating power gain as a function of ambient
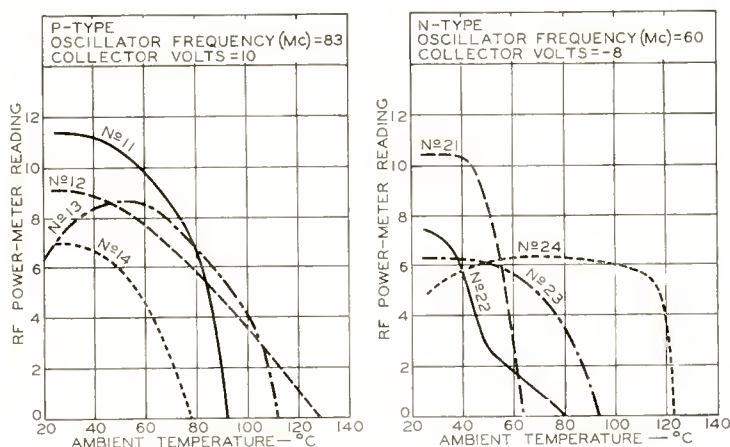
Fig. 11—Effect of variations in ambient temperature on power output of point-contact oscillator transistors.

temperature for four p-type oscillator transistors. These transistors were tested in a small-signal amplifier test set at an emitter current of —0.6 milliampere and a collector bias of 10 volts. The operating power gain was measured at intervals of 5 degrees Centigrade and was found to decrease gradually with increasing temperature. All four units were still operating satisfactorily at a temperature of 75° C.

Figure 13 shows the effect of ambient temperature on the collector current at a collector bias of 15 volts and zero emitter current. The collector current, or I_{c0}, of the four transistors tested decreased gradually with increasing temperature.

The collector resistance of p-type oscillator transistors as a function of ambient temperature is shown in Figure 14. The collector resistance was measured at an emitter current of —0.6 milliampere and
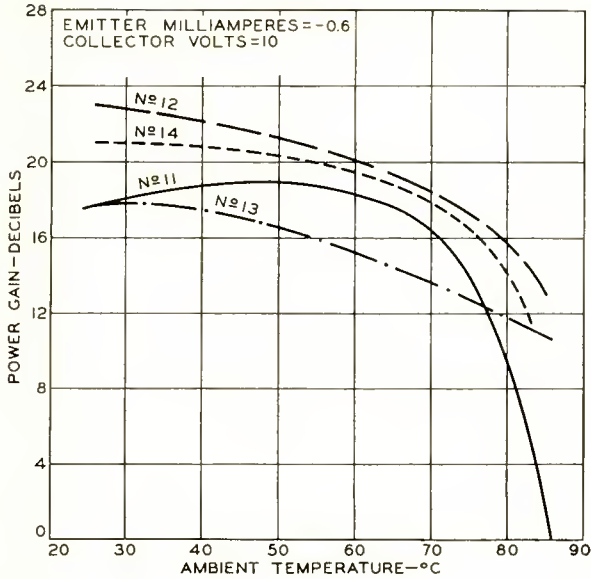
Fig. 12—Effect of variations in ambient temperature on power gain of
p-type point-contact oscillator transistors.
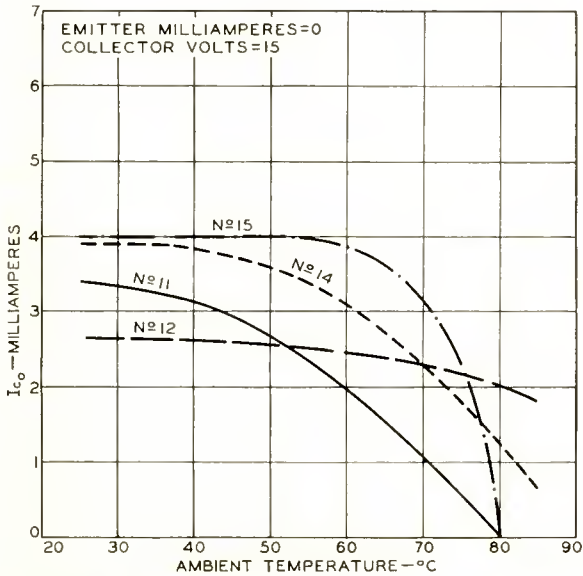
Fig. 13—Effect of variations in ambient temperature on collector current
at zero emitter current for p-type point-contact oscillator transistors.

a collector voltage of 10 volts. The collector resistance remained substantially constant to a temperature of 55° C, and then started rising quite rapidly at higher temperatures.

The curves shown in Figures 13 and 14 may be explained on the basis of the curves of resistivity versus ambient temperature shown in Figure 9. Samples of p-type germanium having resistivities less than 1.8 ohm-centimeters at 25° C were found to have increasing resistivity with increasing temperature up to temperatures of approxi-
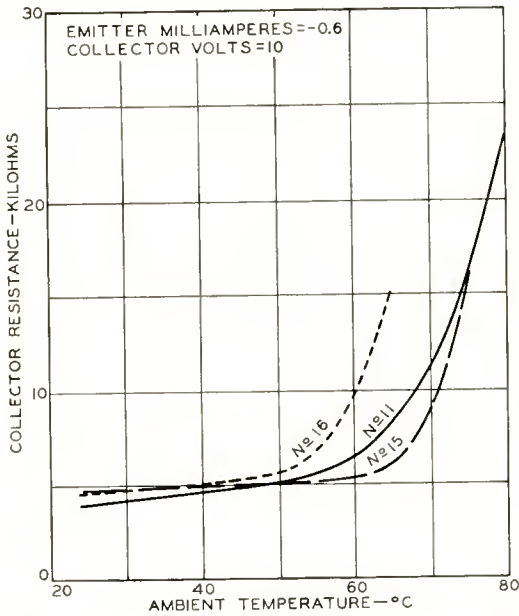
Fig. 14—Effect of variations in ambient temperature on collector resistance of p-type point-contact oscillator transistors.

mately 80° C before the resistivity began to decrease with higher temperatures. Transistors made with this germanium, therefore, would be expected to have collector resistances having positive temperature coefficients up to temperatures of 80° C or more. The positive temperature coefficient of the collector resistance also explains the negative temperature coefficient of I_{c0} shown in Figure 13. The increase in the collector resistance shown in Figure 14 tends to raise the operating power gain shown in Figure 12 at the higher temperatures. The collector current at this operating point, however, decreases with increasing temperature, as does the I_{c0} shown in Figure 13. The current amplification factor, therefore, decreases sufficiently to compensate for the increase of the collector resistance, causing a gradual drop in the

operating power gain. The characteristics of all the transistors used in these ambient-temperature tests returned to their original values when the transistors were cooled to room temperature.

ACKNOWLEDGMENTS

RCA TECHNICAL PAPERS†

Fourth Quarter, 1953

Any request for copies of papers listed herein should be addressed to the publication to which credited.*

---

† Report all corrections or additions to RCA Review, RCA Laboratories, Princeton, N. J.

* *RCA Industry Service Laboratory Bulletins* are not published and are issued only as a service to licensees of the Radio Corporation of America.

AUTHORS

MAURICE ARTZT received the B.S. degree in Electrical Engineering from the University of Texas in 1925 and the M.S. degree in Electrical Engineering from Union College in Schenectady in 1929. From 1925 until 1930 he was in the Radio Test Department and the Radio Engineering Department of the General Electric Company in Schenectady. He was a member of the engineering staff of the RCA Manufacturing Company in Camden, New Jersey from 1930 until 1942, where he was engaged chiefly on the design and development of facsimile equipment. In 1942 he transferred to the RCA Laboratories at Princeton, New Jersey where he has continued to work on facsimile and allied devices. Mr. Artzt is a member of Tau Beta Pi and of Sigma Xi.

STANLEY BLOOM received the B.S. degree in Physics and Mathematics from Rutgers University in 1948. In 1949 he received the M.S. degree in Physics and in 1952, the Ph.D. degree in Physics from Yale University. In 1952 he joined the RCA Laboratories where he has engaged in research on noise problems in traveling-wave tubes. Dr. Bloom is a Member of the American Physical Society, Sigma Xi, and Phi Beta Kappa.
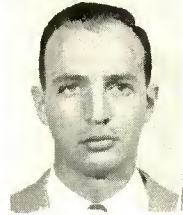
D. G. Burnside—(See *RCA Review*, Volume VII, No. 2, June 1946, p. 284.)
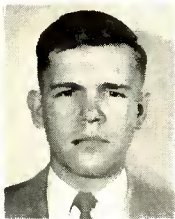
JOHN T. FISCHER received the B.S. degree in Electrical Engineering from Washington University in 1950 and the S.M. degree in Electrical Engineering in 1952 from Massachusetts Institute of Technology where he served as a teaching assistant during his graduate study. Mr. Fischer joined RCA Laboratories in 1952.

THOMAS U. FOLEY received the degree of E.E. from Cornell University in 1937. He joined RCA in 1940 as a student engineer. From 1941 to 1946, he served in the U. S. Army Signal Corps as a member of the Electronics Training Group and later as a radar, communication and technical officer. He returned to RCA Victor, in 1946, where he has since been engaged in product engineering for industrial r-f heating, AM broadcast directional array phasing and UHF television antenna system filter development and design. Mr. Foley is an Associate Member of the Institute of Radio Engineers.

137
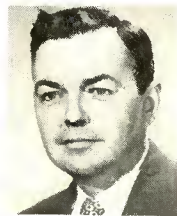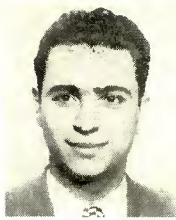
BERNARD HARRIS received the B.E.E. degree from Cooper Union in 1949, and the M.S. degree in Electrical Engineering from Columbia University in 1951. During the period 1946-1947, he served in the United States Army. Since 1951, he has been employed as a television development engineer by the Industry Service Laboratory of RCA Laboratories. He is now pursuing the D.Eng.Sc. degree at Columbia University. Mr. Harris is a member of Tau Beta Pi and an Associate Member of the Institute of Radio Engineers.

WILLIAM D. HOUGHTON graduated from the RCA Institutes in 1939. He joined the Research and Advanced Development group of RCA Communications, Inc. in 1940 and was transferred to the RCA Laboratories in 1942. From 1942 to 1950 he specialized in time-division multiplex research at the Rocky Point, N. Y. laboratory of RCA. In 1950 Mr. Houghton was transferred to the David Sarnoff Research Center in Princeton, N. J. where he has been actively engaged in the color television development program and on systems for video recording on magnetic tape. Mr. Houghton is a Member of Sigma Xi and The Institute of Radio Engineers.

FREDERICK L. HUNTER received the B.S. degree in Electrical Engineering from Syracuse University in 1951. Immediately after graduation, he joined the Advanced Development Group of the RCA Victor Tube Department at Harrison, N. J., where he worked on the development of semiconductor devices. He is now a member of the newly created Semiconductor Advanced Development Group of the Tube Division at Harrison. Mr. Hunter is a Member of the Institute of Radio Engineers.

ALBERT MACOVSKI received the B.E.E. degree from the College of the City of New York in 1950, and the M.E.E. degree from the Polytechnic Institute of Brooklyn in 1953. Since 1950 Mr. Macovski has been engaged in television engineering at the Industry Service Laboratory of RCA Laboratories Division in New York, N. Y.

ADOLPH R. MORGAN received his B.S. degree in Electrical Engineering from the University of California in 1931. In the same year he joined the RCA Manufacturing Company in their Student Training Activities and in 1933 became a research engineer. In 1942 he transferred to RCA Laboratories Division in Princeton, N. J., where he has been engaged in recording and acoustic research problems. Mr. Morgan is a Member of the Acoustical Society of America, Tau Beta Pi, Eta Kappa Nu, Sigma Xi and Phi Beta Kappa.

HARRY F. OLSON received the B.S. degree in 1924, the M.S. degree in 1925, the Ph.D. degree in 1928 and the E.E. degree in 1932 from the University of Iowa. From 1928 to 1930 he was in the Research Department of Radio Corporation of America; from 1930 to 1932, in the Engineering Department of RCA Photophone; from 1932 to 1941, in the Research Division of RCA Manufacturing Company; since 1941, with the RCA Laboratories. Dr. Olson is a member of Tau Beta Pi, Sigma Xi, and the Society of Motion Picture and Television Engineers. He is is a Fellow of the American Physical Society, the Institute of Radio Engineers, the Acoustical Society of America and the Audio Engineering Society. He is a past president of the Acoustical Society of America.

WEN YUAN PAN received the E.E. Degree from Stanford University in 1939, and the Ph.D. Degree in Electrical Engineering in 1940. He served in an advisory capacity to the China Defense and Supplies in 1941 and to the Chinese Delegation to the International Civil Aviation Conference in 1944. He was engaged as a research scientist at the Radio Research Laboratory at Cambridge, Massachusetts, during the war years and was invited to be a member of the Advisory Committee of the United Nations Telecommunications in 1946. Since 1945, he has been with the RCA Victor Division at Camden, New Jersey. Dr. Pan is an honorary member of the Veterans' Wireless Operators Association, a member of Sigma XI and Senior Member of the Institute of Radio Engineers.

JACQUES I. PANKOVE received the B.S. degree in Electrical Engineering in 1944 and the M.S. degree in Electronic Engineering 1948 from the University of California in Berkeley. From 1944 to 1946 he served with the United States Army. Since 1948 he has been engaged in semiconductor research at RCA Laboratories Division in Princeton, N. J. Mr. Pankove is a Member of Sigma Xi and the American Institute of Electronic Engineers and an Associate Member of the Institute of Radio Engineers.

ROLF W. PETER received the M.S. degree in Electrical Engineering in 1944, and the Ph.D. degree in Radio Engineering in 1948 from the Swiss Federal Institute of Technology in Zurich, Switzerland. From 1946 to 1948 he was Assistant Professor of Radio Engineering at the Swiss Federal Institute of Technology. In 1948 he joined the RCA Laboratories Division in Princeton, N. J., where he has been engaged in research on traveling-wave tube amplifiers. Dr. Peter is a Member of Sigma Xi and a Senior Member of the Institute of Radio Engineers.

JOHN A. RUETZ received the B. S. and M. S. degrees in Electrical Engineering from the University of Michigan in 1949 and 1950, respectively. From 1944-1946 he served as an electronic technician in the U. S. Navy. In 1950, he joined the RCA Laboratories Division, Princeton, N.J., where he engaged in work on microwave amplifiers. He is now with the Electronics Research Laboratory at Stanford University. Mr. Ruetz is a Member of the Institute of Radio Engineers.

TERRY M. SHRADER received the B.S. degree in Electrical Engineering from Purdue University in 1925. From 1925 to 1930, he was associated with the General Electric Company as engineer in charge of receiving-tube and test-equipment design. In 1930 he joined the RCA Tube Department as manager of the receiving-tube advanced development group. From 1941 to 1948 he was active in the development of industrial electronic equipment for the Engineering Products Department in Camden and in Indianapolis. Since 1948, he has been concerned with the development of microwave power tubes in the Special Development Group of the Tube Division in Harrison.

BERNARD N. SLADE received the B.S. degree in Electrical Engineering from the University of Wisconsin in 1948. He is now doing graduate work in electrical engineering at Stevens Institute of Technology. Mr. Slade joined the RCA Victor Division in 1948, and was associated with the Advanced Development Group at the Harrison, New Jersey Tube Department until 1953. His work during that time was concerned with the development of semiconductor devices. He is presently Manager of Semiconductor Advanced Development at the Harrison RCA Tube Division. Mr. Slade is a member of the Institute of Radio Engineers.

J. G. WOODWARD received the B.A. degree from North Central College in 1936, the M.S. degree in Physics from Michigan State College in 1938, and the Ph.D. degree in Physics from the Ohio State University in 1941. He held Graduate Assistantships at Michigan State College from 1936 to 1939 and at the Ohio State University from 1939 to March 1941. In March 1941 he joined the Research Division of the RCA Manufacturing Company at Camden, N. J., and later that year transferred to the RCA Laboratories Division at Princeton, N. J. where he has been engaged in research in acoustics. Dr. Woodward is a member of the Acoustical Society of America and Sigma Xi, and is a Fellow of the American Association for the Advancement of Science.
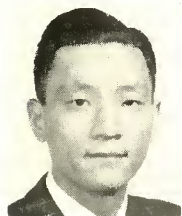
H. B. YIN received the B.S. degree in Physics from the University of Shanghai in 1943 and the M.E.E. degree from Syracuse University in 1950. He then joined the Electronics Measurement Co. In 1951 he joined the Engineering Products Department of RCA in Camden, N. J. where he was engaged in the development of UHF antennas and filters. In 1954 Mr. Yin transferred to the RCA Victor Home Instrument Division where he has been working on transistor circuitry.

JOSEPH A. ZENEL received the B.S. degree in Electrical Engineering from Bucknell University in 1949. Upon graduation, he joined RCA Laboratories in Princeton, N. J. where he is now engaged in work on magnetic recording. He served with the U. S. Army from 1942 to 1945. Mr. Zenel is a member of Tau Beta Pi, Pi Mu Epsilon, American Institute of Electrical Engineers, and the Acoustical Society of America.